Charged Particle Heating in Tokamak Fusion Plasmas(Dissertation_全文)

AUTHOR(S):

Ohnishi, Masami

CHARGED PARTICLE HEATING IN TOKAMAK FUSION PLASMAS

MASAMI OHNISHI

JUNE 1978
INSTITUTE OF ATOMIC ENERGY
KYOTO UNIVERSITY

CHARGED PARTICLE HEATING IN TOKAMAK FUSION PLASMAS

MASAMI OHNISHI

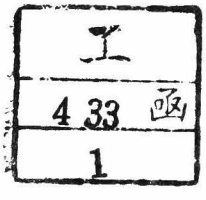

JUNE 1978
INSTITUTE OF ATOMIC ENERGY
KYOTO UNIVERSITY

ABSTRACT

In this thesis two key problems in the area of plasma engineering of fusion reactors have been studied in detail. They are related to the behaviors of reactor-grade plasmas and fusion products, of which works are indispensable for realizing a fusion power reactor.

In chapter 1, the stationary and dynamic characteristics of a D-T fusion reactor were discussed by numerically solving the zero dimensional kinetic equations of a fusion plasma core. The properties of plasma heating due to the energetic ions produced by neutral beam injection and the alpha particles born in D-T reactions were studied by the approximate binary collision model. It is indicated that the thermalization time of the alpha particles should not be neglected in the study on the dynamics or controls of fusion plasma. The calculations of dynamics included the thermalization process of alpha particles as a pure time delay.

In chapter 2, the effects of the thermalization (or slowing down) process of energetic particles on the stability against thermal runaway, the dynamics and the controls of fusion plasma core were investigated by properly dealing with the slowing down process by the multi-group formulation. It is concluded that the slowing down process hardly causes any appreciable change of the thermal stability region, but exerts the important effects which cannot be disregarded in discussing the dynamics and control problems.

In chapter 3, the parameter survey of Cat.D tokamak reactors was

made by solving the density balance equations for five kinds of ions and the temperature balance equation including the effects of convex density and temperature profiles and resulted in obtaining the parameters of reasonable size reactors comparable to a D-T reactor. The possibility to ignite the Cat.D reactor from the D-T burning operation by controlling the fueling rate of deuteriums and tritiums was proposed for reducing the input power needed for start-up of a Cat.D reactor. The transition process during the start-up was calculated and the Cat. D operating mode was attained in a few hundred seconds by adequate controls of the fueling without any additional heating. The effects of additional heating such as to prevent the plasma quench and to improve the transition path were described. The thermal instability and its dynamics in the reactor with arbitrary D-T mixture were also studied in the simplified Cat.D plasma model.

Chapters 4 and 5 dealt with the loss of alpha particles caused by the drift orbit motion in axially symmetric tokamak reactors. The loss of *3.5 MeV* alpha particles was numerically evaluated for various future reactors and was proved to depend strongly on the plasma minor and major radii, the plasma current and its profiles. It was found that a large power reactor could confine alpha particles completely, while small reactors such as zero power experimental devices, fission-fusion hybrid reactors and two-ion-component tokamak reactors would not do so.

In chapter 5, the containment properties of alpha particles during slowing-down process were studied by using Monte Carlo calculations, in which the pitch-angle scattering effects were included. The loss of alpha particles during slowing-down was found to be safely negligible in a pure D-T plasma, but increases proportionally to the effective charge number of the plasma and cannot be ignored in a highly contaminated plasma ($Z_{eff} > 4$), compared with the loss of *3.5 MeV* particles.

ACKNOWLEDGMENTS

The author expresses his sincere gratitude to Professor J. Wakabayashi, Institute of Atomic Energy, Kyoto University, for continuing encouragement, support and advice throughout the course of this research. Appreciation is expressed to Professor A. Iiyoshi, Plasma Physics Laboratory, Kyoto University, for the motivation and discussion on the subject in chapter 3.

The author also thanks Associate Professor T. Hoshino, Institute of Atomic Energy, Kyoto University, for his helpful and stimulating discussion, specifically in chapter 2. The valuable discussion on the material dealt with in chapter 3 is acknowledged to Research Associate O. Motojima, Kyoto University.

The author is indebted to Messrs. T. Sato, H. Tokunaga, N. Ao and Y. Kinoshita for the assistance of numerical calculations and fruitful discussions.

The author thanks Professor G. H. Miley, Nuclear Engineering Laboratory, University of Illinois for his encouragement and interest in this research and deeply appreciates the useful comments on chapter 4 of this thesis made by Research Assistant L. M. Hively, University of Illinois.

The understanding and patience of my wife, Itsuko, were helpful and heartily appreciated.

CONTENTS

NOMENCLATURE

Latin symbols

A	aspect ratio
$\mathbf{A}$	system matrix of a plasma core in I.S.A.
$\mathbf{A}_f$	system matrix of a plasma core with feedback control in I.S.A.
$\vec{A}$	vector potential of magnetic field
a	minor radius of a plasma
$\mathbf{B}$	system matrix of a plasma core in M.S.A.
$\mathbf{B}_f$	system matrix of a plasma core with feedback control in M.S.A.
$\vec{B}$	magnetic field
B	strength of magnetic field
B_ϕ	toroidal magnetic field
B_θ	poloidal magnetic field
C	a parameter of particle confinement time
C_1, C_2	constants
C_D C_T	increasing rates of deuterium and tritium densities
E	energy variable
$\vec{E}$	electric field
E_t	energy of superthermal ions of t-species
E_{th}	thermalization energy
E_{ij}	energy of the charged particle produced by fusion reaction between i and j species ions
E_g	energy of the gth group in the multi-group formulation

$\Delta E_{te}, \Delta E_{ti}$	energy transferred to electrons and ions from an energetic ion of t-species
e, e_{α}	electric charge of an electron and an alpha particle
F_L	total loss fraction of alpha particles
f_L	loss fraction of alpha particles averaged in azimuthal direction
f_{ℓ}	loss fraction of alpha particles at birth position
G	feedback gain constant
H	alpha heating source
j	current density
k	Boltzmann's constant
K_{ℓ}, L_{ℓ}	constants
m_e, m_t	masses of electrons and t-species ions
n	plasma density
n_e, n_j	densities of electrons and j-species ions
N_j	total amount of j-species ions circulating in a fusion reactor
N_{gt}	number of t-species ions in gth group
N_{Et}	number density of energetic ions of t-species
P_f	total fusion power in a fusion reactor
P_H	additional heating power
P_W	wall loading due to fusion products
P_{rad}	energy loss due to radiations
P_c	collision probability density
q	safety factor
R	major radius of a plasma
r_N	uniform random number
$\vec{r}$	position vector of guiding center of an alpha particle
S	fueling rate
S_b	injection rate of neutral beam
S_p	injection rate of pellets, cluster ions or neutral gas
T	plasma temperature
T_e, T_i	electron and ion temperatures

t_{th}	thermalization time
U_b	injection beam energy
V_p	volume of a plasma core
V_d	drift velocity of an alpha particle
$v_\perp, v_\parallel$	velocity components perpendicular and longitudinal to magnetic field
v_x, v_y	velocity components of x-y co-ordinates
v_e	velocity of field electrons
v_t	velocity of superthermal ions of t-species
v_i	velocity of field ions
$<\Delta V_\parallel>$	rate-of-change of mean deviation of longitudinal velocity
$<(\Delta V_\parallel)^2>$	rate-of-change of mean square deviation of longitudinal velocity
$<(\Delta V)_\perp^2>$	rate-of-change of mean square deviation of perpendicular velocity
W_T	thermal output power of a reactor
$\vec{X}, \vec{Y}$	state vectors
x, y, z	rectangular co-ordinates
R, Z, ϕ	cylindrical co-ordinates
Z_{eff}	effective charge number
Z_t	charge number of t-species ions

Greek symbols

β	beta value (=plasma pressure/magnetic pressure)
β_t	toroidal beta value
β_p	poloidal beta value
Γ	reflection rate of cyclotron radiation on the first wall
γ_ℓ	a constant
δ	amplitude of fluctuation of toroidal magnetic field
ε	parameter of direction of a drift motion
ϵ_0	permittivity of vacuum
η	energy multiplication rate of a reactor
η_{bj}	burn-up rate of ions of j-species

θ	azimuthal angle
$\ln\Lambda$	Coulomb logarithum
$\mu(x)$	error function
μ_α	adiabatic invariant
μ_0	permeability of free space
ν_j	relative velocity of alpha particles to j-species ions
ξ	ratio of tritium density to deuterium density
$\langle\sigma v\rangle_{ij}$	fusion reaction rate between i and j species ions
τ_d	deflection time
τ_{Ej}	energy confinement time of j-species ions
τ_{ei}	temperature equalization time
τ_f	a time constant of feedback control
τ_{gt}	expected transition time from $(g-1)$th group to gth group in multi-group formulation
τ_p	particle confinement time
τ_s	slowing down time
τ_{td}	pure time delay of alpha heating
τ_ε	energy exchange time
Φ	electrostatic potential
χ	pitch angle between velocity of an alpha particle and magnetic field

INTRODUCTION

The mankind's demand for the energy goes on increasing rapidly with the great progress in civilization. It is generally predicted that the fossile fuels of coal and oil would be entirely exhausted within a hundred years. The world now envisages the social uneasiness and stress arising from the potential shortage of fossile fuel resources and from the sudden rise of oil prices. One may need the urgent development of the energy resources which take place of the fossile fuel. The solar (including winds and waves) and geothermal energies are anticipated as the favorable energy with the advantages of its abundance and environmental attractiveness, but would be unsuitable for the central electrical power generation because of their diffusible and variable nature in time and space. On the other hand, the atomic energy is regarded as the most promising energy resources from the viewpoint of central power generation.

The nuclear power plant actually generates the electrical power and continuously supplies the energy. The present nuclear reactor makes use of the fission chain-reaction of U^{235} caused by the thermal neutrons. Since the isotope exists merely 0.7% in the natural uranium, the utilization of this type reactor is limited in a few decades. The fast breeder is the reactor which produces the power by the fission reaction of U^{235} and breeds the new fissile fuels of P_u^{239} and U^{233} from U^{238} and T_h^{232}. The F.B.R. will be soon in the stage for practical application

and the utilization of uranium would result in growing several ten times as large as that of the present nuclear reactors. However, for putting the F.B.R. to practical use, we will encounter many problems related to the localized fuel resources, the radioactive waste products, the safety against nuclear explosion, the biological hazard in the events of sabotage or natural disaster, the danger of diversion of weapon grade material.

Controlled thermonuclear fusion is commonly expected as a major energy source, succeeding the F.B.R. Nuclear fusion is the reaction in which light nuclei collide, fuse together and release energy. Its fuels are the light elements such as deuterium, tritium, herium-3 and lithium. The deuterium exists in 0.015 per cent of the hydrogen in ocean waters and meet man's energy needs for millions of years. The fusion reactor appears environmentally to possess potential advantage over fission reactors because the fuel is more abundant, no radioactive wastes are produced and fusion is inherently safe against nuclear explosion. Although the ideal energy resources are still in the elementary stage, recent good progress in the theories and experiments offers the prospects of early demonstration that controlled thermonulear reactions are scientifically feasible.

Two approaches to fusion can be categorized by magnetic and inertia confinements. The power generation, in the inertia confinement fusion, is achieved by rapid heating and compressing small pellets of D-T, D-D or D-H_e^3 fuel by irradiation of lasers, electron or ion beams. For magnetic confinement, three kinds of devices are considered; (a) tokamak and sterallator reactors, long pulsed or steady state toroidal devices with a low or middle beta value, (b) mirror reactors, steady state open end devices with neutral beam injection and (c) theta pinch reactors, high beta and fast pulsed devices. The experimental results which are the most close to the plasma conditions needed in a reactor have been obtained in the tokamak systems. The next generation of tokamak devices now under construction or contemplation is expected to attain the

condition of zero power and the scientific feasibility will be achieved in the early *1980* by tokamak devices. Further more powerful research must be carried out in the areas of not only science but also technology in order to shorten the period from attainment of the scientific feasibility. The subjects of R&D for attainment of the technological (or engineering) feasibility consist of magnetic systems, blanket engineering, tritium processing and handling, vacuum technology, radioactivity, remote handling, divertor and cold gas blanket, heating and fueling systems, reactor kinetics and controls etc.

The future reactor plasma substantially differs from the present laboratory plasma in containing the particles produced by fusion events, since the energetic fusion products would cause various new effects on the plasma core. The predictions of the behaviors of fusion grade plasmas seems to be indispensable for the design and construction of prospective tokamak reactors.

This work aims at the study on the dynamic characteristics and controls of fusion reactors and the heating and confinement properties of alpha particles in D-T tokamak reactors. The subjects in each chapter of this thesis are briefly mentioned as follows:

Chapter 1 treats the properties of the plasma heating due to energetic charged particles produced by D-T reactions and neutral beam injection. The characteristics of the start-up and stationary operation are also discussed by using a zero dimensional fusion plasma model. In chapter 2, the effects of the slowing down process of the energetic alphas on the kinetics and controls of fusion plasma core are studied within the framework of the linearization analysis and the integration of non-linear dynamic equations. Chapter 3 is devoted to discussion of the properties of a Cat.D reactor in comparison with a D-T reactor. The feasible parameters of Cat.D reactor are derived and the methods of ignition from D-T burning plasma to Cat.D operating mode without any auxiliary heating are proposed and the stability of D-T to Cat.D operating points against thermal runaway and the dynamic transition process

of Cat.D ignition are studied.

The confinement of the energetic alphas produced in D-T reactions is an essential problem to realize a tokamak fusion power reactor. The guiding center orbits of high energy particles are largely deviated from the magnetic surface due to the finite giro-radius effects. The alpha particles in a D-T fusion reactor possess so high energy that some of them move away from the plasma surface, collide with the limiter and are lost. The alpha particle loss may cause the serious problems such as the bombardment of the first wall and divertor materials, the production of impurities, the negative electrostatic potential build-up, the plasma rotation and the momentum unbalance of a plasma core. In chapter 4, the orbit loss of *3.5 MeV* alpha particles is predicted for several future reactors and the sensitivity of the loss to various tokamak parameters is studied in a reference reactor. In the last chapter, the loss of alpha particles during the slowing-down process is calculated by Monte Carlo technique. The effects of pitch-angle scattering on the loss and the energy deposition profile of alpha particles are also studied.

Chapter 1

CHARACTERISTICS OF STATIONARY AND START-UP HEATING OF A D-T FUSION REACTOR BY MEANS OF FAST-NEUTRAL-BEAM INJECTION[11]

1.1. Introduction

There are a lot of engineering problems which should be solved in order to realize a commercial fusion power reactor. Most of them need the development of entirely new technology and engineering. One of the most important works seems to be the study on dynamic characteristics of fusion plasma core, which may be indispensable for discussion of safety and feasibility of fusion reactors.

In order to utilize fusion power, the plasma of which density and temperature are respectively about $10^{20}\ m^{-3}$ and *10 KeV* must be confined for a few seconds. These conditions are generally called Lawson criteria. Therefore, heating a D-T plasma up to *10 KeV* is essential problem for attaining Lawson criteria. The following means of plasma heating are considered: (1) Joul heating, (2) R.F. (radio frequency) heating, (3) adiabatic compression heating, (4) N.B.I. (neutral-beam-injection) heating. Joul heating that is plasma heating due to Ohmic loss of plasma current could not attain by itself the ignition of D-T plasmas, because the plasma resistivity decreases in proportion to the *3/2* power of electron temperature. The R.F. heating is due to damping the radio frequency wave in plasmas and it is necessary to develop the oscillator with huge output energy. The plasma heating by compressing

a plasma core adiabatically has difficult problems such as the effects on plasma M.H.D. stability and the constraints in a reactor design. The N.B.I. heating would be most promising for steady-state operation as well as for start-up heating, where the plasma is heated from an initial temperature of about *1 KeV* up to the operating temperature of more than *10 KeV*. The N.B.I. possesses not only a possible benefit of the high input-power density but also a function of fueling.

In this chapter, the author discusses the properties of plasma heating due to the fast ions produced by N.B.I. and the superthermal alpha particles born in D-T reactions and examines the stationary and start-up characteristics of a low β D-T fusion reactor equipped with a system of N.B.I.

1.2. Coulomb Interaction Between Superthermal Ions and Field Plasmas

The slowing down process due to Coulomb interactions of superthermal ions with a pure D-T plasma is given by the approximate binary collision theory[3,4,5] as follows,

$$\frac{dE_t}{dt} = -\frac{Z_t^2 e^4 n_i m_t^{1/2} \ell n\Lambda}{4\sqrt{2}\pi\epsilon_0^2 m_r (kE_t)^{1/2}}\left[1+\frac{4m_r m_e^{1/2} E_t}{3\sqrt{\pi}m_t^{3/2}}\left(\frac{t}{T_e}\right)^{3/2}\right] \qquad (1.1)$$

$$m_r = \frac{m_i m_t}{m_i + m_t}$$

where E_t, m_t and Z_t are the energy, mass and charge number of superthermal ions, respectively, e, ϵ_0 and k the electron charge, permittivity of vacuum and constant, n_i and T_e the ion density and electron temperature, m_e and m_i the masses of electrons and D-T ions, and $\ell n\Lambda$ the Coulomb logarithm, assumed to be *20*. Equation (1.1) holds to a fairly good approximation within the velocity of fast ions such as,

$$v_e \gg v_t \gg v_i \qquad (1.2)$$

where v_e, v_t and v_i are the velocities of field electrons, superthermal ions and field ions. Equation (1.1) can be reduced to a simple form as follows[4,5],

$$\frac{dE_t}{dt} = -\frac{2.5}{\tau_{st}} E_t - \frac{2.5}{\tau_{st}} r_t^3 E_t^{-1/2} \qquad (1.3)$$

$$\tau_{st} = 7.47\times10^{44} \frac{m_t T_e^{3/2}}{n_i Z_t^2} \qquad (1.4)$$

$$r_t^3 = \frac{3\sqrt{\pi}\, m_t^{3/2}}{4 m_r m_e^{1/2}} T_e^{3/2} \qquad (1.5)$$

The first term of the right hand in Eq.(1.3) presents the rate-of-change of energy due to the collisions with electrons and the second term is the rate-of-change due to the collisions with ions. The following time-dependent equation for the energy of superthermal ions can be obtained by integrating Eq.(1.3).

$$E_t(t) = [(r_t^3 + E_{t_0}^{3/2}) \exp(-15t/4\tau_{st}) - r_t^3\ ]^{2/3} \qquad (1.6)$$

where E_{t_0} is the initial energy of superthermal ions.

Figure 1.1 shows the slowing down process of an alpha particle born in the D-T reaction for various temperatures of field electrons. The alpha particles slow down mainly through collisions with electrons at the high energy region and lose their energy due to collisions with field ions when the energy becomes comparable to the energy of field ions. In the former collisions, the rate of energy transfer is very small and the energy gradually decreases below *1 MeV*. The great energy transfer is caused by collisions with ions and the energy rapidly reduces to the thermal energy of field ions. If the thermalization time is defined by the time at which the superthermal ions slow down to the thermalization energy, E_{th} which is the same order value as field ion energy, then the following equation can be obtained from Eq.(1.6),

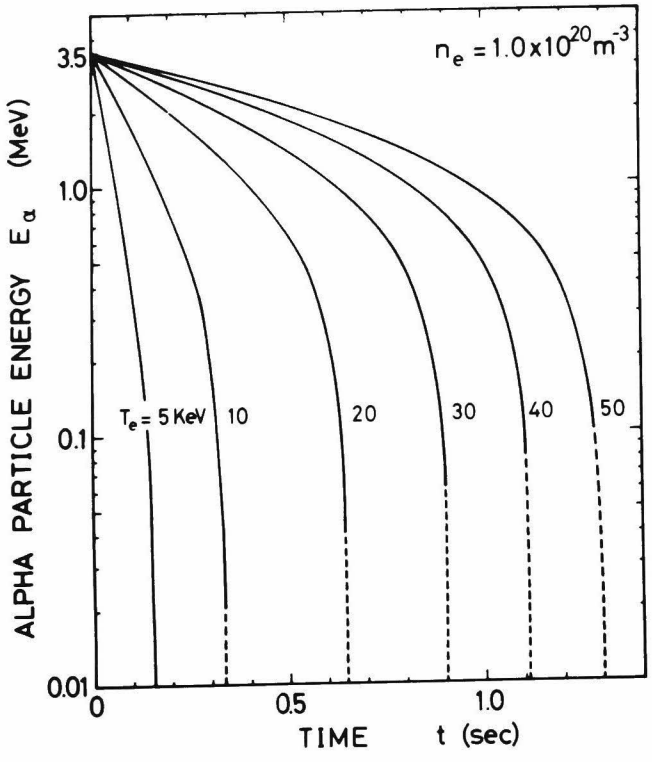

Fig.1.1. Alpha particle energy during slowing down process in fusion plasmas of various electron temperatures.

$$t_{th} = \frac{4}{15} \tau_{st} \ln \frac{E_{to}^{3/2} + r_t^3}{E_{th}^{3/2} + r_t^3}$$

$$\simeq \frac{4}{15} \tau_{st} \ln[(E_{to}^{1/2}/r_t)^3 + 1] \qquad (1.8)$$

Note that the thermalization time is hardly sensitive to the definition of the thermalization energy. **Figure 1.2** shows the dependence of the thermalization time of the alpha particles on electron temperature. The thermalization time strongly depends on the electron temperature and varies over a wide range of *0.1-1.0 sec* correspondingly to the electron temperature of *5-40 KeV*. Figure 1.3 shows the relationship between the thermalization time of fast D-T ions produced from neutral injection beam and electron temperature for various beam energies. The thermalization time of the D-T ions with the energy below *100 KeV* hardly depends on the electron temperature and this tendency becomes

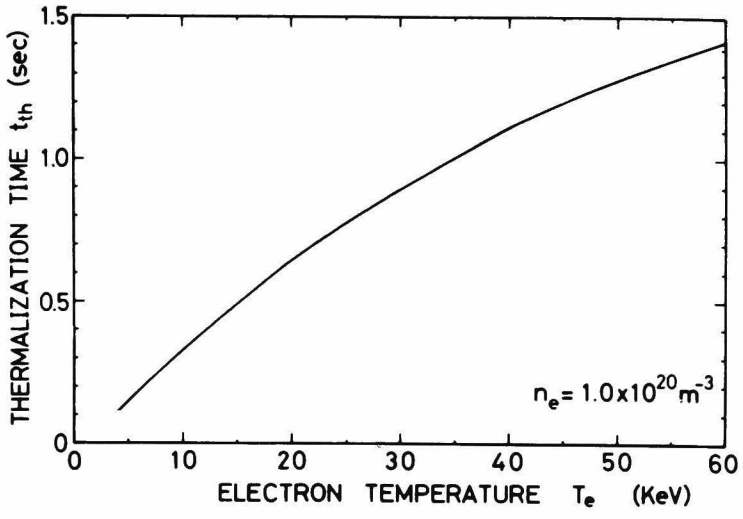

Fig.1.2. Relation between thermalization time of alpha particles and electron temperature.

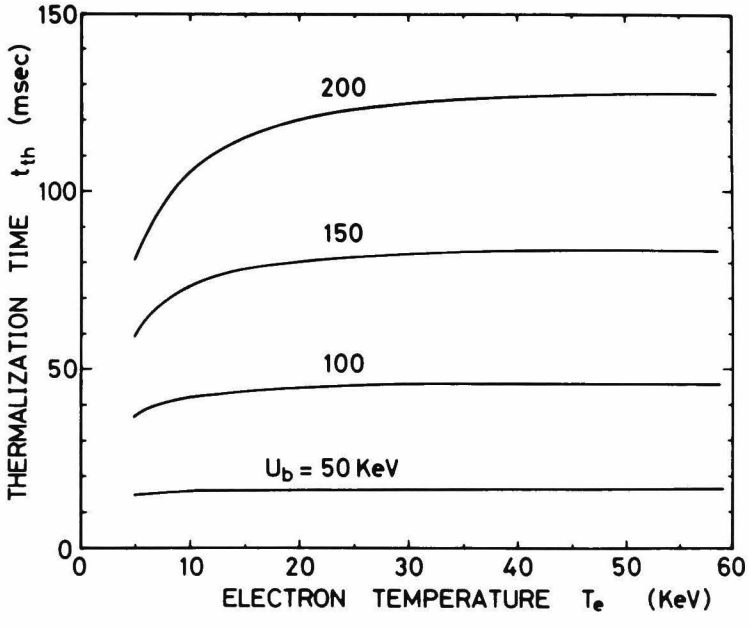

Figl.3. Relations between thermalization time of fast D-T ions and electron temperature for various injection energies.

conspicuous as the energy of the fast ions decreases. This is because the energetic D-T ions are thermalized mainly through the collisions with field ions.

The energy transferred to field ions by a superthermal ion until thermalization can be given by

$$\Delta E_{ti} = \frac{2.5}{\tau_{st}} r_t^3 \int_0^{t_{th}} E_t^{-1/2} \, dt \qquad (1.9)$$

Substituting Eq.(1.6) into Eq.(1.9) and carrying out the integral, we can obtain the following equation.

$$\Delta E_{ti} = \frac{2}{3} r_t^2 \left\{ \ell n \frac{\sqrt{(E_{t_0} - r_t/2)^2 + \frac{3}{4} r_t^2}}{E_t^{1/2} + r_t} + 3 \tan^{-1} \frac{2E_{t_0}^{1/2} - r_t}{\sqrt{3}\, r_t} + \frac{\pi}{2\sqrt{3}} \right\} \qquad (1.10)$$

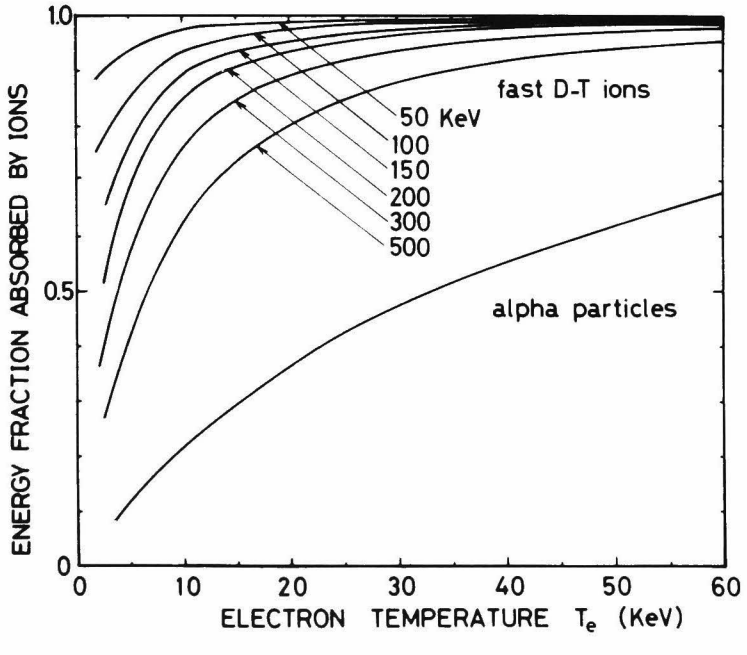

Fig.1.4. Fraction of energy transferred from fast ions and alpha particles to plasma ions vs. electron temperature.

Then, the energy transferred to electrons is given by

$$\Delta E_{te} = E_{t_0} - \Delta E_{ti} \qquad (1.11)$$

Figure 1.4 shows the fractions of energy transferred to the field ions by superthermal ions and alpha particles. When the electron temperature is higher than *10 KeV* and the beam energy is less than *150 KeV*, most of the energy of injection beam is transferred to the field ions. On the other hand, the energy given by alpha particles to ions is equal to the energy given to electrons, when the electron temperature is *33 KeV*. For $T_e < 33$ *KeV*, the energy goes predominantly to the field electrons.

1.3. Physical Models

1.3.1. Assumptions

An infinite and homogeneous fusion plasma with *50%-50%* D-T fuel mixture is assumed in this study. The particle and energy balance equations for field ions and electrons are taken as the fundamental equations. The energy loss is caused by escaping charged particles and bremsstrahlung radiation cooling. The energy production in the plasma is due to the alpha particles born in the D-T reactions and the fast ions produced from neutral beam injection. It is assumed that the energetic alpha particles are confined completely, while the concentrations of thermalized alpha particles and impurity ions are so small that the effects on the density and energy balances of the fusion plasma core can be neglected.

1.3.2. Kinetic equations

The balance equation for the density of ions is given by

$$\frac{dn_i}{dt} = S_b - \frac{n_i}{\tau_p} - \frac{n_i^2 \langle \sigma v \rangle_{DT}}{2} \qquad (1.12)$$

where n_i is ion density, S_b neutral beam injection rate, τ_p particle

confinement times and $\langle\sigma v\rangle_{DT}$ D-T reaction rate, which is given by Tuck's curves[6] as follows,

$$\langle\sigma v\rangle_{DT} = 10^{\{a_1 + a_2 \log_{10} T_i + a_3 (\log_{10} T_i)^2 + a_4 (\log_{10} T_i)^3\}} \qquad (1.13)$$

$$a_1 = -26.176 \qquad a_2 = 6.0276$$
$$a_3 = -1.8223 \qquad a_4 = 0.02822$$

Equation (1.13) holds good for the range of temperature such as $2\ KeV < T_i < 90\ KeV$. The particle confinement time τ_p is assumed to be

$$\tau_p = c\, T_e^{1/2} / n_i \qquad (1.14)$$

as in the classical diffusion, where c is constant taken as a parameter in the following discussion, and T_e electron temperature.

Energy balance equations are given for ions,

$$\frac{3}{2}\frac{d(n_i T_i)}{dt} = U_b S_b \Delta E_{bi} + \frac{n_i^2 \langle\sigma v\rangle_{DT}}{4} \Delta E_{\alpha i} (t-\tau_d) - \frac{3}{2} n_i \frac{T_i - T_e}{\tau_{ei}} - \frac{\frac{3}{2} n_i T_i}{\tau_{Ei}} \qquad (1.15)$$

and for the electrons,

$$\frac{3}{2}\frac{d(n_e T_e)}{dt} = U_b S_b \Delta E_{be} + \frac{n_i^2 \langle\sigma v\rangle_{DT}}{4} \Delta E_{\alpha e} (t-\tau_d) + \frac{3}{2} n_i \frac{T_i - T_e}{\tau_{ei}} - \frac{\frac{3}{2} n_e T_e}{\tau_{Ee}} - 9.6\times10^{-20} n_e^2 \sqrt{T_e} \qquad (1.16)$$

where T_i is ion temperature, n_e electron density equal to ion density, U_b injection energy, τ_{ei} temperature equalization time[7], τ_{Ei} and τ_{Ee} the energy confinement times for ions and electrons which are assumed to be equal to particle confinement time for simplicity in the following

numerical studies, ΔE_{bi} and $\Delta E_{\alpha i}$ energies transferred to ions by the fast D-T ions and the alpha particles, ΔE_{be} and $\Delta E_{\alpha e}$ energies transferred to electrons by the fast ions and the alpha particles, respectively.

When the energy of injection beam is below *150 KeV* and the electron temperature is higher than *10 KeV*, the following approximate equations hold fairly good.

$$\Delta E_{be} \simeq 0 \quad \text{and} \quad \Delta E_{bi} \simeq 1 \tag{1.17}$$

The injected deuterium and tritium ions with the energy smaller than *150 KeV* thermalize within several tens of milliseconds in fusion plasmas, while the alpha particles emitted by the D-T reaction thermalize in about one second. As we are concerned with the dynamics in the time range of seconds, it is reasonable to neglect the thermalization time of injected particles, while that of alpha particles should be taken into consideration, which is approximated as a pure time delay in the following discussion. If the time delay τ_{td} is defined as the time when the energy of alpha particles reduces to E_{α_0}/e, where $E_{\alpha_0}=3.5\ MeV$ and $e=2.718282\cdots$, the following equation can be obtained from Eq.(1.6).

$$\tau_{td} = \frac{4\tau_{s\alpha}}{15} \ell n \frac{E_{\alpha_0}^{3/2} + r_\alpha^3}{(E_{\alpha_0}/e)^{3/2} + r_\alpha^3} \tag{1.18}$$

1.4. Characteristics of Fusion Plasmas

Stationary conditions of plasma density and temperature are derived from Eqs.(1.12), (1.15) and (1.16) by setting $d/dt=0$. Figure 1.5 illustrates the operating ion temperature for a certain injected beam energy for various values of the parameter C in Eq.(1.14). When $C < 0.7\times10^{18}$, the curves have positive gradients for all ion temperatures. On the other hand, if $C > 0.7\times10^{18}$, they have both negative and positive

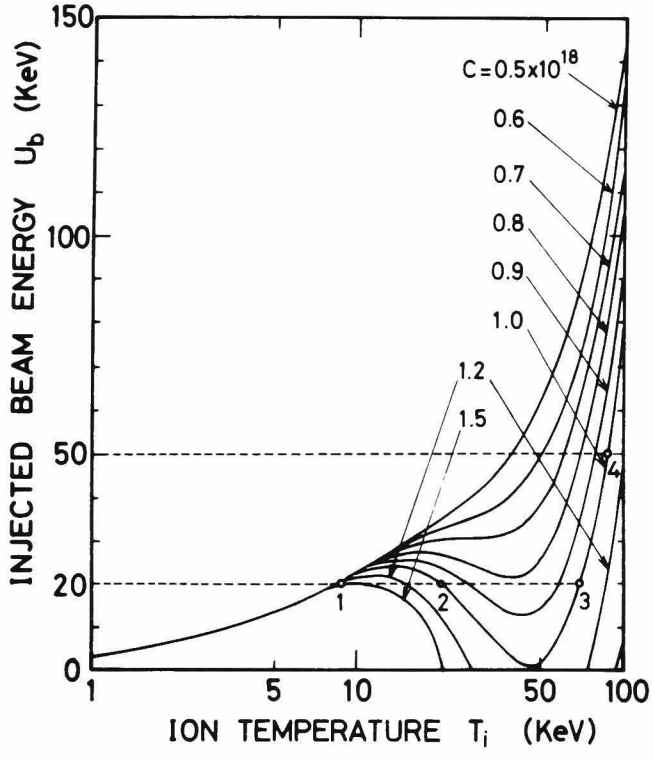

Fig.1.5. Static relation between ion temperature and injection beam energy for various values of C. The points 1, 2 and 3 present operating points in case of $C=1.0\times10^{18}$ for $U_b=20$ KeV. Point 4 corresponds to $U_b=50$ KeV.

gradients. Let us call the part of the curve with positive gradient "*Part A*" and that with negative gradient "*Part B*". When $C > 1.0\times10^{18}$, the curves intersect the ion temperature axis, i.e. $U_b=0$, two points. Let us call the part between the intersecting points "*Part C*".

If the operating point is located above or below the characteristic curves in Fig.1.5, the time derivative of $n_i T_i$ takes a positive or negative value, respectively. If a small disturbance of the injection beam energy or ion temperature is introduced, the operating point on "*Part A*" still remains on "*Part A*". On the other hand, when the stationary operation is disturbed from a point on "*Part B*", it can no longer return to its initial point. This is because, once the disturbance removes the point off and upwards from the curve, the point drifts away from "*Part B*" and goes towards "*Part A*" of the higher temperature due to the positive time derivation of the ion temperature in the region above curve. Similarly, when the point slips off the curve downwards, the

point moves to "*Part A*" of the lower temperature. In this sence, the operation on "*Part B*" could be called "*unstable*".

The dynamic behavior of the ion and electron temperatures induced by a change of injection beam energy is calculated by integrating Eqs. (1.12),(1.15) and (1.16) numerically, as is shown in Fig.1.6. The initial operating points are chosen to be the points 1, 2 and 3 of Fig. 1.5, and the changes of injection energy are taken to be *±10%* from *20 KeV*.

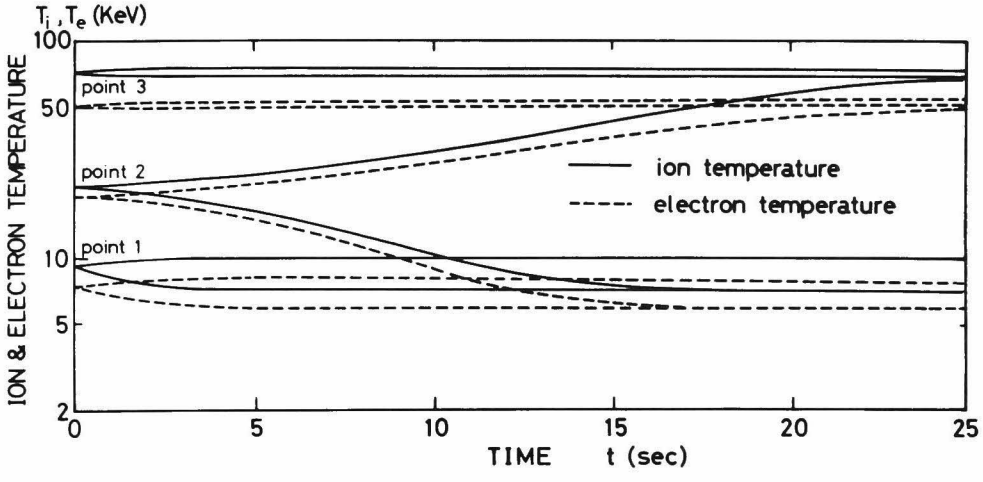

Fig.1.6. Ion and electron temperatures vs. time. The initial beam energy of 20 KeV is changed by ±2 KeV at t=+0, at points 1, 2 and 3 in Fig.1.5.

When the operating point is on "*Part C*", the fusion reactor becomes selfsustaining without any external injection of energy. In this case, the stationary operating point is fixed on the right-end of "*Part C*". The ion temperature cannot be realized on "*Part C*". The stable, unstable and self-sustaining regions are shown in Fig.1.7 with the product of plasma density and confinement time as the longitudinal axis and the ion temperature as the horizontal one. The efficiency η defined by

$$\eta = \frac{\textit{fusion power}}{\textit{injection power}}$$

$$= \frac{\frac{1}{4}n^2\langle\sigma v\rangle_{DT}17.5\times10^6}{U_b\, S_b} \qquad (1.19)$$

is also shown in Fig.1.7.

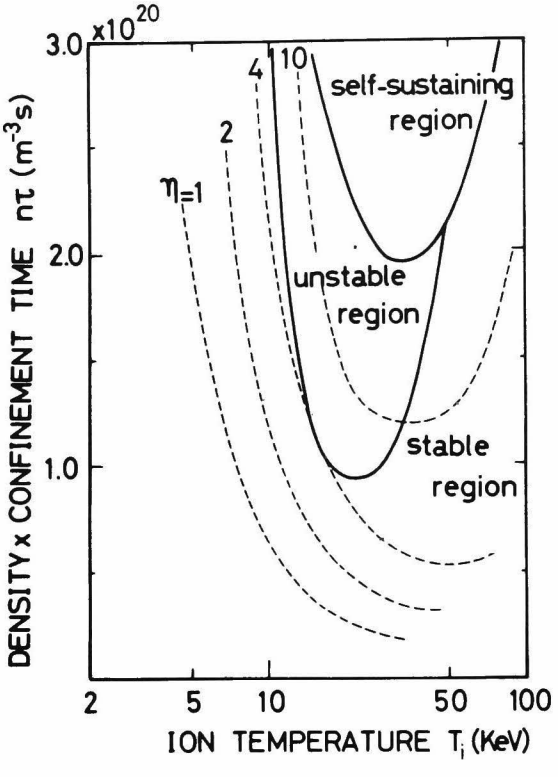

Fig.1.7. $n\tau$-T_i diagram. The solid curves separate the stable, unstable and self-sustaining regions, and the dotted curves indicate efficiency contour lines.

As is seen in Fig.1.7, the efficiency η is improved in the ion temperature region of *20∿70 KeV*. The reactors must be operated inevitably in the unstable region for attaining the high efficiency. Therefore, some proper control mechanisms are necessary to stabilize the operation in "*Part B*". For this purpose, the following methods may be considered: (1) control of injection beam energy, (2) control of fueling rate, (3) control of confinement time, i.e. the parameter C in Eq.(1.14) by varying the magnetic field, and (4) control of the radiation loss by altering impurity concentration. The exploitation of these stabilizing methods would be a problem for the future.

Figure 1.5 also shows that, when the ion temperature is above *50 KeV*, the gradients of the curves have very large **positive** values because of the increased energy loss. This energy loss is mainly caused by the bremsstrahlung.

Figure 1.8 shows the dynamic behavior of start-up in three different cases: $C=1.0\times10^{18}$, 0.7×10^{18} and 0.5×10^{18}, where beam injection of

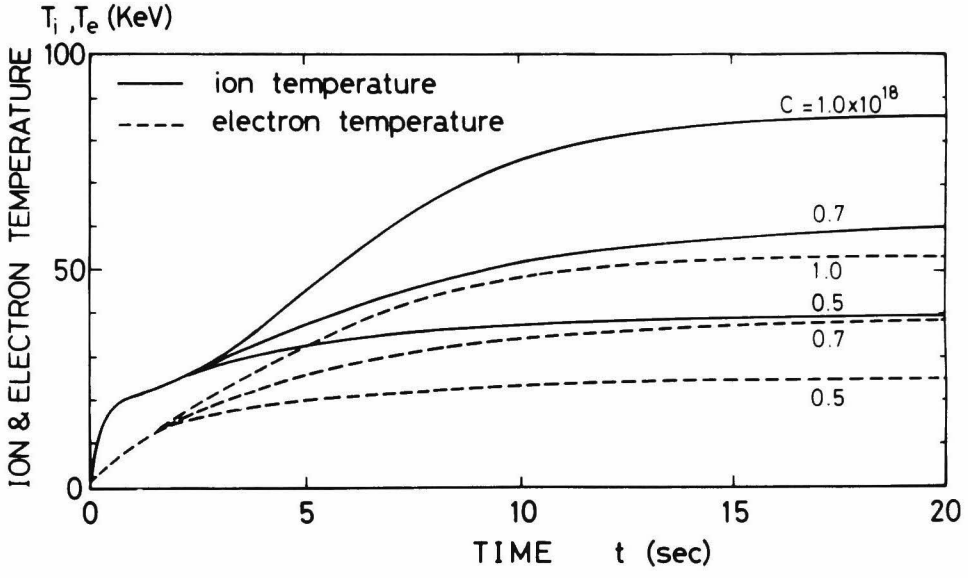

Fig.1.8. T_i and T_e vs. time, for three different values of C, when 50 KeV step-wise injection is made at t=+0 sec. The injection rate S_b is 0.5×10^{20} m^{-3} s^{-1}, and the initial ion and electron temperaturs are assumed to be attained by Joul heating and 0.5 KeV and 1.0 KeV, respectively.

50 KeV energy is performed stepwise at *t=+0 sec*. The final ion temperatures in Fig.1.8 are consistent with those derived from Fig.1.5. Let us consider the start-up of a fusion reactor with $C=1.0\times10^{18}$, and aim at stable operation at point *3* in Fig.1.5. That is accomplished by operation with an injection energy of *20 KeV* after start-up with an energy of *50 KeV*. The operating point moves to point *4* in start-up period, and then moves to point *3*. On the other hand, the start-up control aiming at point *2* would be very complicated, which would be the combination of injection beam energy control, fueling rate control and some other means.

1.5. Concluding Remarks

The characteristics of a D-T fusion reactor are discussed by numerically solving the zero-dimensional kinetic equations of a fusion plasma core. Thermal instability of a D-T plasma is studied by making

use of the static relation between the ion temperature and the injection beam energy, and the stable, unstable and self-sustaining regions are obtained in the $n\tau$-T_i diagram. The dynamic behaviors of plasma temperature induced by the disturbance of injection energy are also examined numerically; the results are consistent with the static analysis. The study of start-up of a fusion reactor due to neutral beam injection indicates that the beam energy of $40 \sim 50$ *KeV* is sufficient for ignition of a D-T plasma. However, the sequence controls of neutral beam energy, fueling rate and magnetic field are needed for attaining the operation temperature of $15 \sim 40$ *KeV*. Finally, although the thermalization process of alpha particles is simply treated as a pure time delay in the kinetic equations of a fusion plasma, more detailed treatments would be necessary for studying the dynamic characteristics of fusion plasmas.

Chapter 2

THERMAL INSTABILITY AND CONTROL OF D-T FUSION PLASMA CONSIDERING THE SLOWING-DOWN PROCESS OF ENERGETIC IONS[18]

2.1. Introduction

The energy balance (or thermal) instability of a fusion plasma has been studied by several workers[1,2,8-11]. Most of previous studies were carried out under assuming the alpha particles transfer instantaneously all their energy to the field plasma as soon as they are born from D-T fusion events. In the previous studies, it has been concluded that the energy balance instability of a fusion plasma may occur because, at low temperature, any change in temperature causes a greater change in the reaction rate than in the rate of energy losses due to radiation, thermal conduction and particle diffusion. In reality, however, the alpha particles transfer their energy to the field plasma during their slowing-down process. Main process for the transfer is through Coulomb collisions with the field plasma. It is assumed, in this work, that the energetic ions slow down due to Coulomb collisions with the field plasma. This classical slowing-down time of the alpha particles in the fusion plasma should not be neglected[11], compared to the time constants characterizing the dynamics of the plasma density and temperature which are reportedly on the order of several seconds[1, 2]. Moreover, it has been reported that the alpha particle energy distribution behaves as if it possesses an inertia against plasma

temperature perturbations[12]. Therefore, the slowing-down process of the alpha particles should be included in the fundamental process of dynamics and control of a fusion plasma core.

Saito et al.[13] have indicated that the inertia property of alpha particle energy distribution gives rise to pronounced effects on the problems of start-up and thermal instability by numerically solving the coupled equations consisting of a Fokker Plank equation for alpha particles, and the particle and energy conservation equations for the background plasma. The present approach treats the slowing-down process of the energetic ions in the multi-group formulation. The superthermal ions for which a slowing-down process is considered in this study are (1) the alpha particles born in D-T fusion reactions, and (2) the fast ions produced from the injected neutral beam. The effects of the slowing-down process on the thermal stability, dynamics and control will be clarified by means of a linear stability analysis and the numerical analysis of the non-linear dynamics.

2.2. Analytical Model

2.2.1. Basic equations

The same physical model as in chapter 1 is used in this study. The particle and temperature balance equations for plasma core are taken as the basic equations. The ion density balance equation is given by Eq.(1.12). The energy of injected neutral beam must be adequately assumed to be so high as to penetrate into the center of plasma column[14]. Therefore, if D-T fuel is fed exclusively by means of the neutral beam injection, the input power would become too large for the reactor to operate at the feasible operating points. Hence, in this chapter, it is assumed that the source S consists of two terms i.e. neutral injection rate, S_b and fueling rate by means of pellet injection, cluster ion injection, gas fueling, etc., S_p.

The temperature balance equations for ions and electrons are derived from Eqs.(1.15) and (1.16) as follows,

$$\frac{dT_i}{dt} = \frac{1}{n_i}\left(\frac{2}{3}\Delta W_{bi} + T_i S_b\right) - \frac{S_p}{n_i} T_i + \frac{2}{3n_i}\Delta W_{\alpha i} + \frac{n_i\langle\sigma v\rangle DT}{2} T_i - \frac{T_i - T_e}{\tau_{ei}} \qquad (2.1)$$

and

$$\frac{dT_e}{dt} = \frac{1}{n_i}\frac{2}{3}\Delta W_{be} - \frac{S}{n_i} T_e + \frac{2}{3n_i}\Delta W_{\alpha e} + \frac{T_i - T_e}{\tau_{ei}} + \frac{n_i\langle\sigma v\rangle DT}{2} T_e - 6.4\times10^{-20} n_i Z_{eff}\sqrt{T_e} \qquad (2.2)$$

where ΔW_{bj} and ΔW_{j} $(j=i,e)$ denote heating powers of neutral beam and alphas, and Z_{eff} is effective charge number. If the impurities consist of highly ionized heavy ions and the effective charge number is relatively low, the ion density would be almost the same as the electron density. In deriving Eqs.(2.1) and (2.2), the assumption is made that the energy confinement time is equal to the particle confinement time. The particle confinement time is pressumed to have the following dependence;

$$\tau_p \propto n^{\ell} T_e^{m} \qquad (2.3)$$

The following two cases are examined in the numerical analysis.

(i) $\ell = 0,\ m = -1$ (Bohm)

(ii) $\ell = -1,\ m = 1/2$ (Classical)

2.2.2. Plasma heating by energetic ions

a) Instantaneous slowing-down approximation (I.S.A.)

The transport equation of the energetic ions in the energy space can be given in Ref.[15,16] as follows,

$$\frac{\partial N_{Et}}{\partial t} = \frac{2.5}{\tau_{st}}\frac{\partial}{\partial E}\left[N_{Et}\left(E + r_t^3/E^{1/2}\right)\right] \qquad (2.4)$$

where r_t and τ_{st} are given in chapter 1. N_{Et} is the number density of

energetic ions of t-spacies per volume per energy interval, E the energy of energetic ions. Equation (2.4) is approximately derived from a Fokker Planck equation under the condition that the velocities of the energetic ions are far less than the thermal velocity of the field electrons and far greater than that of the field ions. Therefore, the approach of the velocities of the energetic ions to the thermal ion velocity violates the condition and Eq.(2.4) does not hold for the ions of which velocities become comparable to the thermal velocity of the field ions. However, since those ions have little effects on the energy balance of the fusion plasma core, Eq.(2.4) can be used in this study.

The familiar slowing-down equation [4,16] of a single particle given by Eq.(1.3) is obtained by substituting $E'\delta(E'-E_t)$ ($\delta(x)$; a Dirac delta function) into N_{Et} and integrating Eq.(2.4) over the entire energy range of E'. If the energetic ions are assumed to give their energy to the plasma core instantaneously at the moment of production, the terms of plasma heating are given by Eqs.(1.10) and (1.11).

b) Multi-group slowing-down approximation (M.S.A.)

The multi-group formulation given by Corman et al.[15] may be adequate means to investigate the effects of the energetic ions on the thermal stability. Defining the number of t-species ions in group g by

$$N_{gt} = \int_{E_g}^{E_{g-1}} N_{Et}\, dE \qquad (2.5)$$

where E_{g-1} and E_g are the energies at the upper and lower boundaries of the gth group, and integrating Eq.(2.4) within the energy group, we can write the particle balance equation of t-spacies ions within gth group as follows,

$$\frac{\partial N_{gt}}{\partial t} = \int_{E_g}^{E_{g-1}} \frac{2.5}{\tau_{st}} \frac{\partial}{\partial E} [\, N_{Et}(E + r_t^3/E^{1/2})\,]\, dE$$

$$= \frac{N_{g-1\,t}}{\tau_{g-1\,t}} - \frac{N_{g\,t}}{\tau_{g\,t}} \qquad (g=2,\cdots\cdots,M) \tag{2.6}$$

where M is the number of energy group, and τ_{gt} the expected transition time from the $(g-1)$th group to the gth group, which is obtained under the steady state assumption within a group as follows,

$$\tau_{gt} = \frac{4\tau_{st}}{15} \ln \frac{E_{g-1}^{3/2} + r_t^3}{E_g^{3/2} + r_t^3} \qquad (g=1,\cdots\cdots,M) \tag{2.7}$$

Specifically, the balance equation in the 1st group is given by

$$\frac{\partial N_{1t}}{\partial t} = S_t - \frac{N_{1t}}{\tau_{1t}} \tag{2.8}$$

where S_t is the production rate of energetic particles. The ion and electron heating due to energetic ions of t-species can be expressed respectively by

$$\Delta W_{ti} = \sum_{g=1}^{M} \frac{N_{gt}}{\tau_{gt}} F_{gt}^{i} \tag{2.9}$$

and

$$\Delta W_{te} = \sum_{g=1}^{M} \frac{N_{gt}}{\tau_{gt}} (E_{g-1} - E_g - F_{gt}^{i}) \tag{2.10}$$

where F_{gt}^{i} is the energy transferred to ions from an energetic ion of t-species within the gth group, that is given by

$$F^{i}_{gt} = r_t^3 \int_{E_g}^{E_{g-1}} \frac{dE}{E^{3/2}+r_t^3}$$

$$= r_t^3 \left[\frac{1}{3r_t} \ln \left| \frac{x^3+r_t^3}{(x+r_t)^3} \right| + \frac{2}{\sqrt{3}\,r_t} \arctan \frac{2x-r_t}{\sqrt{3}\,r_t} \right]_{x_1=E_g^{1/2}}^{x_1=E_{g-1}^{1/2}} \qquad (2.11)$$

If the group stracture is adequately made so that the changes of plasma density and temperature within the transition time can be neglected, Eqs.(2.9) and (2.10) could be used for the plasma heating terms even in the non-steady state plasma dynamics.

2.2.3. Equilibrium operating points

The feasible operating points can be determined from Eqs.(1.12), (2.1) and (2.2) by letting the time derivatives zero. However, these equations are highly non-linear, so that the numerical analysis is only

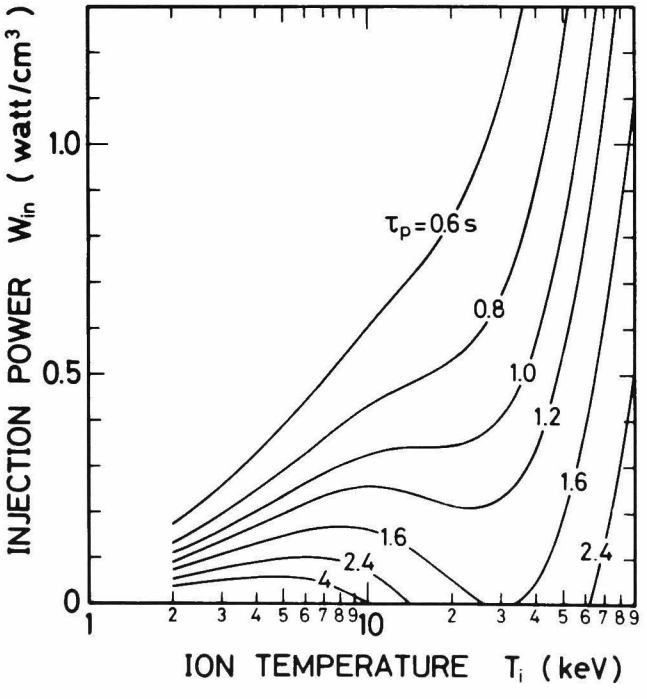

Fig.2.1. Static relation between ion temperature and injection power for various confinement times. n_e=1.0 $\times 10^{20}$ m^{-3}, Z_{eff}=2.0 and U_b= 200 KeV.

means to get the operating points. Figure 2.1. depicts the injection power vs. the ion temperature in the stationary operation for various confinement times. In case of the confinement time larger than *1.6 sec*, the curves intersects the ion temperature axis. Such two equilibrium operating points appear for zero injection energy[11]. These two operating points are called self-sustaining operating points. Note that the equilibrium operation at the ion temperature between the two self-sustaining operating points is impossible. As seen in Fig.2.1, the injection power necessary for sustaining steady state operation decreases as the confinement time increases. But when the confinement time becomes greater than *1.6 sec*, the range of the feasible operating temperature reduces. The energy balance instability at the equilibrium operating points given by Fig.2.1 will be discussed in the following sections.

2.3. Linear Stability Analysis

If the energetic alpha particles born in D-T reactions and the fast ions produced by the injected neutral beam are assumed to transfer instantaneously all their energies to the field plasma, the plasma heating due to the superthermal ions could be given by Eqs.(1.10) and (1.11).

The plasma density and temperature are expressed by the sum of the equilibrium values and the small deviations as follows;

$$\begin{aligned} n(t) &= n_0 + \delta n(t) \\ T_i(t) &= T_{i_0} + \delta T_i(t) \\ T_e(t) &= T_{e_0} + \delta T_e(t) \end{aligned} \qquad (2.12)$$

Substituting Eq.(2.12) into Eqs.(1.12), (2.1) and (2.2) and neglecting non-linear terms, we obtain the linearized state-equation as follows,

$$\frac{d\vec{X}}{dt} = A\vec{X} \qquad (2.13)$$

where $\vec{X}$ denotes the state vector, given by

$$\vec{X} = \begin{pmatrix} \delta n/n_0 \\ \delta T_i/T_{i_0} \\ \delta T_e/T_{e_0} \end{pmatrix} \tag{2.14}$$

and A denotes the system matrix, given by

$$A = \begin{pmatrix} a_{11} & a_{12} & a_{13} \\ a_{21} & a_{22} & a_{23} \\ a_{31} & a_{32} & a_{33} \end{pmatrix} \tag{2.15}$$

The stability criterion can be obtained by calculating the largest eigenvalue of matrix A.

However, the instantaneous slowing-down approximation would not be adequate to the analysis of the non-steady-state fusion plasma core, because the plasma density and temperature have significant effects on the slowing-down process of the energetic ions. Since the energy transfer rate is affected by the change in the plasma parameters, the slowing down process should be considered in the stability analysis[12]. The number of the energetic ions within the ith group and the number of the alpha particles within the jth group are respectively expressed in terms of the equilibrium values and the deviations as follows;

$$N_{ib}(t) = N_{ib_0} + \delta N_{ib}(t) \qquad (i=1,\cdots,I) \tag{2.16}$$

and

$$N_{j\alpha}(t) = N_{j\alpha_0} + \delta N_{j\alpha}(t) \qquad (j=1,\cdots,J) \tag{2.17}$$

where I and J are numbers of energy groups for the fast ions and the alpha particles, respectively. Substituting Eqs.(2.12), (2.16) and (2.7) into Eqs.(1.12),(2.1),(2.2),(2.9) and (2.10), and neglecting non-linear terms, we get the linearized state equation as follows,

$$\frac{d\vec{Y}}{dt} = B\vec{Y} \tag{2.18}$$

where $\vec{Y}$ is the state vector, given by

$$\vec{Y}^T = (\delta n/n_0 \ \delta T_i/T_{i0} \ \delta T_e/T_{e0} \ \delta N_{1b}/N_{1b0} \cdots \delta N_{Ib}/N_{Ib0} \ \delta N_{1\alpha}/N_{1\alpha 0} \cdots \delta N_{J\alpha}/N_{J\alpha 0}) \tag{2.19}$$

and B is the system matrix, given by

$$B = \begin{pmatrix} b_{11} & b_{12} & b_{13} & \cdots\cdots & b_{1\ 3+I+J} \\ b_{21} & b_{22} & b_{23} & \cdots\cdots & b_{2\ 3+I+J} \\ \cdots\cdots & & & & \\ b_{3+I+J\ 1} & & \cdots\cdots & & b_{3+I+J\ 3+I+J} \end{pmatrix} \tag{2.20}$$

The effects of the slowing-down process of the energetic particles on the thermal stability can be discussed by comparing the eigenvalues of the system matrixes A and B.

Figure 2.2 illustrates the largest eigenvalues (=stability indexes) of the system matrixes A and B at all feasible operating points for various

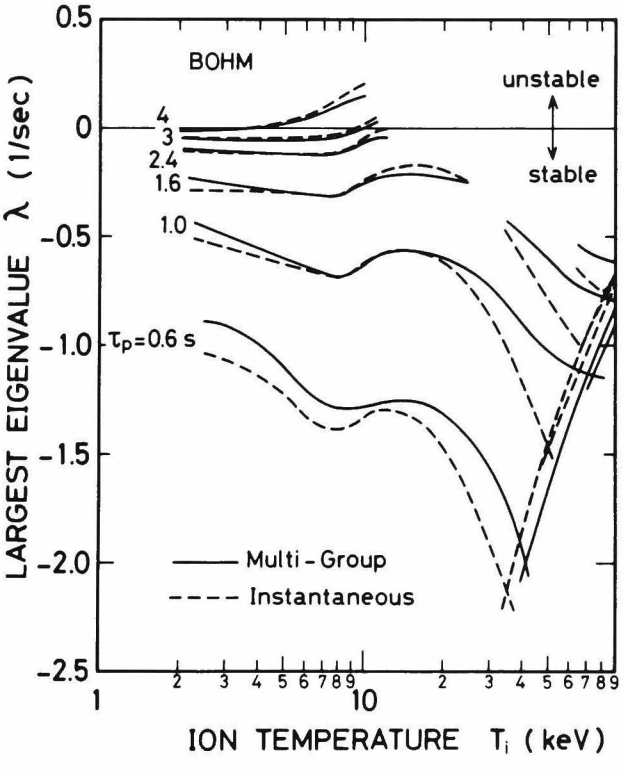

Fig.2.2. The largest real part of eigenvalues vs. ion temperature for various confinement times of Bohm type.

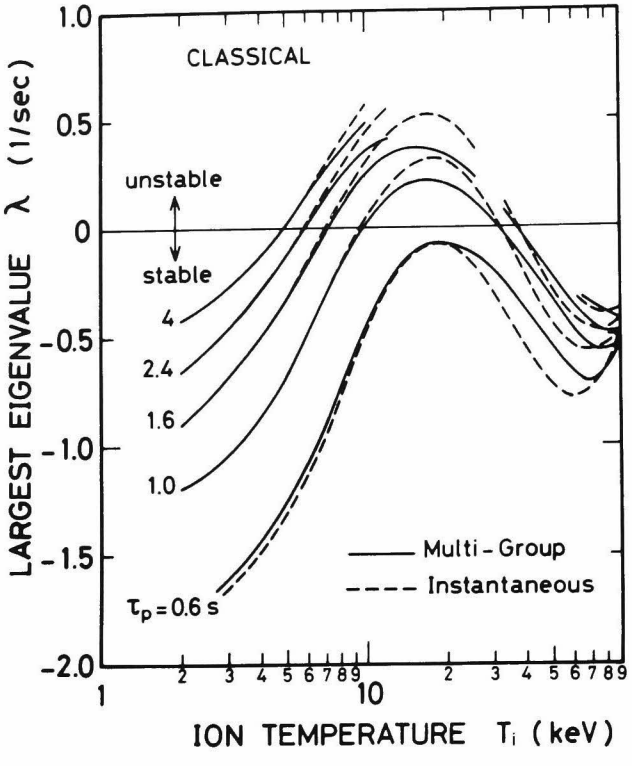

Fig.2.3. The largest real part of eigenvalue vs. ion temperature for various confinement times of classical type.

confinement times of Bohm type.* The broken curves show the largest eigenvalues of the system matrix A, i.e. the stability index of the plasma in case of I.S.A. The solid curves show the similar stability indexes in case of M.S.A., in which 2-group and 5-group approximations are made for the fast ions and for the alpha particles, respectively. The group structure seems adequate, because the increase in the number of groups does not make any appreciable change in the numerical results.

Figure 2.3 illustrates the similar relation to Fig.2.2, but the confinement laws are assumed to be classical type. In each of the above confinement laws, though the stable region may be hardly different between the two approximations, the positive largest eigenvalues in M.S.A. are about 30% smaller than those in I.S.A.

2.4. Physical Interpretation in a Simplified Model

The intuitive interpretation within the framework of the linear approximate analysis around the equilibrium points may be possible as follows. The plasma density is assumed to

*Curves in Fig.2.2 and Fig.2.3 are plotted for T_i ranging from 2 to 90 KeV as well as for the entire feasible operating points.

be constant for simplicity. The plasma temperature T depends on the heating source H through the cooling time constant τ_c, i.e.

$$\tau_c \frac{dT}{dt} = -T + C_1 H \tag{2.21}$$

where C_1 is a constant.
The heating source H is generated by the slowing-down of the energetic alpha particles, of which production rate is proportional to T, through the slowing down time τ_s, i.e.

$$\tau_s \frac{dH}{dt} = -H + C_2 T \tag{2.22}$$

where C_2 is a constant.
Eigenvalues of the set of equations are derived from the equation;

$$\begin{vmatrix} 1 + \lambda\tau_c & -C_1 \\ -C_2 & 1 + \lambda\tau_s \end{vmatrix} = 0 \tag{2.23}$$

Assuming $\lambda\tau_s \ll 1$, we can obtain the approximate evaluation of the largest eigenvalue λ_d as follows,

$$\lambda_d \simeq \lambda_i (1 - C_1 C_2 \tau_s / \tau_c) \tag{2.24}$$

where λ_i is the eigenvalue when $\tau_s = 0$, i.e. under I.S.A. and is given by

$$\lambda_i = \frac{C_1 C_2 - 1}{\tau_c} \tag{2.25}$$

Eigenvalues could be positive or negative, dependent on the loop gain $C_1 C_2$. In either case, the eigenvalue decreases its absolute value by the factor $(1 - C_1 C_2 \tau_s / \tau_c)$, which interprets the observation in Fig.2.2 and 2.3. The thermal instability, if it occurs, comes from the possitive feedback loop of the alpha heating mechanism. The slowing down time

makes the feedback effect smaller, hence the slowing down process must be adequately treated in the dynamic analysis[11,12].

2.5 Analysis of Non-linear Dynamics and Feedback Control

2.5.1. Dynamics

The dynamic behaviors of the plasma density and temperature can be obtained by numerical integrations of Eqs.(1.12), (2.1) and (2.2) with the perturbed initial conditions. Figure 2.4 shows, in the initial condition of the classical confinement time of *1 sec*, the dynamic behaviors of the ion and electron temperatures induced by both ion and electron temperature deviations of *±10%* of the equilibrium values. The broken and solid curves show the cases of I.S.A. and M.S.A., respectively. In M.S.A., the temporal inverse responces are observed at the initial period. Figure 2.5 shows the corresponding behaviors of the plasma density, and the upper and lower curves are caused by positive and negative temperature deviations, respectively. The time constants of the dynamics obtained in M.S.A. become about two times of those obtained in I.S.A. The time constants of dynamics are consistent with the eigenvalues shown in Fig.2.3.

The difference of the above dynamics between I.S.A. and M.S.A. can be interpreted as follows. There are four possible mechanisms that affect the alpha heating:

(a) The increase in plasma density increases the energetic alpha particles through the increase in the D-T reaction rate.

(b) The increase in plasma density increases the energy transfer rate of alpha particles to plasma due to the decrease in the slowing down time.

(c) The increase in ion temperature increases the birth rate of energetic alpha particles.

(d) The increase in electron temperature makes the slowing down time longer and consequently causes the decrease in energy

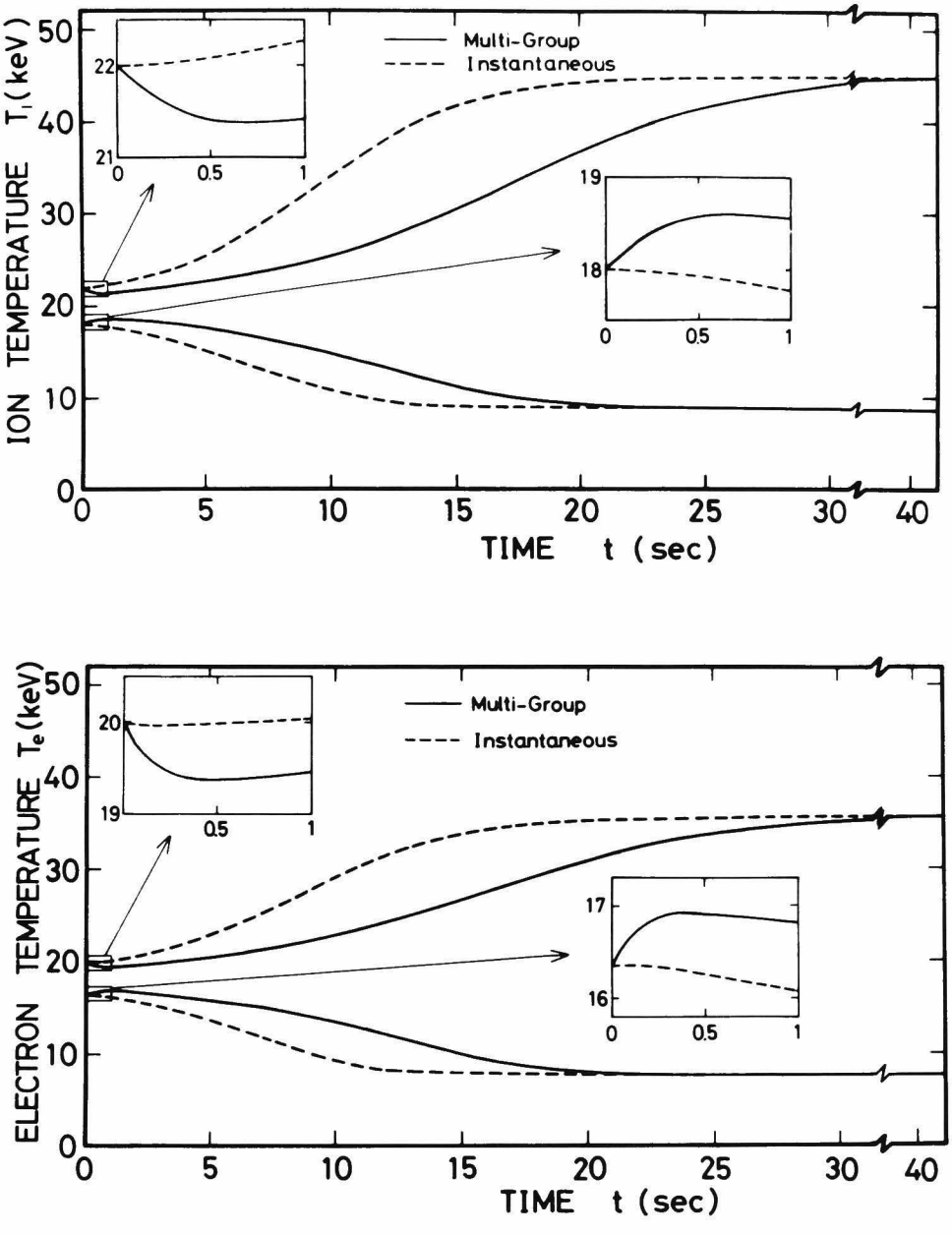

Fig.2.4. Dynamic behaviors of ion and electron temperatures induced by the temperature deviations of ±10%. The initial ion and electron temperatures are 20 and 18 KeV, respectively.

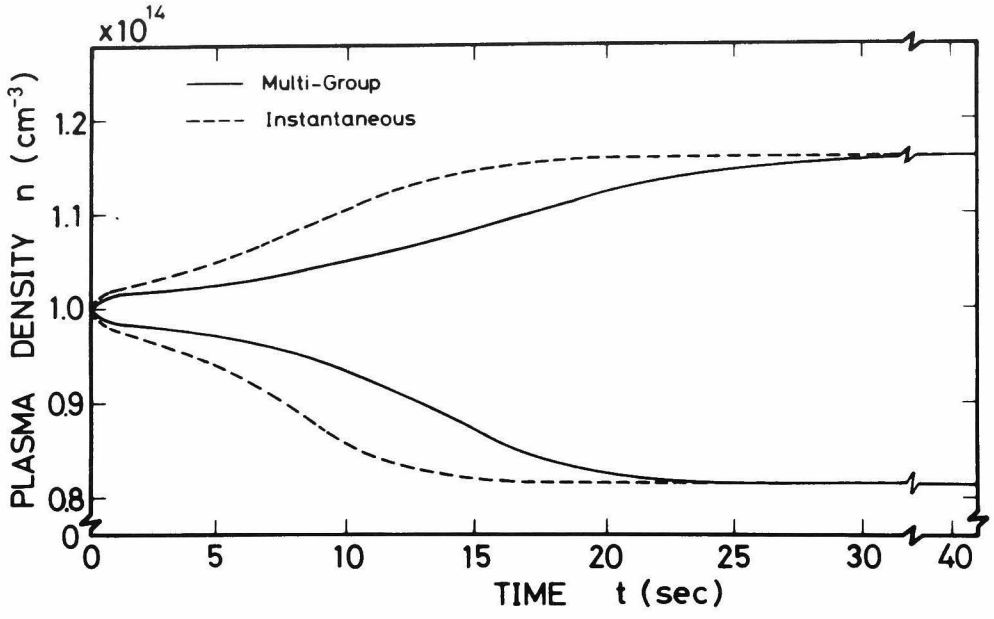

Fig.2.5. Dynamic behaviors of plasma density induced by the temperature deviations of +10%.

transfer rate from energetic particles to plasma[12]. Although the model used in I.S.A. excludes the effects (b) and (d), the model used in M.S.A. includes all these effects. The effects (a), (b) and (c) altogether constitute the positive feedback effect to the plasma heating. On the other hand, the effect (d) acts as a negative feedback.

The initial temperature perturbations bring about effects (c) and (d). Since effect (d) dominates over effect (c) at the initial period, the inverse responses appear particularly in M.S.A. About one second later, effects (a) and (b) become important due to the increase in plasma density. Effect (d) gets smaller than these three effects, as time goes on. Hence, except at the initial period, the positive deviations force the ion and electron temperatures to rise in both in I.S.A. and M.S.A.

2.5.2. Feedback control

The feedback control system with one exponential time lag can be

presented by Eq.(2.26), where the neutral beam injection rate is regulated according to the deviation of the ion temperature from the equilibrium value.

$$\tau_f \frac{d}{dt}\left(\frac{\delta S_b}{S_{b_0}}\right) = -G\,\frac{\delta T_i}{T_{i_0}} - \frac{\delta S_b}{S_{b_0}} \tag{2.26}$$

where τ_f and G are time lag and gain constant of the feedback control, respectively. Variable δS_b denotes the change of injection rate.

The linearized state equations of the plasma core with the feedback control system are given, in case of I.S.A., by

$$\frac{d\vec{X}_f}{dt} = A_f \vec{X}_f \tag{2.27}$$

where

$$\vec{X}_f = \begin{pmatrix} \vec{X} \\ \delta S_b/S_{b_0} \end{pmatrix}, \quad A_f = \begin{pmatrix} & & S_b/n \\ A & & (\frac{2}{3}\Delta W_{bi} + S_{b_0} T_{i_0})/n_0 \\ & & (\frac{2}{3}\Delta W_{be} - S_{b_0} T_{e_0})/n_0 \\ 0 \;\; -G/\tau_f \;\; 0 & & -1/\tau_f \end{pmatrix} \tag{2.28}$$

and, in case of M.S.A., by

$$\frac{d\vec{Y}_f}{dt} = B_f \vec{Y}_f \tag{2.29}$$

where

$$\vec{Y}_f = \begin{pmatrix} \vec{Y} \\ \delta S_b/S_{b_0} \end{pmatrix} \quad \text{and} \quad B_f = \begin{pmatrix} & & 0 \\ & & 0 \\ & & 0 \\ B & & S_b/N_{f1} \\ & & 0 \\ & & \vdots \\ & & 0 \\ 0 \;\; -G/\tau_f \;\; 0 \cdots \; 0 & & -1/\tau_f \end{pmatrix} \tag{2.30}$$

The marginal stability conditions on the gain constant G and the time constant τ_f can be obtained by setting the maximum eigenvalues of

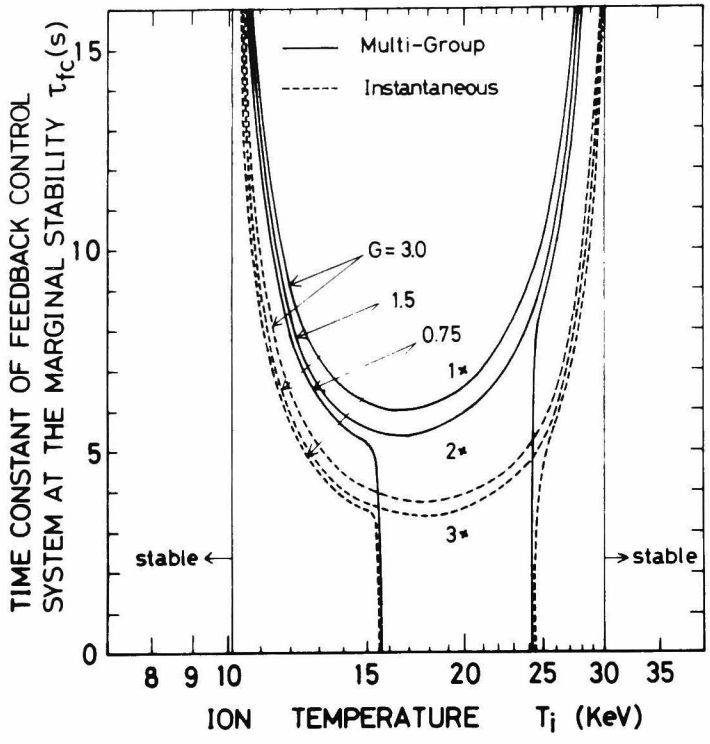

Fig.2.6. Relation between time constant of feedback control system and ion temperature for three feedback gains at the marginal stability.

matrixes A_f and B_f zero. Figure 2.6 depicts the relation between the time constant and the ion temperature for three gain constants at the marginal stability. The time constant of the marginal stability τ_{fc} obtained in M.S.A. are more than *1.5* times as large as in I.S.A. When the gain constant *G* is equal to *0.75*, the fusion plasma in the range of temperature between *16 KeV* and *24 KeV* cannot be stabilized by any time lag not only in case of I.S.A. but also in M.S.A.

Figure 2.7 illustrates dynamic behaviors of the ion and electron temperatures where the beam injection rate is regulated by the feedback control given by Eq.(2.26) and the same initial conditions as those adopted in the section 2.5.1 are used. Figures 2.7 a) and b) correspond to the results obtained in I.S.A. and M.S.A., respectively. The same

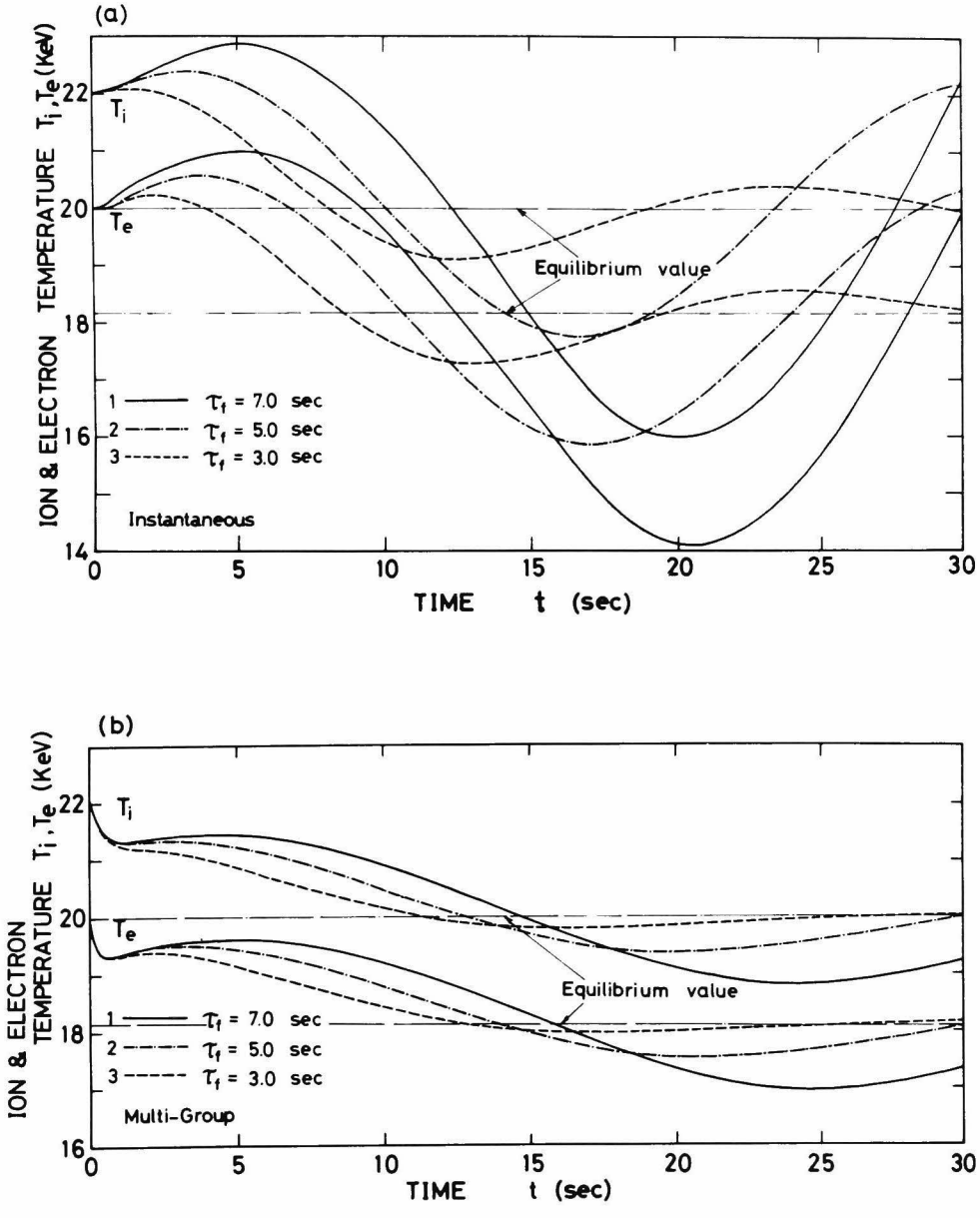

Fig.2.7. Dynamic behaviors of plasma temperature with feedback control of gain constant G=1.5, where a) and b) are calculated in I.S.A. and M.S.A., respectively.

three time constants as marked in Fig.2.6 are assumed in these cases. Note that, in case of τ_f=5.0 sec, the calculations in I.S.A. and in M.S.A. lead to the different results, where the plasma can be stabilized in M.S.A., while it remains unstable in I.S.A. Thus, the slowing down process should be treated accurately in studying the dynamics and control problems.

2.6. Concluding Remarks

The energy balance instability of an infinite and homogeneous D-T fusion plasma was studied within the framework of linearization comparing two alternative approximations; the instantaneous slowing down approximation and the multi-group slowing down approximation. The stability indexes which are obtained by the linear approximation agreed well with the numerical results of non-linear dynamics. The comparison between these approximations made it clear that the slowing down process of the energetic ions hardly changes the stability region obtained by I.S.A. Therefore, I.S.A. may be applied to the static analysis of the thermal stability. However, the neglect of the slowing down process of energetic ions results in underestimation of time constants of the plasma density and temperature dynamics, which arises the serious problem on the design of feedback control system. The process should be taken into consideration in the analysis of dynamics and control of a fusion plasma.

Chapter 3

CHARACTERISTICS OF CATALYZED DEUTERIUM REACTORS

3.1. Introduction

It is commonly accepted that the present goal of fusion research lies in attaining the plasma condition which satisfies the Lawson criterion of D-T reactor and in developing D-T power reactor. However, the advanced reactors with D-D, D-H_e^3 and p-B^{11} fuel cycles possess the advantages of the abundant fuels, the elimination of tritium breeding and the reduced production of neutrons. Hence, continuous effort should be made in developing the advanced fuel reactors. Catalyzed deuterium (*Cat.D*) [19] among the advanced fuels is the most likely candidate for the toroidal reactor after D-T reactor because of non-breeding and the highest reactivity next to D-T reaction.

Recent design studies of Cat.D fueled tokamak result in economically interesting reactors, when the plasma β (= *plasma pressure/ magnetic field pressure*) is of the order of a few tens of per cent.[20] In this chapter, the reactor parameters of Cat.D tokamak are examined by solving the particle and energy balances under the MHD stability constraints and the sensitivity analysis of the parameters is also made for the sake of the optimal design study of Cat.D reactors.

Another engineering problem dealt with in this chapter is concerned with the kinetics of Cat.D reactors. Since the energy required to ignite the Cat.D reactor is one order greater than that of D-T

reactors, it is necessary to find out advanced start-up techniques for saving the additional heating energy. Gerdin et al.[21] discussed some ignition techniques of Cat.D using a moving limiter and burn propagation in order to reduce energy requirement. If the Cat.D ignition can be attained by means of the thermal run away induced by excessively fueling the cold deuterium and tritium in a D-T burning plasma, then the input power required for start-up of the Cat.D reactor could remain same order as that required to the D-T reactors. Then, the other start-up technique using thermal run away is proposed and the transition dynamics from the D-T burning mode to Cat.D operating mode are investigated by the control of the fuel injection rate and mixture. The thermal stability and dynamics are studied on the reactor operating in the trapped-ion-instability region with arbitrary D-T mixture (*including Cat.D*).

3.2. Properties of Cat.D reactors

The D-D reactions are composed of the following chain reactions;

Principal Reactions

$$D + D \longrightarrow H_e^3\ (0.82\ MeV) + n\ (2.45\ MeV) \qquad (3.1)$$

$$D + D \longrightarrow T\ (1.01\ MeV) + p\ (3.03\ MeV) \qquad (3.2)$$

where each reaction occurs with almost equal probability.

Secondary Reactions

$$D + T \longrightarrow H_e^4\ (3.52\ MeV) + n\ (14.06\ MeV) \qquad (3.3)$$

$$D + H_e^3 \longrightarrow H_e^4\ (3.67\ MeV) + p\ (14.67\ MeV) \qquad (3.4)$$

If the products T and H_e^3 are both burned at the rates equal to their productions, the reactions (3.1)-(3.4) are reduced to

$$6D \longrightarrow 2H_e^4 + 2n + 2p + (43.23\ MeV) \qquad (3.5)$$

This is called Cat.D reaction, because it does not explicitly include T and H_e^3. When the entire T and H_e^3 leaving the plasma core are re-injected, the concentrations of T and H_e^3 for Cat.D reaction are given by

$$n_T = \frac{\langle\sigma v\rangle_{DD}}{4\langle\sigma v\rangle_{DT}} n_D, \qquad n_{H_e^3} = \frac{\langle\sigma v\rangle_{DD}}{4\langle\sigma v\rangle_{DH_e^3}} n_D \tag{3.6}$$

The burn-up rates η_b of D, T and H_e^3 are presented by

$$\eta_{bD} = \frac{n_D^2\langle\sigma v\rangle_{DD}}{n_D/\tau_p + n_D^2\langle\sigma v\rangle_{DD}} \tag{3.7}$$

$$\eta_{bT} = \frac{n_D n_T\langle\sigma v\rangle_{DT}}{n_T/\tau_p + n_D n_T\langle\sigma v\rangle_{DT}} \tag{3.8}$$

$$\eta_{bH_e^3} = \frac{n_D n_{H_e^3}\langle\sigma v\rangle_{DH_e^3}}{n_{H_e^3}/\tau_p + n_D n_{H_e^3}\langle\sigma v\rangle_{DH_e^3}} \tag{3.9}$$

When the reactor parameters of Cat.D illustrated in table 3.1 are used for numerical calculations, the burn-up rates are evaluated as follows,

$$\eta_{bD} \simeq 0.04, \ \eta_{bT} \simeq 0.61 \text{ and } \eta_{bH_e^3} \simeq 0.10$$

Although the tritiums are fairly well burned in the plasma core, most of helium-3 escape from the plasma before burning. The total amounts of the tritium and helium-3 circulating in the Cat.D reactor, $N_T(Cat.D)$ and $N_{H_e}(Cat.D)$ and the tritium in the D-T reactor, $N_T(D\text{-}T)$ are written by

$$N_T(Cat.D) = \frac{n_T}{\tau_p} V_p \tag{3.10}$$

$$N_{H_e^3}(Cat.D) = \frac{n_{H_e^3}}{\tau_p} V_p \tag{3.11}$$

Table 3.1 Reference reactor parameters

Parameters	D-T reactor (Mills[22])	Cat.D reactor (present study)
Temperature (KeV)	30	50
Density (m^{-3})	5×10^{19}	2.7×10^{20} (deuterium)
Confinement time (s)	3.3	6.8
Minor radius (m)	3.25	4
Major radius (m)	10.5	12.9
Toroidal field (T)	6	6
Beta value (%)	$4 \sim 10$	30
Output power (GW)	3.2	11 (graphite blanket) 18 (sodium blanket)
Neutron flux (m^{-2})	6.0×10^{17}	1.48×10^{18} (2.45 MeV neutron+14.1 MeV neutron)
Wall loading (MW/m^2)	2.15	4.9 (graphite blanket)

$$N_T(D\text{-}T) = \frac{n'_T}{\tau'_p} V'_p \qquad (3.12)$$

where V_p and τ_p denote plasma volume and particle confinement time and the dash refers to the D-T reactor. The ratio of the amounts of the helium-3 in Cat.D and of the tritium in D-T to that of the tritium in Cat.D are obtained for the reference reactors as follows,

$$N_{H_e^3}(Cat.D)/N_T(Cat.D) \simeq 14 \qquad (3.13)$$

$$N_T(D\text{-}T)/N_T(Cat.D) \simeq 16 \qquad (3.14)$$

Thus, Cat.D reactors have the potential benefits of not only the flexible design due to the elimination of tritium breeding but also the reduced tritium handling.

3.3. Parameter Study of Cat.D Reactors

The design of self-sustaining Cat.D fueled tokamak reactors is studied by surveying the large range of plasma and reactor parameters. The similar methods to the design study on the D-T fueled tokamak reactor[23,24] are applied to the present study. The parameters are obtained by selfconsistently solving the particle and energy balances under the MHD stability constraints.

3.3.1. Basic equations

The space-averaged particle balance equations for five plasma spacies; deuterium, tritium, helium-3, alpha and proton are given by

$$\frac{d\bar{n}_D}{dt} = \bar{S}_D - \frac{\bar{n}_D}{\tau_{pD}} - \overline{n_D^2 \langle\sigma v\rangle}_{DD} - \overline{n_D n_T \langle\sigma v\rangle}_{DT} - \overline{n_D n_{H_e^3} \langle\sigma v\rangle}_{DH_e^3} \tag{3.15}$$

$$\frac{d\bar{n}_T}{dt} = \bar{S}_T - \frac{\bar{n}_T}{\tau_{pT}} - \overline{n_D n_T \langle\sigma v\rangle}_{DT} + \frac{1}{2}\overline{n_D^2 \langle\sigma v\rangle}_{DD-T} \tag{3.16}$$

$$\frac{d\bar{n}_{H_e^3}}{dt} = \bar{S}_{H_e^3} - \frac{\bar{n}_{H_e^3}}{\tau_{pH_e^3}} - \overline{n_D n_{H_e^3} \langle\sigma v\rangle}_{DH_e^3} + \frac{1}{2}\overline{n_D^2 \langle\sigma v\rangle}_{DD-H_e^3} \tag{3.17}$$

$$\frac{d\bar{n}_{H_e^4}}{dt} = -\frac{\bar{n}_{H_e^4}}{\tau_{pH_e^4}} + \overline{n_D n_T \langle\sigma v\rangle}_{DT} + \overline{n_D n_{H_e^3} \langle\sigma v\rangle}_{DH_e^3} \tag{3.18}$$

$$\frac{d\bar{n}_p}{dt} = -\frac{\bar{n}_p}{\tau_{pp}} + \frac{1}{2}\overline{n_D^2 \langle\sigma v\rangle}_{DD-T} + \overline{n_D n_{H_e^3} \langle\sigma v\rangle}_{DH_e^3} \tag{3.19}$$

where $\bar{n}$ stands for the space-averaged quantity of n. $\langle\sigma v\rangle_{ij}$ presents the fusion reaction rate between i and j spacies ions with Maxwellian distributions. $\langle\sigma v\rangle_{DD-T}$ and $\langle\sigma v\rangle_{DD-H_e^3}$ are the reaction rates of T and H_e^3 branches of D-D reactions. The reactions between superthermal ions and thermal ions are neglected in this study (Appendix A). S_D, S_T and $S_{H_e^3}$ are the fuel injection rates of D, T and H_e^3. Note that $S_T =$

n_T/τ_{pT} and $S_{He^3}=n_{He^3}/\tau_{pHe^3}$ should be satisfied under the Cat.D operation condition. τ_{pj} is the particle confinement time of j species ions. The scaling laws for the plasma confinement have not been established experimentally, but theoretical prediction shows that the plasma parameters in the D-T and Cat.D reactors lie in the trapped-ion-regime. The particle and energy confinement times can be set equal ($\tau_p=\tau_E=\tau$) and are given by

$$\tau = 4\times10^{-9} \frac{B^2\bar{\phi}\bar{n}_e a^4 Z_{eff} A^{5/2}}{T_e^{7/2}} \quad (sec) \tag{3.20}$$

where A is aspect ratio given by R/a. T_e is the electron temperature in eV unit. The confinement times for all species of ions are presumed to be equal to Eq.(3.20).

If the electron and ion temperatures are taken to be equal, the energy balance equation is given by

$$3\frac{\overline{dn_eT}}{dt} = \overline{\frac{1}{2}n_D^2\langle\sigma v\rangle}_{DD\text{-}He^3}E_{DD\text{-}He^3} + \overline{\frac{1}{2}n_D^2\langle\sigma v\rangle}_{DD\text{-}T}E_{DD\text{-}T} + \overline{n_Dn_T\langle\sigma v\rangle}_{DT}E_{DT} + \overline{n_Dn_{He^3}\langle\sigma v\rangle}_{DHe^3}E_{DHe^3} - \bar{P}_{rad} - \sum\frac{\overline{3n_jT}}{\tau} + \bar{P}_H \tag{3.21}$$

where E_{ij} denotes the energy of the charged particles produced by fusion reaction between i and j species of ions, given by $E_{DD\text{-}He^3}=0.82\ MeV$, $E_{DD\text{-}T}=4.04\ MeV$, $E_{DT}=3.52\ MeV$ and $E_{DHe^3}=18.34\ MeV$. n_e is the electron density given by

$$n_e = n_D + n_T + 2n_{He^3} + 2n_{He^4} + n_p \tag{3.22}$$

P_{rad} is the energy loss caused by bremsstrahlung and cyclotron radiations, written by[50]

$$P_{rad} = P_{brem} + P_{cyc}$$

$$P_{brem} = 9.6\times10^{-20}\ Z_{eff}\ n_e^2\ \sqrt{T_e} \quad (ev/m^3\ s) \tag{3.23}$$

$$P_{cyc} = 0.416\ \frac{\sqrt{n_e}\,B_\phi}{\sqrt{a}}\ [T_e^{11/4} + 0.490\times10^{-5}T_e^{15/4}]\ (1-\Gamma)$$

$$(eV/m^3\ s) \tag{3.24}$$

where Γ is the reflection rate on the first wall, assumed to be 0.9 in the numerical calculations. P_H is the input power due to the additional heating,such as R.F. heating or neutral beam injection heating. The stability of plasma column depends on the parameter, $q(r)=r/R\cdot B_\phi/B_\theta$, where r is minor radius, B_ϕ toroidal magnetic field and B_θ poloidal magnetic field. The condition $q(a) > 1$ is always necessary to ensure stability against herical kinking of the plasma pinch. The most optimistic condition;

$$q(a) = 1 \tag{3.25}$$

is taken for this study. Another stability constraint is concearned with the poloidal beta value β_p. To stabilize the ballooning mode, the poloidal beta must be less than R/a or $\sqrt{R/a}$. When the following equation

$$\beta_p = \sqrt{R/a} \tag{3.26}$$

is assumed, then the toroidal beta β_t are given by

$$\beta_t = \beta_p/A^2q^2 = A^{-3/2} \tag{3.27}$$

The density and temperature are presumed to have the following radial profiles,

$$n_j = n_{j_0}[1-(r/a)^2]^{m_1} \tag{3.28}$$

$$T = T_0[1-(r/a)^2]^{m_2} \tag{3.29}$$

where n_{j_0} and T_0 are the ion density of j species and the plasma temperature at the plasma center, respectively. The toroidal current density profile is taken as follows,

$$j = j_0[1-(r/a)^2]^{\frac{3}{2}m_2} \tag{3.30}$$

where j_0 is the current density at the plasma center. The fusion power P_f and the wall loading P_w due to charged fusion products of a core plasma are written by

$$P_f = 2\pi^2 a^2 R \left[\frac{1}{2}\overline{n_D^2\langle\sigma v\rangle}_{DD\text{-}H_e^3}(E_{DD\text{-}H_e^3} + E_{DH_e^3}) + \frac{1}{2}\overline{n_D^2\langle\sigma v\rangle}_{DD\text{-}T}(E_{DD\text{-}T} + E_{DT})\right]$$

$$\simeq \pi^2 a^2 R\ \overline{n_D^2\langle\sigma v\rangle}_{DD}\ E_{tot} \tag{3.31}$$

$$P_w = P_f/4\pi^2 r_w R$$

$$\simeq \frac{a^2}{4r_w}\overline{n_D^2\langle\sigma v\rangle}_{DD}\ E_{tot} \tag{3.32}$$

where r_w is the wall radius and E_{tot} is equal to *13.36 MeV*.

3.3.2. Parameter analysis

The reactor parameters such as minor and major radii, plasma current, beta value and total fusion power are obtained by solving Eqs. (3.15)-(3.24), (3.25) and (3.26) depending on the plasma density and temperature. Figure 3.1 shows the dependence of the reactor parameters on the density and temperature with the flat profiles. The ignition is impossible below the temperature of *30 KeV*. The minor and major radii have the minimum values at *T=35 KeV* and increase proportionally to the temperature. The increase of density allows the great reduction of the major radius and the plasma current, but results in the high beta and large fusion power.

It is known that $n\tau_E$ value required for ignition can be reduced remarkably from that of an uniform plasma, if the density and temperature profiles possess strong axial peaking [25,26]. The effects of the shape of the density and temperature profiles on the reactor parameters are examined. Figures 3.2 and 3.3 show the similar relations to Fig.3.1

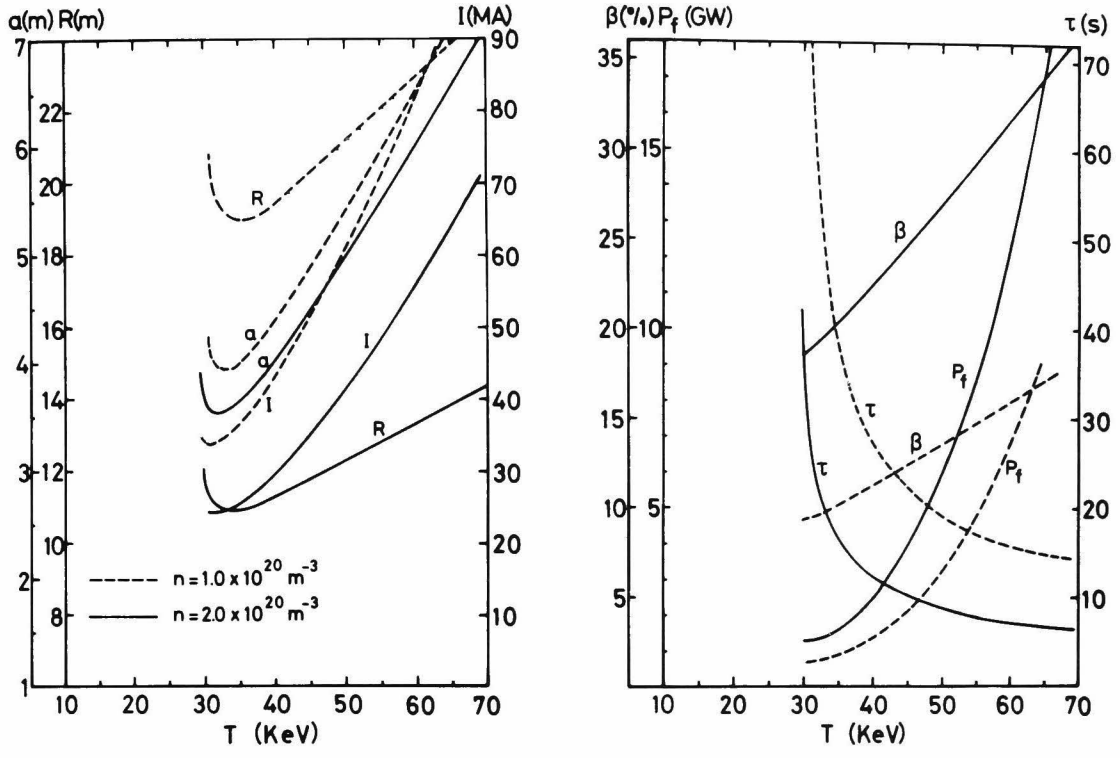

Fig.3.1. Reactor parameters vs. ion temperature for flat density and temperature profiles ($m_1=m_2=0$). The solid and broken curves correspond to the electron density of 1.0 $\times 10^{20}$ m^{-3} and 2.0$\times 10^{20}$ m^{-3}, respectively.

except that the density and temperature profiles are assumed to have peaking at the plasma center. The flat density and parabolic temperature profiles make ignition of Cat.D plasma possible at the averaged temperature of *25 KeV* (the peak temperature of *50 KeV*). The Cat.D plasma with the more peaking profiles can be ignited even at the temperture lower than *15 KeV*.

The peaking profile effects bring the marked reduction of the size of Cat.D plasma required for ignition, which leads to the compact design of the reactors. If cold gas blanket[17,27] could be used successfully, the assumption of the flat density and peaked temperature profiles appears to be reasonable in a fusion grade plasma, which is heated by fusion products mainly in the center region. The following Cat.D

reactor parameters, for example, are obtained from Fig.3.2;

$n=2.0\times10^{20}\ m^{-3}$, $\bar{T}=40$ KeV, $a=3.7$ m, $R=10.7$ m,
$B_\phi=5.5$ T, $I=27$ MA, $\beta_t=21$ % and $P_f=2.3$ GW.

These Cat.D reactor parameters would be attained by the simple extension of the D-T tokamak reactor parameters excepting the beta value. The recent experiments of tokamak (e.g. in ATC) have attained central β-values of only about 2 %. Although it is a very difficult task to raise beta value in tokamak, the attainment of high β-values of $10\sim20$ % will be achieved by intensive heating in an optimized tokamak MHD configuration[28]. The β-value greater than 20% may not be an impractical value for the asymmetric toroidal systems like heliotron[29].

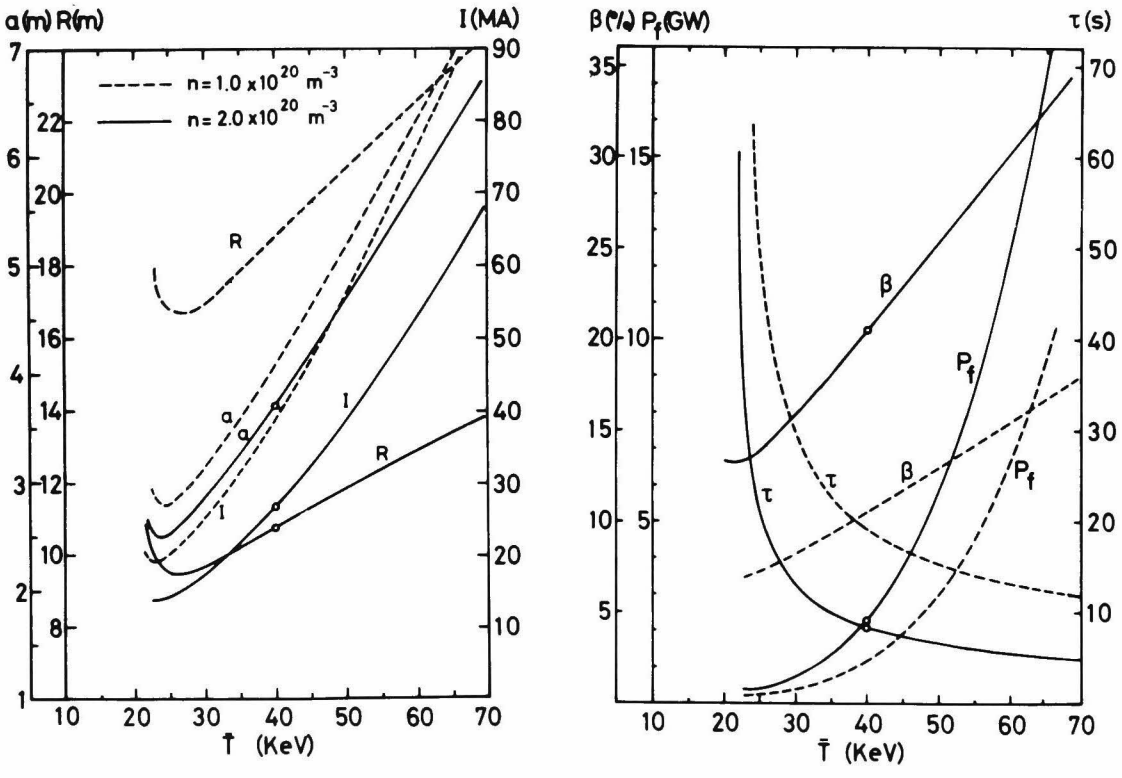

Fig.3.2. Reactor parameters vs. averaged ion temperature for flat density and peaked temperature profiles ($m_1=0$, $m_2=1$). The small circles on solid curves denote the reference operating points used in the sensitivity study.

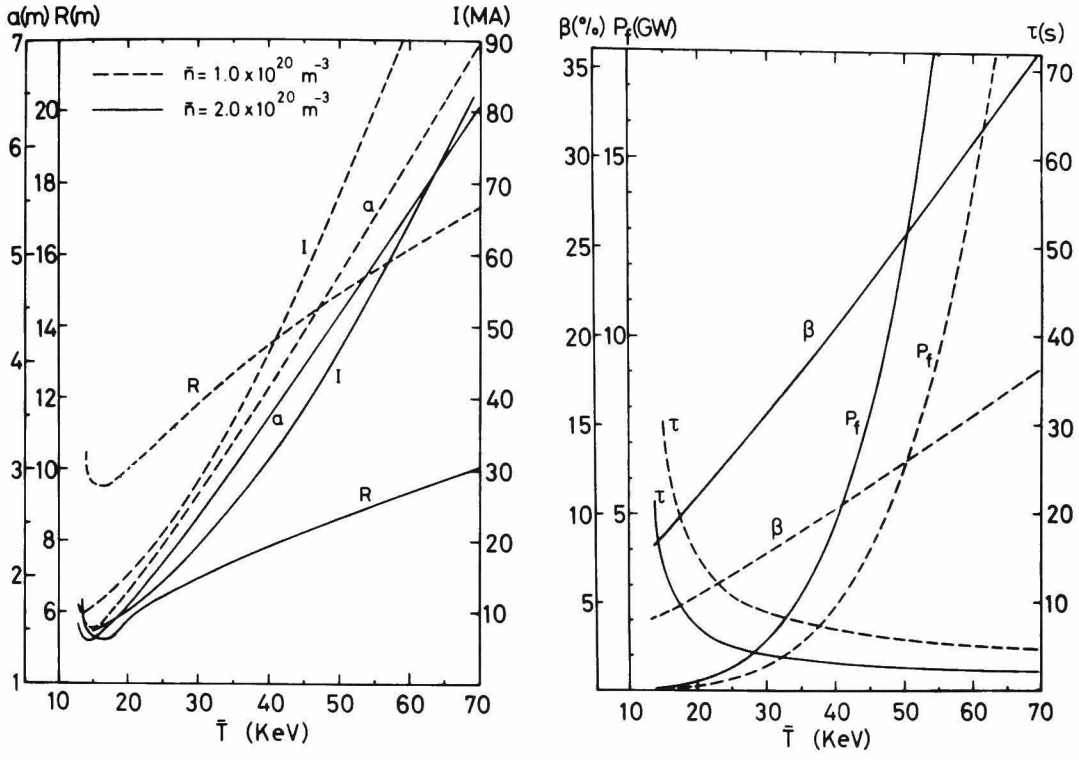

Fig.3.3. Reactor parameters vs. averaged ion temperature for peaked density and peaked temperature profiles (m_1=1, m_2=2).

3.3.3. Sensitivity Analysis

The sensitivity of various reactor parameters to the deuterium density, magnetic field and shape of the temperature profile are examined for the reference parameters cited in the section 3.3.2. Figure 3.4 shows the dependence of the parameters on the deuterium density. Although the major radius and wall loading are very sensitive, the minor radius is relatively insensitive to the density. The increase of the density reduces greatly the major radius, but on the other hand raises the beta and wall loading. The high density operation permits the compact design of Cat.D reactor but aggravates the difficulty of the first wall engineering. Figure 3.5 indicates the change of the parameters caused by the variation of the toroidal

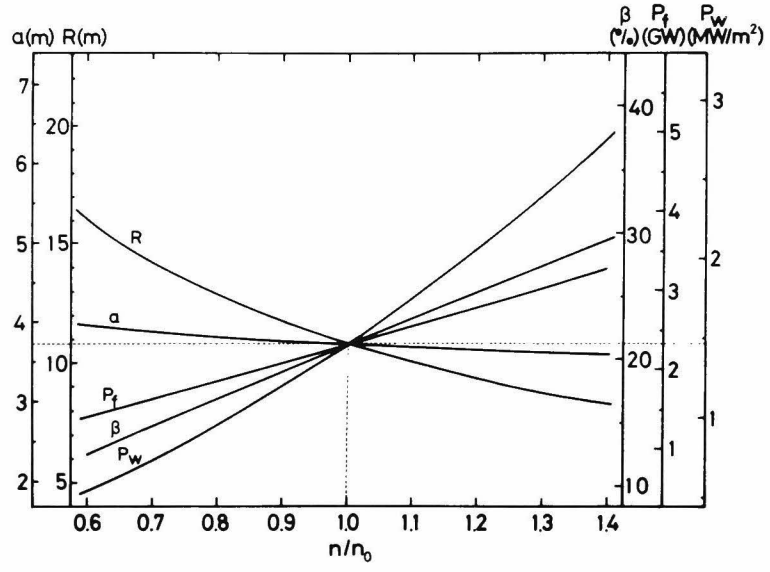

Fig.3.4. Reactor parameters vs. deuterium density.

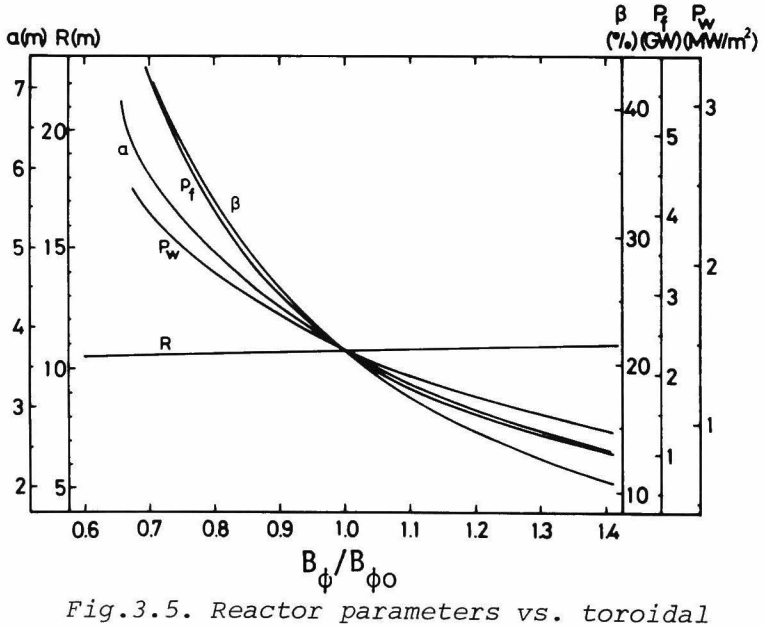

Fig.3.5. Reactor parameters vs. toroidal magnetic field.

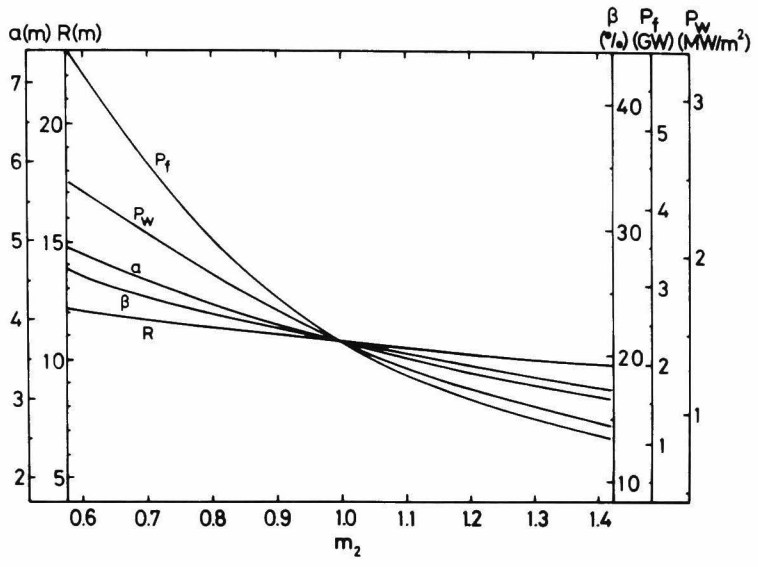

Fig.3.6. Reactor parameters vs. shape of ion temperature profile.

magnetic field. All parameters except major radius are found to depend strongly on the magnetic field. Although the higher magnetic field is more desirable from the viewpoints of plasma engineering and reactor design, the maximum values are limited within *18 (T)* for Nb_3Sn and *12 (T)* for *NbTi* at the magnetic winding. Figure 3.6 reveals the effects of the shape of temperature profile on the reactor parameters. The more steep peaking of temperature profile decreases every parameter and brings about the advantageous effects as well as the high magnetic field. However, the means of controlling the temperature profile are unknown and it may be a difficult problem to attain the desired temperature profile.

3.4. Ignition of Cat.D Reactor from D-T Burning[30]

3.4.1. Stability on the operating points of pure D-T to Cat.D

If it is assumed that (1) the concentrations of proton and helium-*4* are negligible small, (2) the helium-*3* and tritium produced by D-D reactions are burnt at the rates equal to their production, and (3) particle loss caused by fusion events and energy loss due to cyclotron

radiation are neglected, then Eqs.(3.15)-(3.19) and (3.21) are reduced to the simplified equations as follows,

$$\frac{dn}{dt} = S - \frac{n}{\tau} \tag{3.33}$$

$$3\frac{dnT}{dt} = \frac{n_D^2}{2}\langle\sigma v\rangle_{DD}E_{DD} + n_D n_T\langle\sigma v\rangle_{DT}E_{DT} - P_{brem} - \frac{3nT}{\tau} \tag{3.34}$$

where $n=n_D+n_T$ and $E_{DD}=13.36\ MeV$. Introducing the parameter $\xi=n_T/n_D$, the ignition condition for any ξ is given by

$$n\tau = \frac{3T}{\frac{1}{2}\langle\sigma v\rangle_{DD}E_{DD}/(1+\xi)^2 + \langle\sigma v\rangle_{DT}E_{DT}\xi/(1+\xi)^2 - P_{brem}/n^2} \tag{3.35}$$

where $\xi=1-\frac{\langle\sigma v\rangle_{DD}}{4\langle\sigma v\rangle_{DT}} \simeq 1$ corresponds to pure D-T and $\xi=0$ to Cat.D. Note that n_T does not include the density of tritium born in D-D reactions. The ignition criteria calculated from Eq.(3.35) are depicted in Fig.3.7 for various ξ. The linear stability analysis used in capter 2 is performed for the sake of examining the thermal stability of the plasma with arbitrary D-T mixture. Figure 3.8 indicates the real parts and imaginary parts of eigenvalues of linearized systems derived from Eqs.(3.33) and (3.34). The marginal stability region on the $n\tau$-T diagram is shown by the fine broken curves in Fig.3.7. The critical temperature at the marginal point of stability

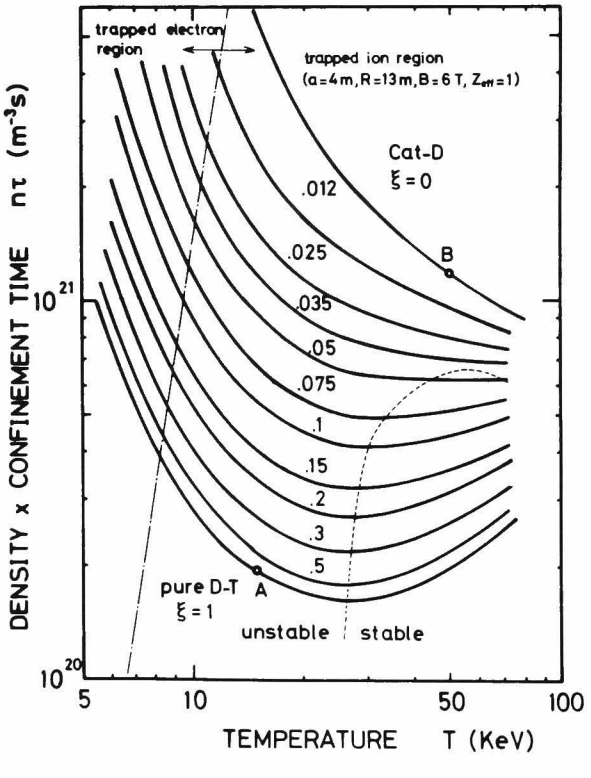

Fig.3.7. The ignition conditions of the reactor with arbitrary D-T mixture.

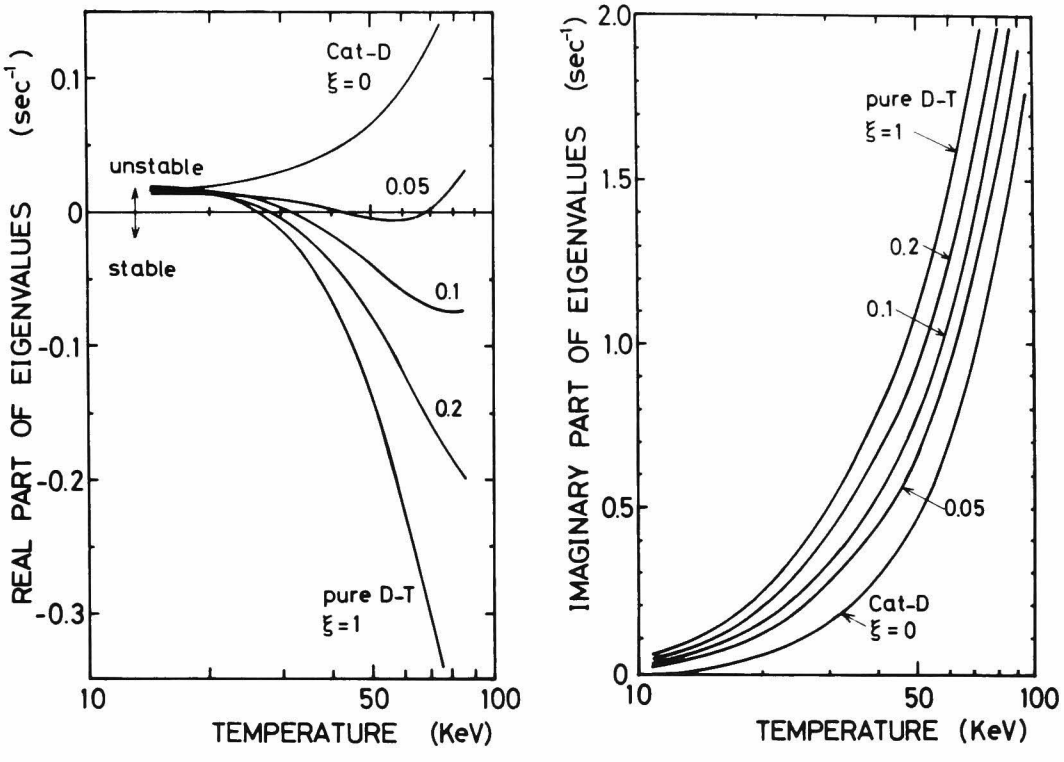

Fig.3.8. The real parts and the imaginary parts of eigenvalues of the linealized system of the fusion plasma with the arbitrary D-T mixture.

is *26 KeV* for pure D-T. For smaller ξ, the plasma is more oscillatory unstable and for the Cat.D plasma the entire temperature region is unstable and the growth rate and oscillation frequency of the instability increase as the temperature rises.

Figures 3.9 and 3.10 show the dynamic behaviors of the temperature and density initiated by *10%* density perturbation from the equilibrium values in pure D-T and Cat.D reactors, respectively. These indicate that adequate feedback controls of plasma parameters are necessary to get the stationary operation of Cat.D as well as the D-T. The tritium controls seems to be most effective method because of its high reactivity. Further discussion of this problem will be made in the following section with relation to the dynamic transition process from pure D-T to Cat.D.

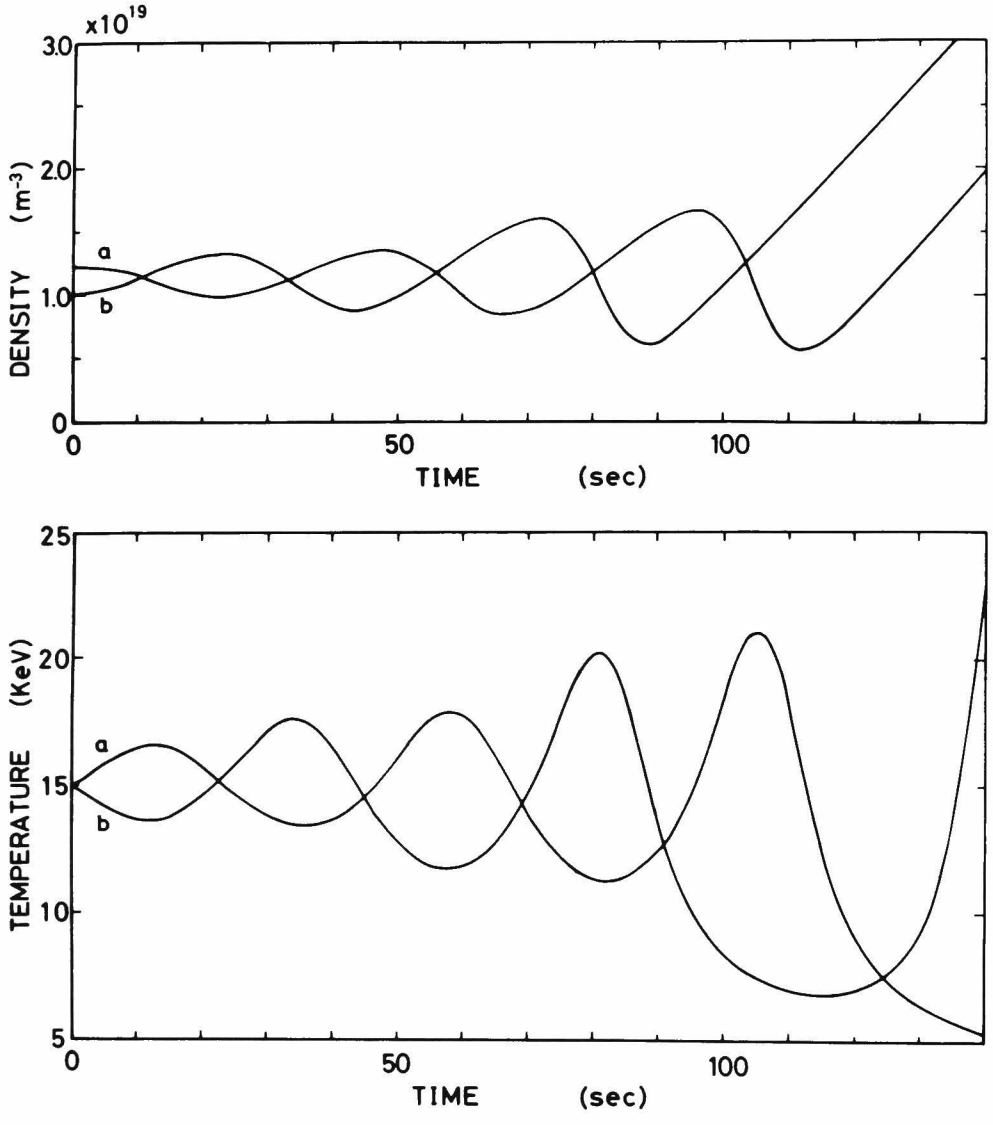

Fig.3.9. The density and temperature dynamics of D-T reactor induced by ±10% density perturbations. The equilibrium operating point is assumed to be point A in Fig.3.7.

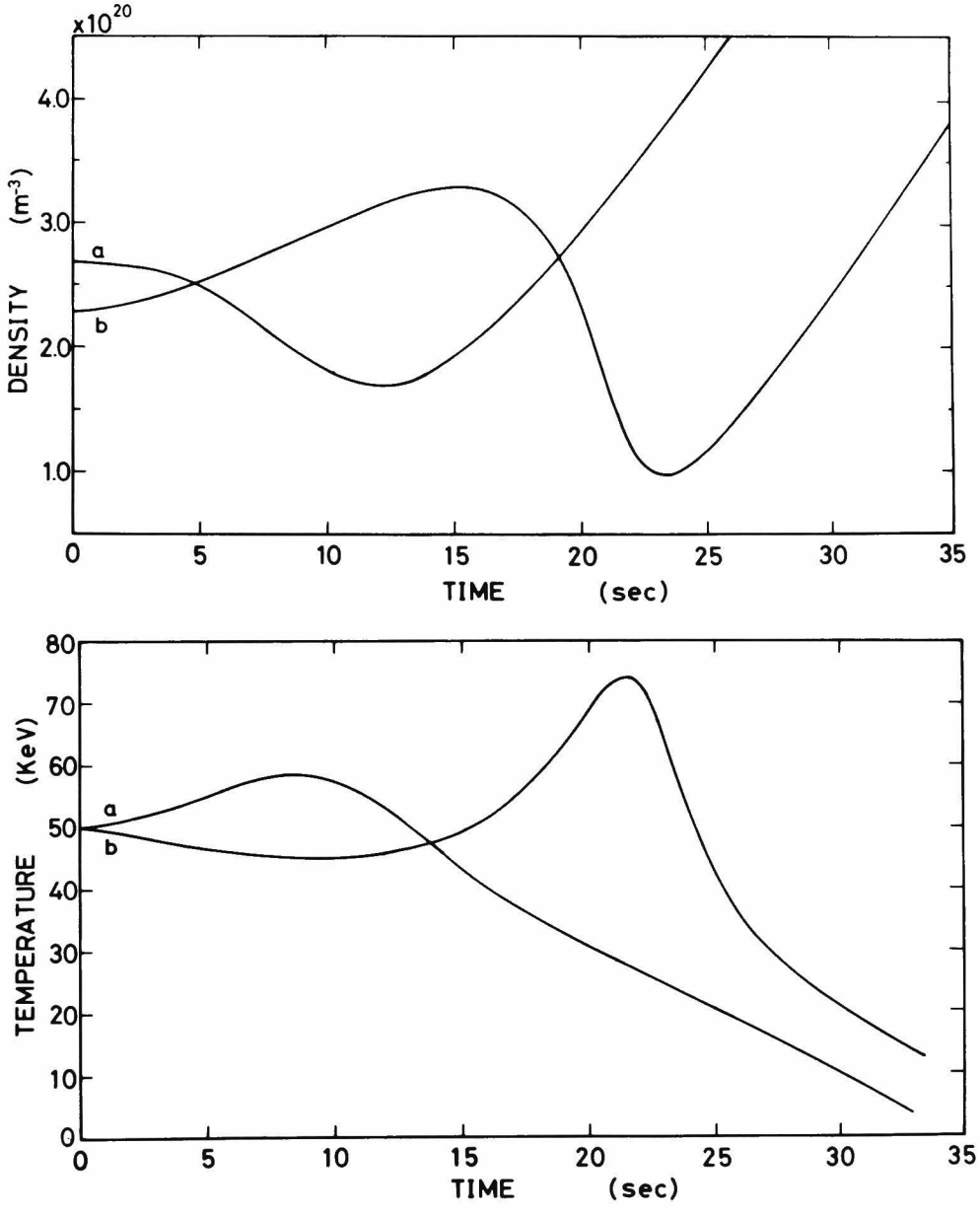

Fig.3.10. The density and temperature dynamics of Cat.D reactor induced by ±10% density perturbations. The equilibrium operating point is assumed to be point B in Fig.3.7.

3.4.2. Dynamic transition process from D-T to Cat.D

In order to investigate the transition process from D-T burning to Cat.D operation, the relatively conservative parameters given in section 3.2 are used as a reference reactor. The dynamics of the process is obtained by numerical integration of Eqs.(3.15)-(3.19) and (3.21) with the adequate initial conditions. The plasma parameters of the initial state of D-T burning mode are chosen as follows; $T=15$ KeV, $n=1.1\times10^{19}$ m^{-3}, $\beta_t=0.0017$, $W_T=110$ MW, $n\tau=1.75\times10^{20}$ $m^{-3}s$ (point A in Fig.3.7). The outline of control of the fuel injection during the transition process is;

For deuterium

$$\dot{n}_D = C_D \qquad 0 < t < t_T$$
$$\dot{n}_D = C_D + C_T \qquad t_T \leq t < t_D$$
$$\dot{n}_D = 0 \qquad t \geq t_D$$

where C_D and C_T denote the increasing rates of the deuterium and tritium densities caused by the excessive fueling, t_T is the time when the plasma temperature rises to the ignition temperature ($T_0=50$ KeV) and t_D is the time when the plasma density reaches the ignition density ($n_D=1.9\times10^{20}$ m^{-3}). The values C_D and C_T are taken to be constants. These linear increase in the densities may be realized by the appropriate fueling rates proportional to T^m ($m \gtrsim 3.5$ due to Eq.(3.20))

For tritium

$$\dot{n}_T = C_T \qquad 0 < t < t_T$$
$$\dot{n}_T = -G\,(T-T_0)/T_0 \qquad t \geq t_T$$

where G is a feedback gain constant. The time delay required for the feedback control is neglected for simplicity. The temperature control is possible for the wide range of G, i.e. $10^{19}<G<10^{21}$. G is taken to be 10^{20} in the following dynamic calculations. For $t \geq t_T$, the tritium

density is reduced holding the temperature almost constant around $T \simeq T_2$. The numerical values of C_D and C_T used in the calculation are listed in table 3.2. For case *C* and case *E*, the additional heating power P_H is applied at the initial phase of the transition.

Table 3.2 Fuel injection rates and additional heating during transition process.

	case A	case B	case C	case D	case E
C_D $(m^{-3}\,s^{-1})$	1.5×10^{18}	1.5×10^{18}	1.5×10^{18}	3.0×10^{18}	3.0×10^{18}
C_T $(m^{-3}\,s^{-1})$	1.0×10^{18}	1.0×10^{17}	1.0×10^{17}	1.0×10^{17}	1.0×10^{17}
P_H (MW)	0	0	65 for 25 sec	0	65 for 20 sec

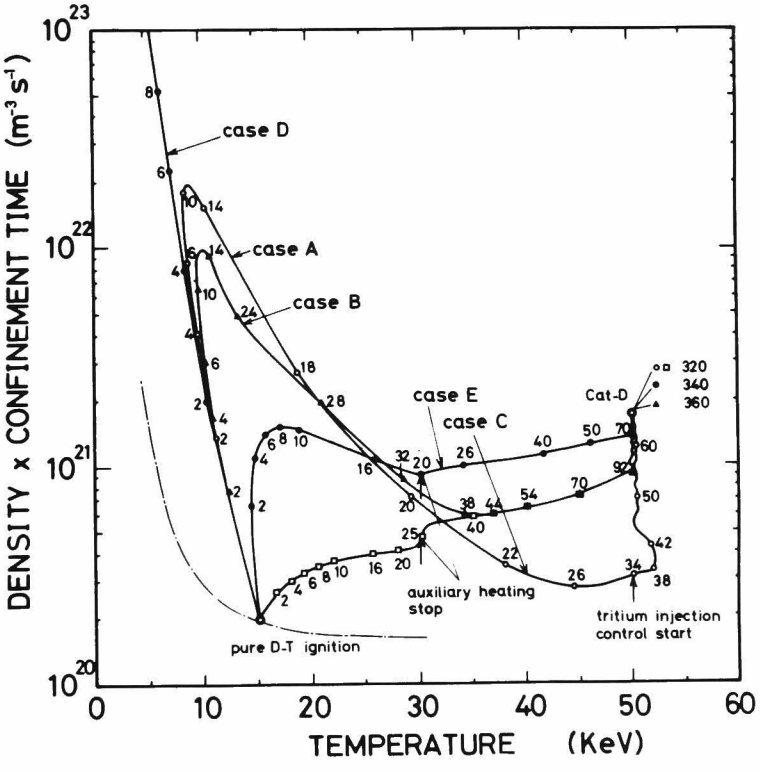

Fig.3.11. The paths of the transition from pure D-T burning to Cat.D operation mode. The numbers show the lapse time in second.

Figure 3.11 shows the transition paths on the $n\tau$-T diagram. Successive points on each line indicate the time required. Initially excessive fuel injection results in cooling the plasma, but since the plasma density increases due to the scaling law ($n_e\tau \propto n_e T^{-7/2}$), the temperature recovers gradually and the plasma can reach the ignition point (*case A* and *case B*). If the fuel injection rate exceeds a certain value, the temperature cannot recover again and the plasma stops burning (*case D*). The upper limit of the rising rate of density is about $C(=C_D+C_T)=3\times10^{18}m^{-3}sec^{-1}$. Evidently, an additional heating may sustain burning even in this case (*case E*) because the temperature decrease is suppressed. The input power of the heating is *65 MW* and the duration is *25 seconds* for *case C* and *20 seconds* for *case E*. Note that comparing *case C* with *case B*, the additional heating gives no effect to reduce the transition time, if the rising rate of density *C* is the same.

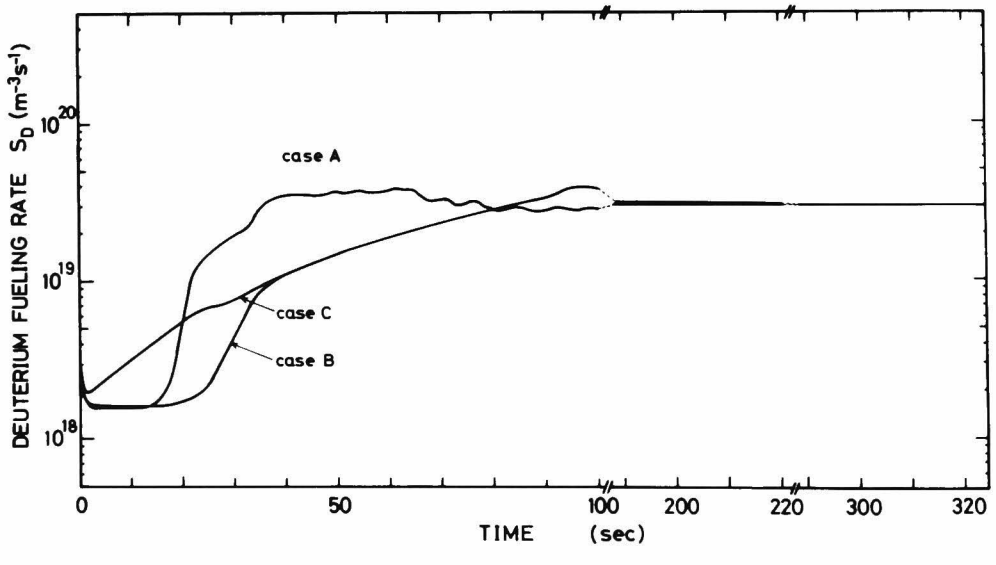

Fig.3.12. The deuterium fueling rate during the transition process.

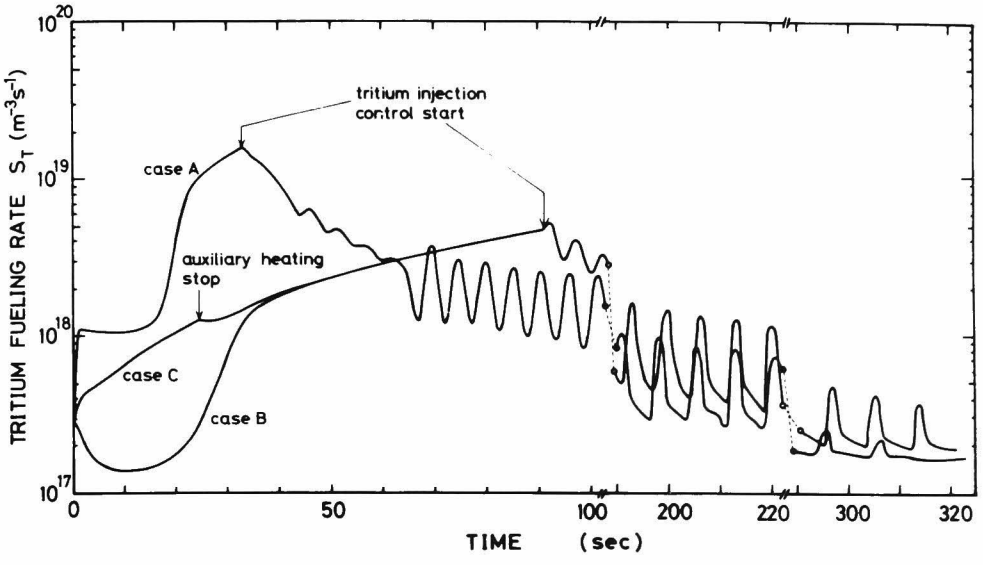

Fig.3.13. The tritium fueling rate during the transition process.

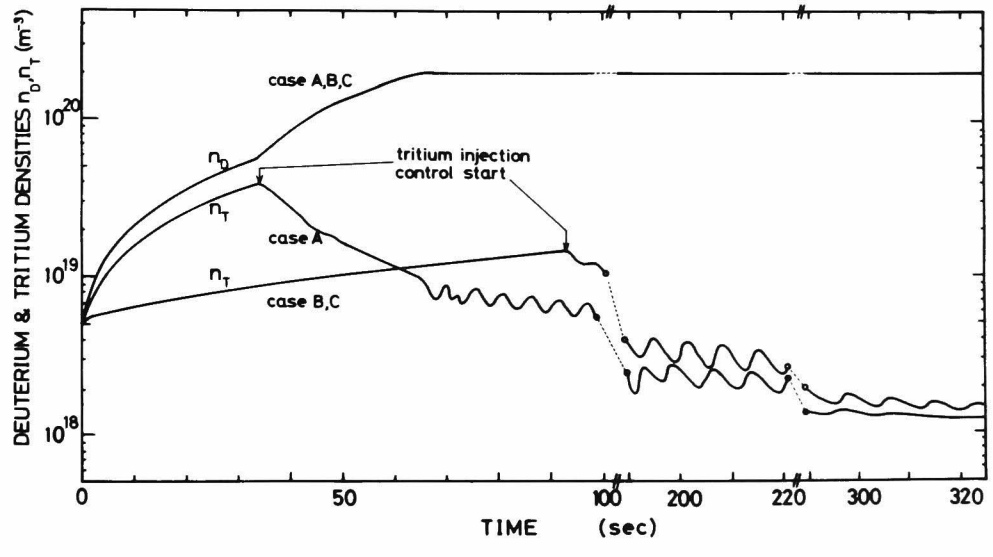

Fig.3.14. The deuterium and tritium density dynamics during the transition process.

In practice, the injection rates S_D and S_T are important quantities for controlling the density, which are shown in Fig.3.12 and Fig. 3.13. The corresponding density dynamics are given in Fig.3.14. The time t_T becomes shorter as the value of C_T/C_D approaches unity for a constant C_D or when the additional heating is applied. Hence, the tritium injection as well as the additional heating at the initial transition phase is effective for reducing the time required to reach the ignition temperature. However, the transition times to reach the final goal of Cat.D are almost same for two cases, i.e. roughly *300 seconds*. This time is almost same for *case E*. This is due to the fact that the transition times depend mainly on the times which are necessary for controlling the tritium density down to the level of Cat.D holding the temperature almost constant. The tritium density cannot be reduced rapidly since the operating plasma conditions are unstable against density deviation.

3.5. Concluding Remarks

The self-sustaining reactor parameters of Cat.D tokamak are obtained by solving the particle and energy balances of the plasma core under the restrictions of MHD stability. The increase of density in Cat.D reactor leads to the remarkable reduction of the major radius, but to the rise of beta value. The compact design due to the high density operation of Cat.D reactor are restricted by the allowable beta values. However, the effects of peaking temperature profile realize the compact reactor comparable to the D-T reactor keeping the averaged beta value to be reasonable ($\beta < 10\%$).

The possibility to ignite the D-D reactor from D-T reactor without any auxiliary heating power is proposed. The Cat.D operation mode is attained in roughly three hundred seconds only by adequate controls of the fuel injection rate and mixture. The required transition time is mainly restricted by the time for reducing the tritium concentration to the level of the Cat.D mode suppressing the temperature excurtion. The additional heating would not contribute to cut down the transition

time. Probably, the long transition time provides us no serious problem in practice, because the D-T mixture modes satisfy the self-sustaining condition and the reactor continues to supply the output power through the transition. The feedback control to keep the stationary operation is one of the most important tasks for the Cat.D reactor, since the plasma is always unstable for the density and temperature deviations.

Chapter 4

LOSS OF 3.5 MEV ALPHA PARTICLES IN TOKAMAK REACTORS[35]

4.1. Introduction

Studies have recently been taken up in order to estimate the drift loss of energetic particles in tokamak plasmas resulting from finite-giro-radius effects[31-34]. As is generally known, the drift-orbit surface of charged particles shifts outward or inward relative to the magnetic surface according to the angle between the direction of motion of the charged particles and that of the magnetic field due to the rotational transform in a tokamak. And charged particles with a small velocity component along the direction of the magnetic field are trapped in the mirror field inevitably associated with the geometry of the torus. Generally, the displacement of the drift orbit surface of the trapped particles from the magnetic surface is larger than that of the passing particles, and the displacement of the drift surface of the charged particles is evaluated to be approximately proportional to the Larmor radius, hence to the energy of the charged particles. The energies of some of the alpha particles produced by the D-T reaction and of the fast ions produced by neutral beam injection are so high that they escape directly and instantly from the plasma core, owing to the displacement referred to above.

Rome et al.[33] calculated the particle loss region for protons in

the $v_{//}$-$v_{\perp}$ plane and discussed the effects of the loss on neutral injection heating in ORMAK. McAlees[34] has evaluated the range of the loss corn of *3.5 MeV* alpha particles in a tokamak reactor and derived the radial dependence of the loss fraction of alpha particles in a form useful for the design of fusion reactors. In this chapter, the author aims at discussing the material similar to that treated in Ref.[34], but,in more detail, calculates the loss pattern of alpha particles in the vertical cross section of the plasma columm. The sensitivity of some reactor parameters to the loss is studied and the confinement property of *3.5 MeV* alpha particles is examined in the various tokamak reactors.

4.2. Drift Orbits of Alpha Particles

4.2.1. Equations of drift orbit

A drift motion of charged particles in an electromagnetic field is reviewed in detail elsewhere (e.g. Ref.[36]) and will not be repeated here. The drift equation for motion of a single alpha particle in stationary electromagnetic fields $\vec{E}$ and $\vec{B}$ is given by

$$\frac{d\vec{r}}{dt} = \frac{v_{//}}{|\vec{B}|}\, rot\left(\vec{A} + \frac{m_\alpha v_{//} \vec{B}}{e_\alpha |\vec{B}|}\right) \qquad (4.1)$$

where $\vec{r}$, $\vec{A}$ and $\vec{B}$ are the position vector of the guiding center of an alpha particle, the vector potential of magnetic field and the magnetic field, respectively; m_α,e_α and $v_{//}$ are the alpha particle mass, the alpha particle charge and the alpha particle velocity parallel to the magnetic field, respectively. If $\vec{E}$ and $\vec{B}$ are independent of the time, the particle energy E_α and adiabatic invariant μ_α are conserved:

$$E_\alpha = \frac{1}{2} m_\alpha v^2 + e\,\Phi = const. \qquad (4.2)$$

$$\mu_\alpha = \frac{1}{2} m_\alpha v_{\perp}^2 / B = const. \qquad (4.3)$$

where v is the particle velocity, Φ the electrostatic potential, $v_\perp$ the velocity perpendicular to the magnetic field and B the strength of magnetic field.

If the beta value is assumed to be so low that the diamagnetic effects of field plasma can be neglected and that the magnetic surfaces are concentric circle, then the magnetic field in a tokamak is given as follows in the cylindrical co-ordinates shown in Fig.4.1:

$$B_R = B_\theta(r)\,\frac{R_0}{R}\frac{Z}{R} \tag{4.4}$$

$$B_Z = B_\theta(r)\,\frac{R_0}{R}\left(-\frac{R-R_0}{R}\right) \tag{4.5}$$

$$B_\phi = B_{\phi_0}\,\frac{R_0}{R}[1+\delta\cos(m\phi)] \tag{4.6}$$

where R_0, B_{ϕ_0}, δ and m are the major radius, the toroidal magnetic field on the magnetic axis, the relative amplitude of the oscillation in the toroidal magnetic field and the number of coils generating the toroidal field, respectively. Assuming the current density profiles of

$$j = j_0\,[1-\gamma_j(r/a)^{K_j}]^{L_j} \tag{4.7}$$

where j_0 is the current density on the plasma center axis, and γ_j, K_j and L_j(integer) are constants, the poloidal field $B_\theta(r)$ can be given by

$$B_\theta(r) = \frac{\mu_0}{r}\int_0^r j(r')r'dr'$$

$$= \mu_0 j_0 a \sum_{k=0}^{L_j}(-\gamma_j)^k \frac{L_j!}{k!\,(L_j-k)!\,(K_jk+2)}\left(\frac{r}{a}\right)^{K_jk+1} \tag{4.8}$$

where μ_0 is the permeability of free space.

In the ideal case where the field possesses strictly axial symmetry i.e. $\delta = 0$ in Eq.(4.6), the motion of alpha particles is independent of the ϕ-direction, and the drift orbit projected on the R-Z plane is closed. However, in practice, the magnetic field modulation due to the

discrete nature of the toroidal field coils destroys the axial symmetry and creates an open drift surface. Thus, the orbit of alpha particles must be solved with the use of Eq.(4.1) in the strict sense. The particles with sufficiently small $v_{//}/v_{\perp}$ are trapped in the toroidal magnetic well. However, for a small field ripple of $\delta \sim 0.1$ to 1%, the fraction of such trapped particles is negligible small[37]. Hence, in this study, we consider a tokamak reactor with an exactly axisymmetric field.

The equation of motion of alpha particles in an axisymmetric tokamak can be given, in x-y co-ordinates, by

$$\frac{dx}{dt} = \left(v_{//} \frac{B_\theta(r)}{B_\phi} - \frac{E}{B}\right) \frac{x}{r} \tag{4.9}$$

$$\frac{dy}{dt} = -\left(v_{//} \frac{B_\theta(r)}{B_\phi} - \frac{E}{B}\right) \frac{y}{r} + \frac{m_\alpha}{e_\alpha B_\phi R_0} \left(v_{//}^2 + \frac{1}{2} v_{\perp}^2\right) \tag{4.10}$$

where B_ϕ and B are the toroidal magnetic field and total magnetic field. When $\frac{R}{a} q \gg 1$, the following approximate equations hold,

$$B_\phi \simeq B_{\phi_0}, \quad B = \sqrt{B_\phi^2 + B_\theta^2} \simeq B_{\phi_0} \tag{4.11}$$

where B_{ϕ_0} is the magnetic field at the plasma center axis. E is the radial electric field obtained by

$$\vec{E} = -\frac{\partial \Phi(r)}{\partial r} \tag{4.12}$$

In case of axial symmetry, we can obtain an integral of the drift equation directly from Eq.(4.1) as is done in ordinary mechanics,

$$R \left(A_\phi + \frac{m_\alpha}{e_\alpha} v_{//}\right) = const. \tag{4.13}$$

The vector potential A_ϕ is evaluated by Maxwell equation, i.e. $rot\ \vec{A} = \vec{B}$ as follows,

$$\Psi(r) \equiv R A_\phi = -\int_0^r B_\theta(r)\, R_0\, dr$$

$$= -\mu_0 j_0 R_0 a^2 \sum_{k=0}^{L_j} (-\gamma)^k \frac{L_j!}{k!(L_j-k)!(kK_j+2)^2} \left(\frac{r}{a}\right)^{kK_j+2} \qquad (4.14)$$

Using Eqs.(4.2) and (4.3), the perpendicular and longitudinal velocities are given by

$$v_\perp = \sqrt{\frac{2}{m_\alpha} \mu_\alpha B} \qquad (4.15)$$

$$v_{//} = \varepsilon \sqrt{\frac{2}{m_\alpha} (E_\alpha - e_\alpha \Phi(r) - \mu_\alpha B)} \qquad (4.16)$$

$$\varepsilon = \begin{cases} +1 \cdots \vec{v} \cdot \vec{j} \geq 0 \\ -1 \cdots \vec{v} \cdot \vec{j} < 0 \end{cases}$$

Therefore, the drift orbit equation can be obtained from Eqs.(4.13) and (4.16) as follows,

$$P_\phi = -e_\alpha R A_\phi(r) + \varepsilon \sqrt{2m_\alpha (E_\alpha - e_\alpha \Phi(r) - \mu_\alpha B)}\, R \qquad (4.17)$$

where P_ϕ is an integration constant determined by the initial conditions of motion.

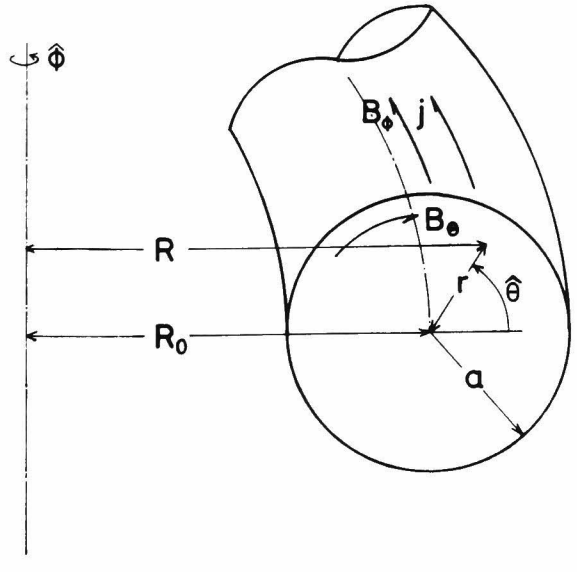

Fig.4.1. Co-ordinate systems.

4.2.2. Property of drift orbit

The reactor parameters shown in Table 4.1 are used for the numerical examples of the drift orbits. The reactor satisfies the zero-power

Table 4.1 Parameters of reference reactor

Major Radius (R_0)	*5 m*	*Minor Radius (a)*	*1.5 m*
Toroidal Magnetic Field (B_ϕ)	*4.0 T*	*Safety Factor (q)*	*2.5*
Plasma Density (n)	*1.0×10^{20} m^{-3}*	*Plasma Temperature (T)*	*8.0 KeV*

conditions given by the trapped-ion-instability law[38]. The drift orbits of alpha particles can be obtained by integrating Eqs.(4.9) and (4.10) on digital computer. Figure 4.2 shows the drift orbits of the alpha particles born at *(0.4,0)* in Cartesian co-ordinates with various pitch-angles. It is assumed that the toroidal current flows uniformly on the plasma vertical cross section and no electrical potential exists.

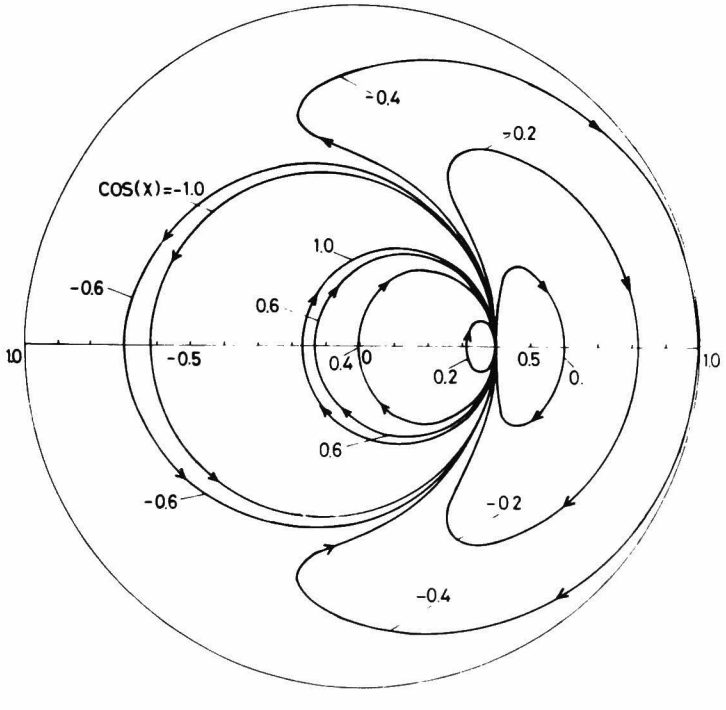

Fig.4.2. Drift orbits of alpha particles born at (0.4,0) in Cartesian co-ordinates. χ denotes the pitch-angle and arrows show the directions of drift motions.

Arrows on the orbits indicate the direction of motions. The trajectories of the alpha particles of $\cos\chi=-0.6$ and -1.0 circle counter-clockwise on x-y plane, while those of the particles of $\cos\chi=0.2$, 0.4, 0.6 and 1.0 go round clockwise. The particle of $\cos\chi=-0.2$ is reflected by the poloidal magnetic mirror caused by the toroidal geometry and go back along another trajectory. The former and the latter are generally called "passing particles" and "banana particles", respectively.

The particles of which trajectories intersect the plasma boundary are lost from plasma core in colliding with mechanical limiter or running away along the magnetic field of divertor. Figure 4.3 illustrates the loss and confinement orbits. The alpha particles with the pitch-angles of $\cos\chi=-0.4$, -0.5 and -0.6 are lost, while the particles with $\cos\chi=-0.3$ are confined. Since the drift orbits of banana particles remarkably deviate from magnetic surface, the banana particles are much more probable to be lost than the passing particles.

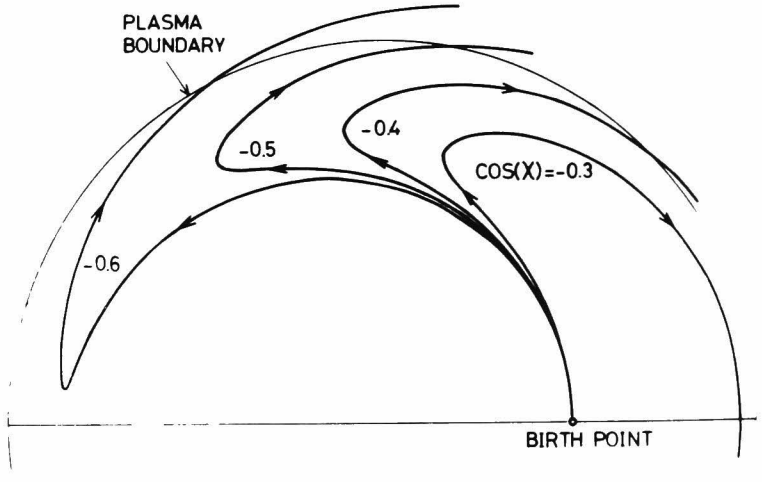

Fig.4.3. The loss and confinement orbits of alpha particles.

The loss of alpha particles from the plasma core causes an electrostatic potential build-up. Figure 4.4 shows the drift orbits similar to Fig.4.2 except for existence of the uniform electric field towards the plasma center (*-500 KV/m*). Since the electric field causes the additional drift of $E \times B$ to the poloidal direction, the number of banana particles decreases and that of passing particles moving clockwise increases. Hence, the radial electric field affects the influence of decreasing the particle loss. However, since the background plasma subject to ambipolar diffusion may prevent the development of an electrostatic potential high enough to change the orbit of *3.5 MeV* alpha particles, the effects of the electrostatic potential on the loss of these alpha particles are assumed to be neglected in this study.

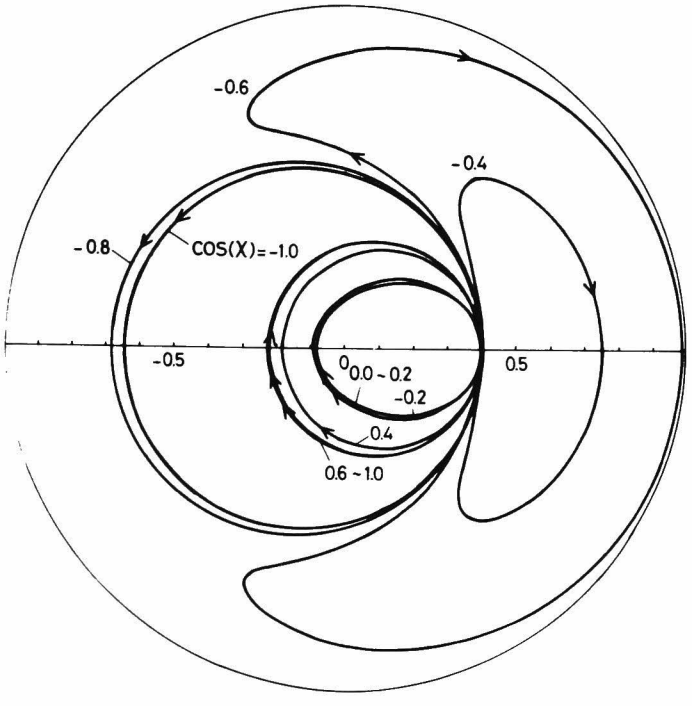

Fig.4.4. Drift orbit in existence of the electric field towards the plasma center axis (-500 KV/m).

4.3. Loss of Alpha Particles

When the alpha particles are assumed to be isotropically born, the loss fraction at the birth point (r_b, θ_b), $f_\ell(r_b, \theta_b)$ is given by using

pitch-angle χ (i.e. the angle between direction of particle velocity and that of magnetic field):

$$f_{\ell}(r_b,\theta_b) = \frac{1}{2}\,(\cos\chi_1 - \cos\chi_2) \tag{4.18}$$

where χ_1 and χ_2 are the minimum and maximum values at which the orbits intersect the plasma surface. The pitch-angle χ can be expressed by the adiabatic invariant μ_α as follows,

$$\begin{aligned}\chi &= \sin^{-1}(v_\perp/v)\\ &= \sin^{-1}(\sqrt{\mu_\alpha B_b/E_0})\end{aligned} \tag{4.19}$$

where E_0 is the kinetic energy of alpha particles, B_b the magnetic field at the birth point. If the maximum and minimum values of the adiabatic invariants with which the alpha particles are lost are found, then the loss fraction can be evaluated from Eqs.(4.18) and (4.19).

The equation for R at which the particles are lost can be given by setting $r=a$ in Eq.(4.17);

$$\frac{1}{R} = \frac{\varepsilon_a}{F(\mu_\alpha)}\sqrt{2m_\alpha\{E_\alpha - e_\alpha\Phi(a) - \mu_\alpha B_{\phi_0}\frac{R_0}{R}\}} \tag{4.20}$$

$$F(\mu_\alpha) = e_\alpha\{\Psi(a) - \Psi(r_b)\} + \varepsilon_b\sqrt{2m_\alpha\{E_\alpha - e_\alpha\Phi(r_b) - \mu_\alpha B_b\}}\,R_b \tag{4.21}$$

where the suffix b denotes the values at the birth position. When the particles are lost, the following inequalities should hold,

$$\frac{1}{R_0+a} < \frac{1}{R} < \frac{1}{R_0-a} \tag{4.22}$$

The quadratic equation of $(\frac{1}{R})$ can be derived by squaring the both sides of Eq.(4.20), and setting $\Phi(a)$ zero,

$$G(\mu_\alpha,R) = (\frac{1}{R})^2 + 2\frac{m_\alpha B_{\phi_0} R_0}{F^2(\mu_\alpha)/\mu_\alpha}(\frac{1}{R}) - 2\frac{m_\alpha E_\alpha}{F^2(\mu_\alpha)} = 0 \tag{4.23}$$

Then, the inequalities which an adiavatic invariant μ_α should satisfy are:

$$G(\mu_\alpha, R_0+a) \leq 0 \tag{4.24}$$

$$G(\mu_\alpha, R_0-a) \geq 0 \tag{4.25}$$

$$\varepsilon_a/F(\mu_\alpha) \geq 0 \tag{4.26}$$

Therefore, the range of μ_α at which the particles are lost is determined by solving Eqs.(4.24)-(4.26).

The loss fraction of alpha particles at minor radius r_b, $f_L(r_b)$ and the total loss fraction F_L can be given by

$$f_L(r_b) = \frac{1}{\pi}\int_0^{\pi} f_\ell(r_b,\theta_b)\, d\theta_b \tag{4.27}$$

and

$$F_L = \frac{\int_0^a r_b S_\alpha(r_b/a) f_L(r_b)\, dr_b}{\int_0^a r_b S_\alpha(r_b/a)\, dr_b} \tag{4.28}$$

where $S_\alpha(r_b/a)$ is the radial profile of alpha particle formation.

4.4. Numerical Analysis

4.4.1 Dependence of loss on reactor parameters

The percentage loss of alpha particles on vertical cross-section of the reference reactor is shown in Fig.4.5, where (a),(b) and (c) correspond to q=*1.0*, *2.5* and *3.5*, respectively and the current profile is assumed to be flat. The contour line of *20%* in Fig.4.5 indicates that *20%* of the alpha particles born on its line are lost from the plasma core.. The loss is highly sensitive to q-value, i.e. toroidal plasma current. When q equals to *1*, the particles born more than *30 cm* inside the plasma surface are almost completely confined. On the other hand, when q is

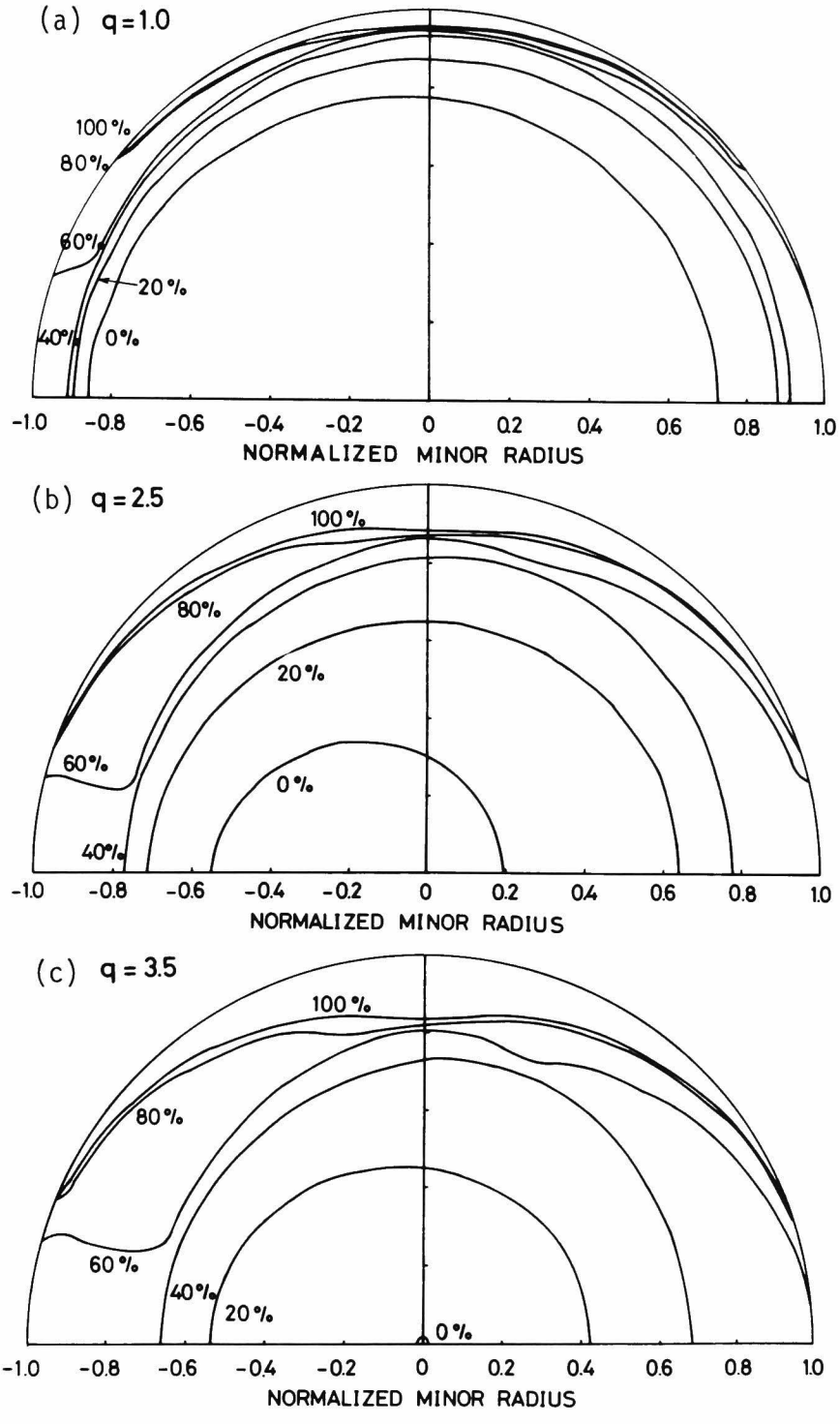

Fig.4.5. Alpha-particle loss patterns at plasma cross-section for three q-values, in assuming the flat current profile.

greater than 3.5, some particles born at the plasma center axis are lost. Figure 4.6 shows a loss pattern similar to that of Fig.4.5(b) except the convex plasma current distribution given by

$$j = j_0[1-0.8(r/a)^4]^3. \qquad (4.29)$$

Although the loss at the region near the plasma surface hardly differs from that of flat current distribution, the confinement of the particles born at the inner region are fairly improved. It is because the current profile peaking does not change q-value near the plasma surface, but makes q-value at the inner region much smaller than the value in the flat current profiles.

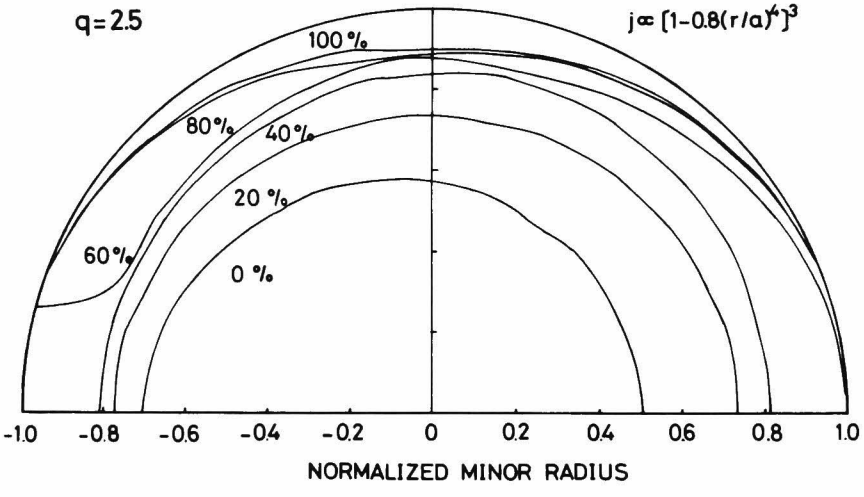

Fig.4.6 Alpha-particle loss pattern for q=2.5 in assuming the convex current profile of $j = j_0[1-0.8(r/a)^4]^3$.

The total loss fraction of alpha particles depends on the radial profile of alpha particle formation, $S_\alpha(r/a)$, which exhibits a strong dependence on both ion density $n(r/a)$ m^{-3} and ion temperature $T(r/a)$ *KeV*; it is expressed by

$$S_\alpha(r/a) = 3.7\times10^{-18}\left(\frac{n(r/a)}{2}\right)^2 exp[-19.9\ T^{-\frac{1}{3}}(r/a)]/T^{\frac{2}{3}}(r/a)\ m^{-3}s \qquad (4.30)$$

in the region of ion temperature less than *10 KeV*.

Since the ion density and temperature profiles depend on unknown factors such as diffusion and conductivity coefficients of the fusion plasma, boundary conditions, fueling and auxiliary heating methods in a fusion reactor, etc., the exact profiles cannot be known. Therefore, the following four cases are assumed for further studies:

(a) $T = const.,\quad n \propto \sqrt{1-(r/a)^3}$

(b) $T = const.,\quad n \propto [1-0.8(r/a)^2]$

(c) $T \propto [1-0.8(r/a)^4]^2,\quad n = const.$

(d) $T \propto [1-0.8(r/a)^4]^2,\quad n \propto [1-0.8(r/a)^2]$

The profiles shown in case (a) are derived from the neoclassical transport theory applied to fusion plasma[39] and the profiles in case (d) are close to those measures in recent tokamak experiments. The current density profile is assumed to be given by the following classical relation[7],

$$j \propto T^{3/2} \qquad (4.31)$$

Figure 4.7 shows the loss of alpha particles from the plasma core with respect to q-value for various profiles referred to above, where the minor

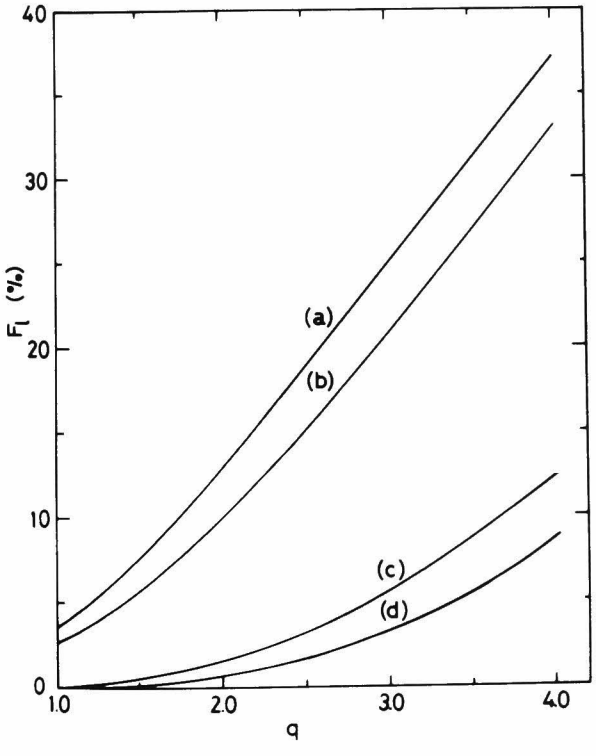

Fig.4.7. Alpha-particle loss vs. q-value for different temperature, T and ion density, n_i profiles, where plasma minor and major radii and toroidal magnetic field are fixed.

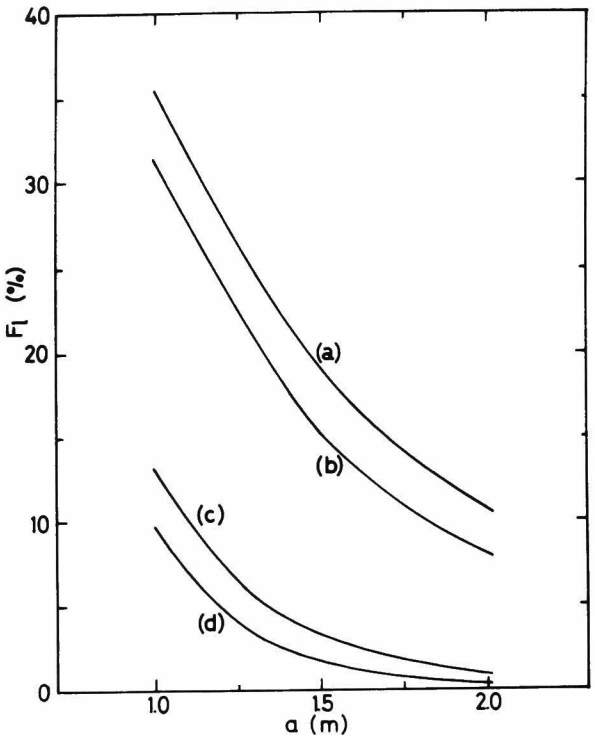

Fig.4.8. Alpha-particle loss vs. plasma minor radius, where major radius, toroidal field and q-value are fixed.

and major radii and toroidal field are kept constant. It is seen that, for q larger than *2.5*, the loss increases proportionally to q. This is because the displacement between magnetic surface and orbit of both trapped and passing particles is proportional to poloidal field. Figure 4.8 shows the dependence of the loss on the plasma minor radius, where major radius, toroidal field and q-value are fixed. The loss decreases roughly at the rate of the inverse square of the minor radius for cases (a) and (b), and decreases at the rate of the inverse cube of the minor radius for cases (c) and (d). Hence, the minor radius becomes less than *1 m*, the rapid increase of loss occurs. Figure 4.9 shows the dependence of the loss on the plasma major radius, when the plasma current is fixed to be *3.6 MA*. The loss is found to vary inversely as $R^{1.4\sim2.0}$. Figure 4.10 is similar to Fig.4.9 except for keeping q-value constant. The loss increases proportionally to major radius. Figure 4.11 shows the dependence on the toroidal magnetic field, when the major and minor radii and q-value are kept constant. The loss decreases proportionally to $B_{\phi_0}^{-1.6}$ in cases (a) and (b) and decreases at the rate of $B_{\phi_0}^{-3\sim-4}$ in cases (c) and (d).

Summarizing the above results, the sensitivity of various parameters to the loss are shown in Fig.4.12 where the density and temperature profiles of case (a) are used. The sensitivity to q-value is calculated

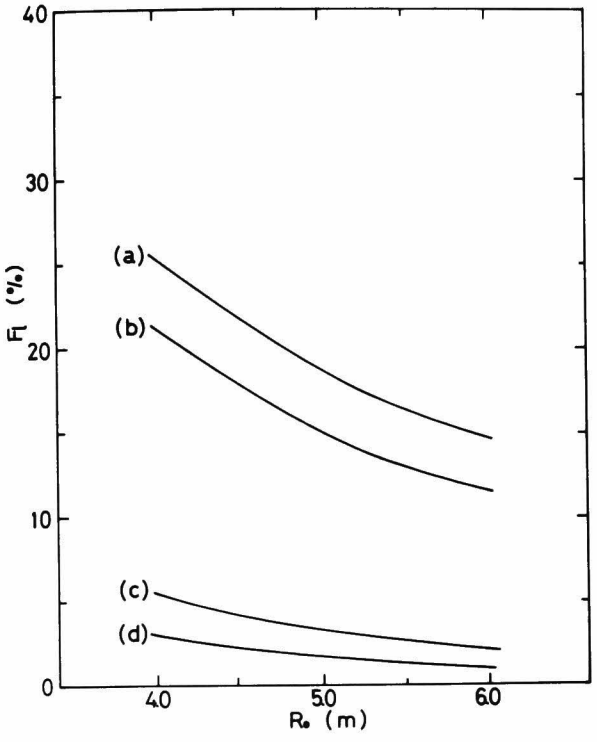

Fig.4.9. Alpha-particle loss vs. plasma major radius, when the plsma current is fixed to be 3.6 MA.

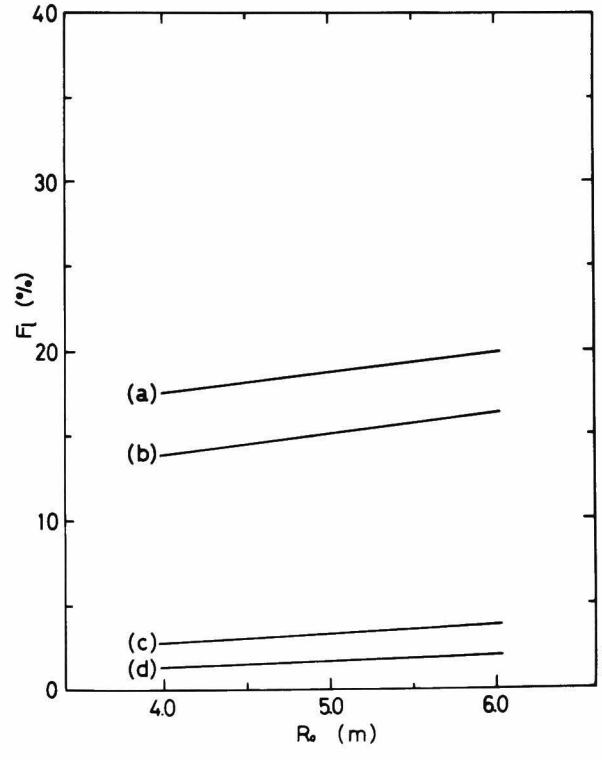

Fig.4.10. Alpha-particle loss vs. plasma major radius, when q-value is fixed to be 2.5.

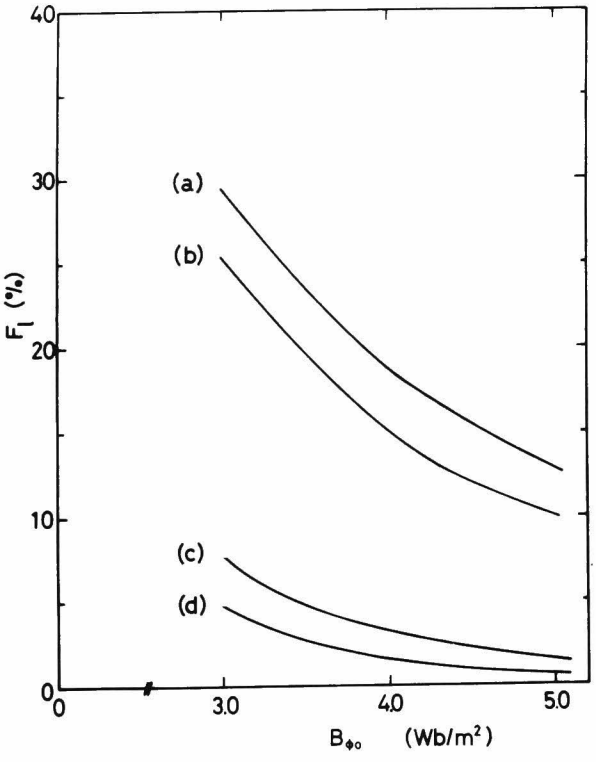

Fig.4.11. Alpha-particle loss vs. toroidal magnetic field, when q-value is 2.5.

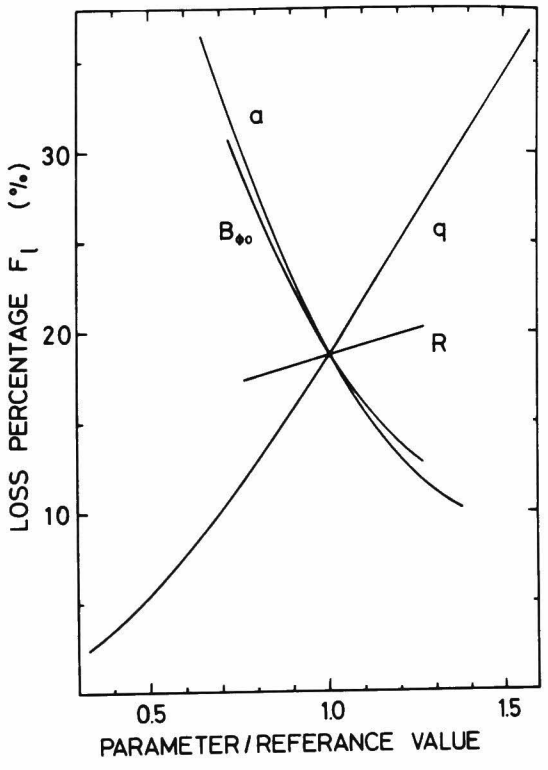

Fig.4.12. Sensitivity of various parameters (a, R_0, B_ϕ and q) to alpha-particle loss.

in varying only toroidal current and the other sensitivity curves are obtained by keeping q constant. The following equation which approximately expresses the sensitivity for the loss can be found from Fig.4.12,

$$F_L \propto q^{1.7} R^{0.3} a^{-2} B_{\phi_0}^{-1.9} \qquad (4.32)$$

When q-value is fixed constant, the minor radius is the most sensitive to the loss and the sensitivity of the major radius is the least.

4.4.2. Property of alpha particle confinement in future tokamaks

The property of confinement of *3.5 MeV* alpha particles are studied in future tokamaks whose parameters are illustrated in Table 4.2 , where

Table 4.2. Parameters of various future tokamak reactors*

(i) Near Term Experimental Devices

	HFITR	TFTR	T-20
a (m)	0.6	0.85	2.0
R_0 (m)	2.0	2.48	5.0
q	3	3	2.3
B_ϕ (T)	14	5.2	3.5
T (KeV)	$14[1-(r/a)^2]$	$6[1-(r/a)^2]^2$	$10[1-(r/a)^2]^2$
n_i (m^{-3})	$1.2\times10^{21}[1-(r/a)^3]$	$4\times10^{19}[1-(r/a)^4]$	$2\times10^{19}[1-(r/a)^4]$
j (MA/m^2)	3.7†	$4.45[1-(r/a)^2]^3$	$1.94[1-(r/a)^2]^3$
F_L (%)	2.89	0.90	0.106

(ii) Mid Term Experimental Reactors

	ETES-1	ORNL-EPR	JAERI
a (m)	1.6	2.25	2
R_0 (m)	6.4	6.75	10
q	2.5	2.5	1.5
B_ϕ (T)	5.0	4.8	6.0
T (KeV)	$14[1-(r/a)^2]$	$6[1-(r/a)^2]^2$	$10[1-(r/a)^2]^2$
n_i (m^{-3})	$5\times10^{19}[1-(r/a)^4]$	$6.5\times10^{19}[1-(r/a)^4]$	1.0×10^{20}
j (MA/m^2)	$2.0[1-(r/a)^2]^3$	$1.81[1-(r/a)^2]^3$	$2.55[1-(r/a)^2]^3$
F_L (%)	0.296	1.1×10^{-2}	6.9×10^{-3}

(iii) Long Range Power Reactors

	CULHAM 1	ORNL	UWMAK-II
a (m)	2.8	2.5	5
R_0 (m)	10.5	12.5	13
q	1.4	2.5	2.3
B_ϕ (T)	2.45	9.5	3.57
T (KeV)	$20[1-(r/a)^2]^2$	$20[1-(r/a)^2]^2$	$13.2[1-(r/a)^2]^2$
n_i (m^{-3})	$2.0\times10^{20}[1-(r/a)^4]$	$1.8\times10^{20}[1-(r/a)^4]$	$7.3\times10^{19}[1-(r/a)^4]$
j (MA/m^2)	$1.06[1-(r/a)^2]^3$	$1.93[1-(r/a)^2]^3$	$0.76[1-(r/a)^2]^3$
F_L (%)	2.9×10^{-2}	3.9×10^{-4}	1.6×10^{-4}

*The plasma and reactor parameters are quoted from Ref.[40].
†This current profile is exceptionally assumed to be flat.

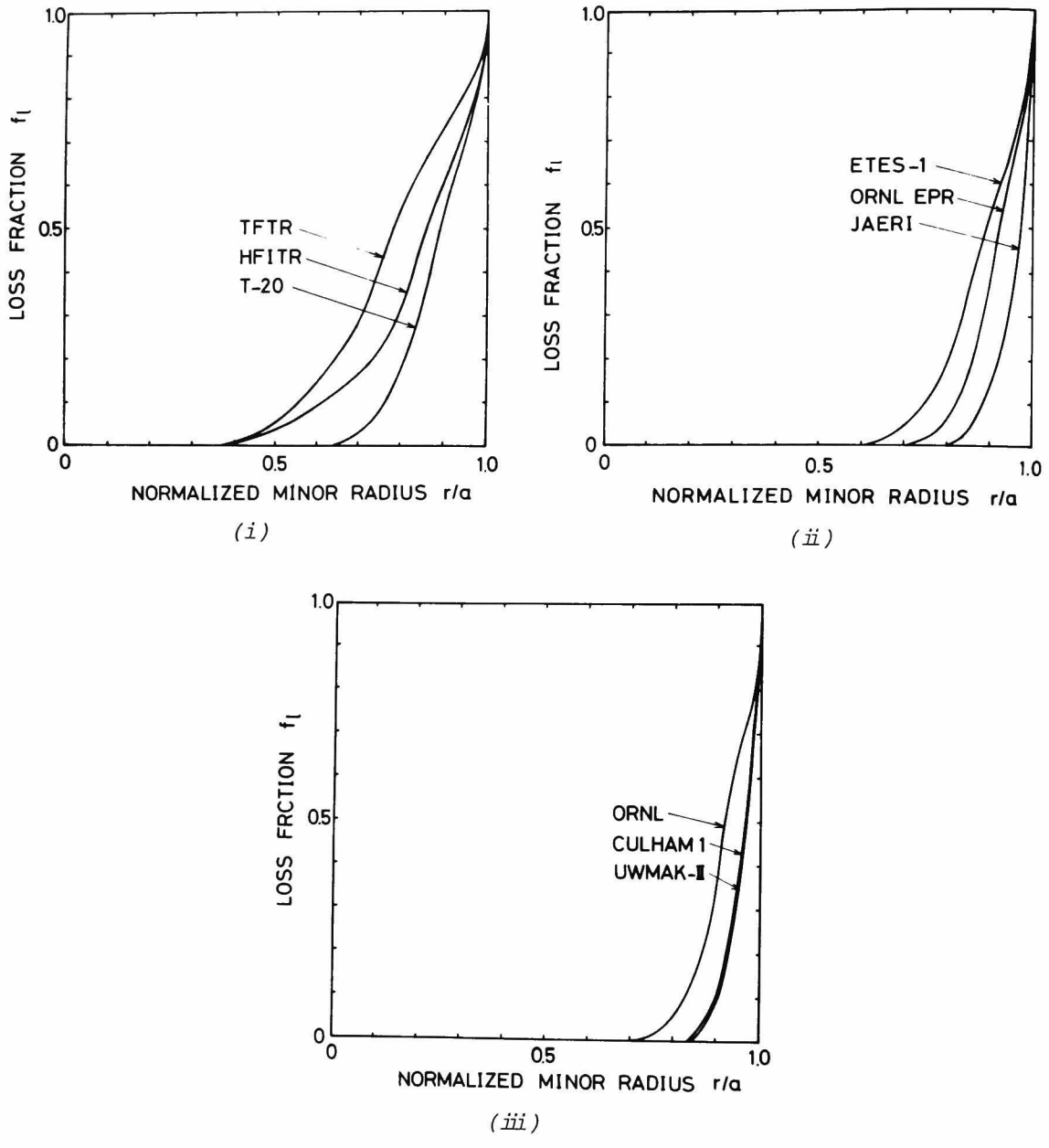

Fig.4.13. Alpha particle loss fraction at the radial position normalized by minor radius in (i) Near Term Experimental Devices, (ii) Mid Term Experimental Reactors and (iii) Long Range Power Reactors.

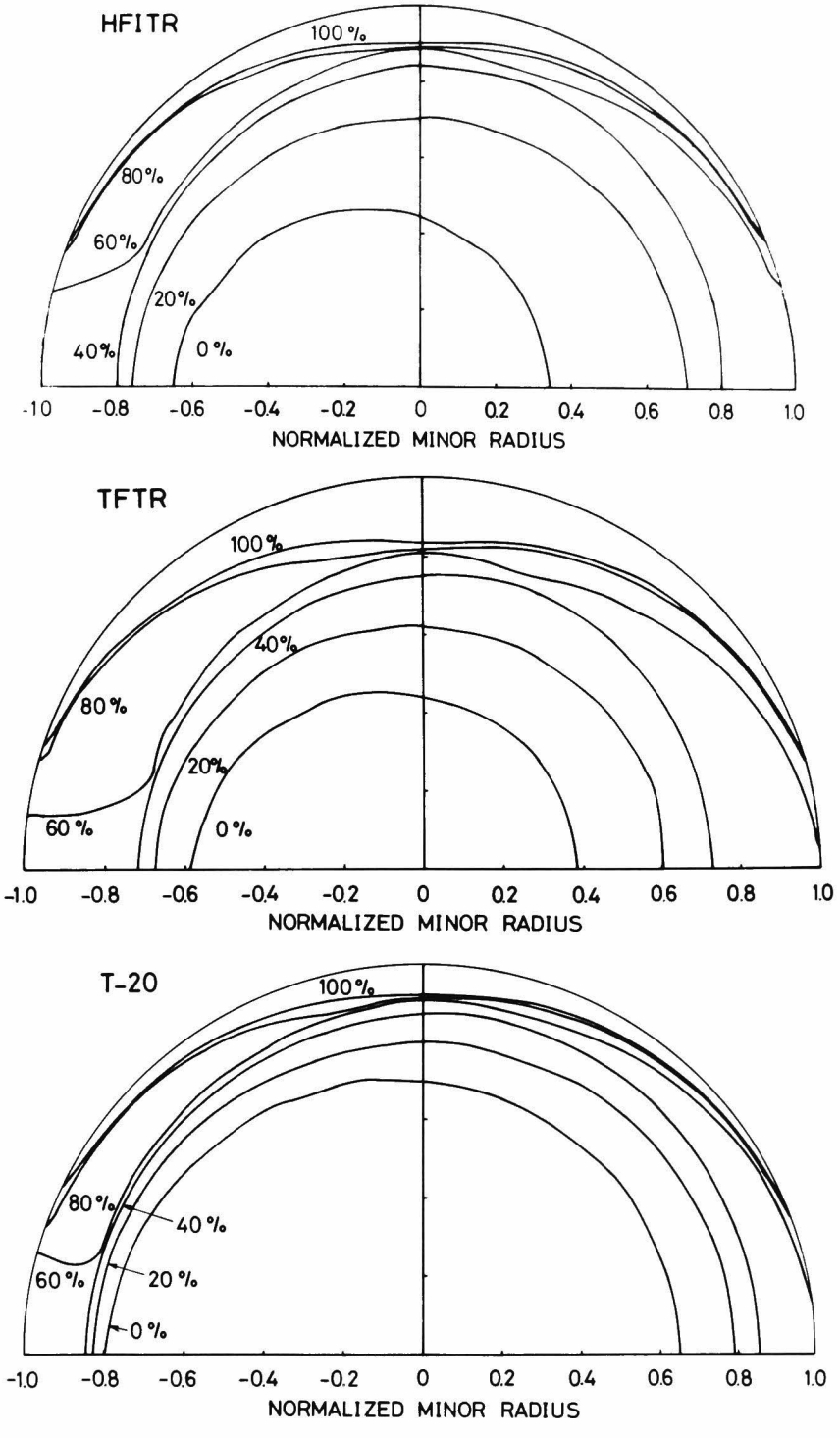

Fig.4.14. Alpha-particle loss patterns at plasma cross section in Near Term Experimental Devices.

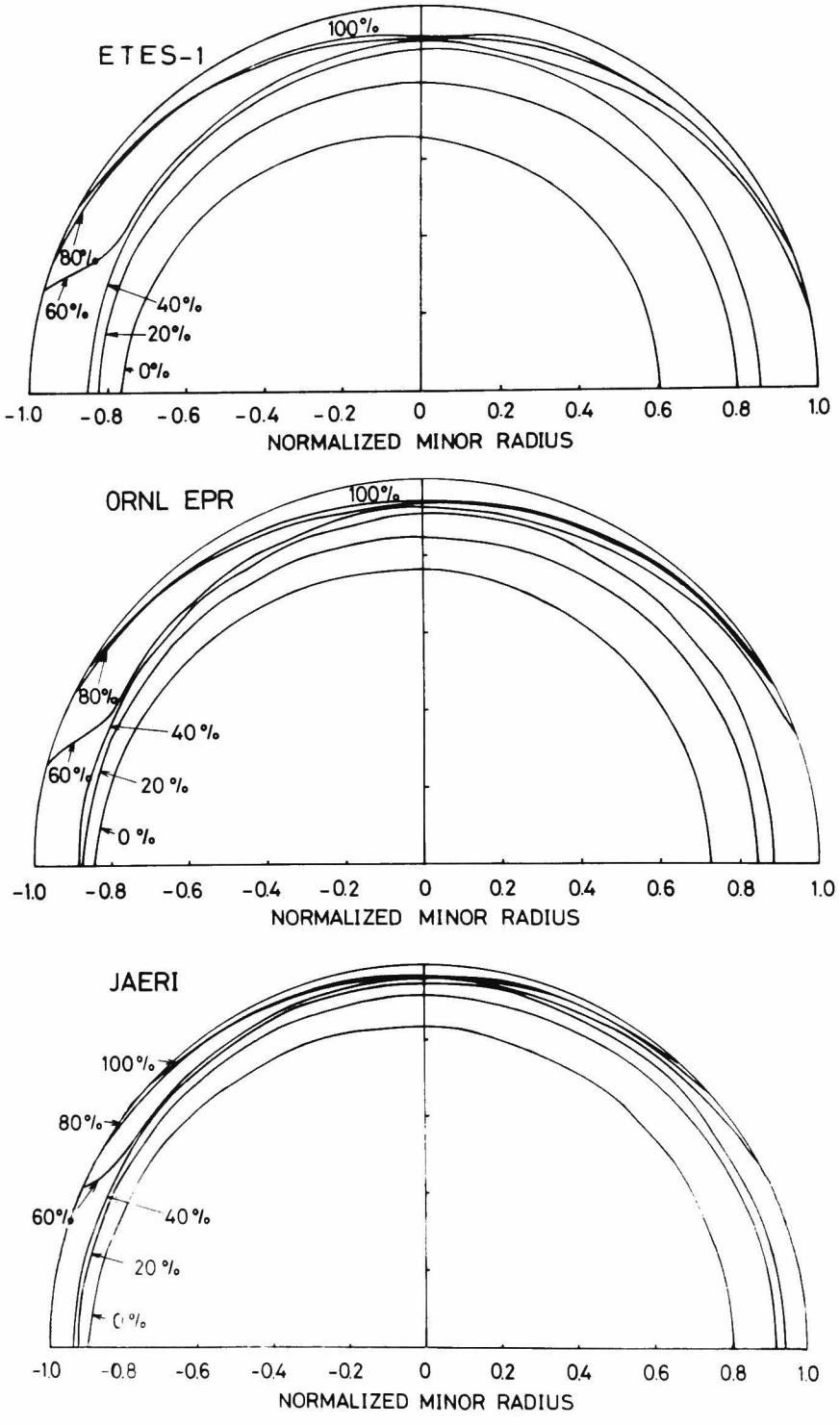

Fig.4.15. Alpha-particle loss patterns at plasma cross sections in Mid Term Experimental Reactors.

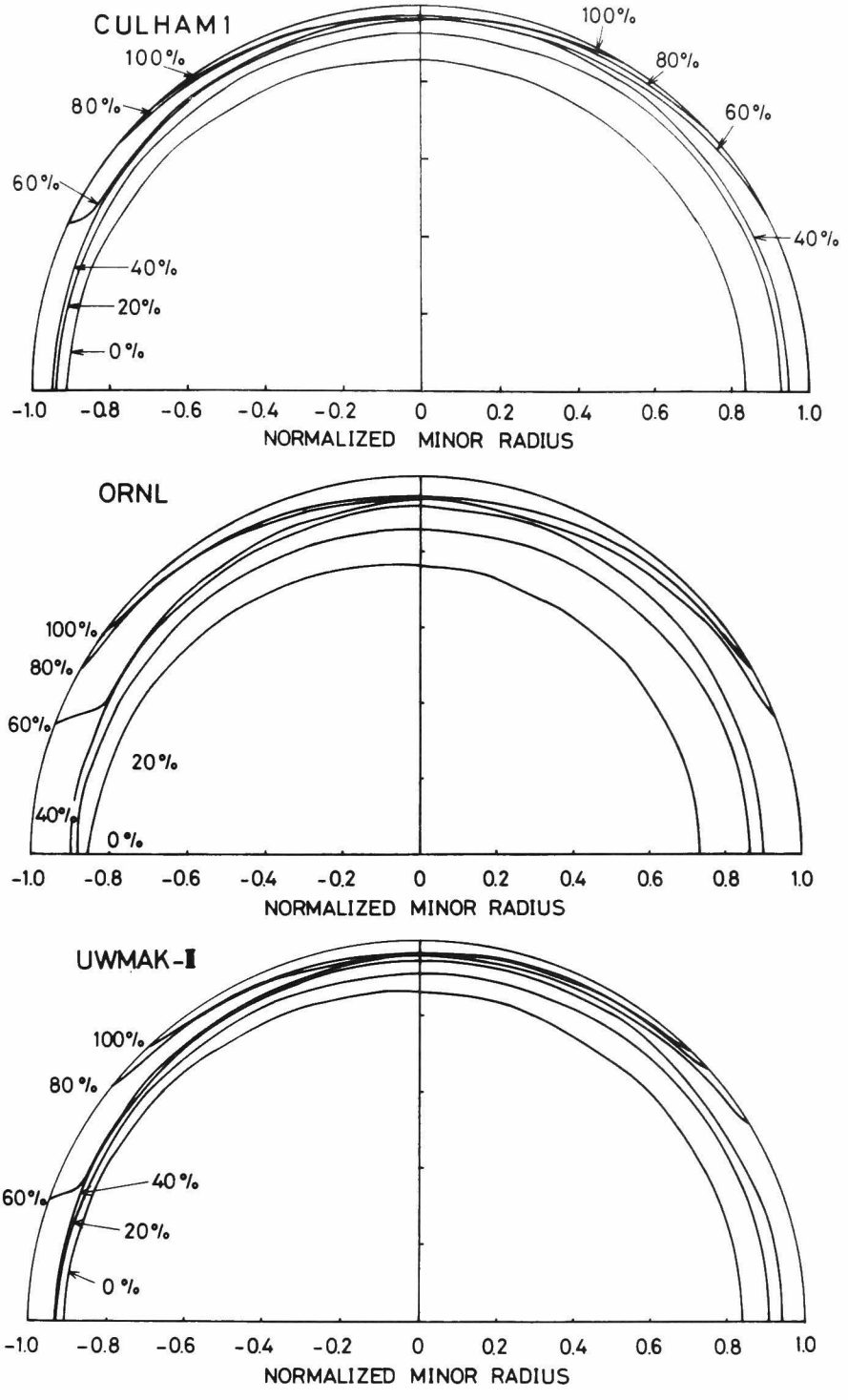

Fig.4.16. Alpha-particle loss patterns at plasma cross sections in Long Range Power Reactors.

hypothetical profiles of density and temperature are taken for numerical calculations. Figure 4.13 shows the loss fractions at the radial position normalized by minor radius in various devices. Near term experimental devices (HFTR, TFTR, T-20) poorly confine the alpha particles and the loss of alpha particles may cause the serious problems such as production of impurities due to the bombardment of the first wall, negative potential build-up, plasma rotation due to the electric field, etc. The confinement property are fairly improved in the mid term experimental reactors (ETES-1, ORNL EPR, JAERI). The problems caused by the loss of alpha particles are fairly reduced but should be taken into consideration for the reactor design. The long range power reactors (CULHAM 1, ORNL, UWMAK II) could almost completely confine the particles. The effects of alpha-particle loss may be neglected in the power reactors, since the loss flux of alpha particles reduces to much less than *1%* of that of zero power experimental reactors.

Figure 4.14 depicts the loss patterns in various reactors. Since many particles born near the plasma surface are lost even in the power reactors, it may be necessary to attain the profile of temperature which is low enough for fusion reactions to be negligible at the region neighboring the plasma surface.

4.5. Concluding Remarks

The orbit loss of *3.5 MeV* alpha particles in axially symmetric tokamak reactors is evaluated and it is found that the loss depends on the plasma minor and major radii, the plasma current and the current density profiles. A large power reactor could confine alpha particles (*3.5 MeV*) completely, while small reactors such as zero power experimental devices, fission-fusion hybrid reactors and two-ion-component (beam driven) tokamak reactors will not do so. When the plasma minor radius is less than *1.5 m* and the plasma current is below *3 MA*, the the plasma core of the reference reactor with the relatively flat density and temperature prifiles. Although the power loss due to the loss of alpha

particles is found to be comparable to bremsstrahlung in small tokamak reactors, alpha heating does not play an important role in plasma heating, and the loss of alpha particles has only a slight effect on the power balance of the fusion plasma core. On the other hand, the damage of first wall and divertor materials, and the production of impurity ions due to bombardment of *3.5 MeV* alpha particles escaping from the plasma core may cause the serious problems. The electrostatic potential build-up by the loss of alpha particles not only helps the impurities to enter the plasma core but also causes the rotation of field plasma in the toroidal and poloidal directions. The plasma rotation may cause the serious influence on the plasma equilibrium. The more detailed studies of these problems related to the loss of alpha particles must be carried out for the sake of construction of the future D-T burning devices.

Chapter 5

LOSS OF ALPHA PARTICLES DURING SLOWING DOWN IN AN AXISYMMETRIC TOKAMAK REACTOR[49]

5.1. Introduction

The containment properties of alpha particles born in a tokamak reactor have been studied in several works. McAlees[34] calculated the radial dependence of the loss fraction of the 3.5 MeV alpha particles and the source profiles of alpha particles modified by drift motions. Stringer[32] obtained an analytical expression for the alpha particle source distribution considering the drift orbit effects. Ohnishi et al [35] studied the sensitivity of alpha particle loss to some tokamak reactor parameters by using numerical integrations of the drift orbits. Kolesnichenko et al.[41] studied the confinement of alpha particles, together with the streaming of these particles towards the first wall in an axisymmetric tokamak. Hively et al.[42] examined the fusion-product bombardment of the first wall in several tokamak facilities. Petrie and Miley[43] obtained alpha-heating profiles and *500 KeV* alpha particle source profiles by tracking the alpha-particle trajectories of each phase space group. All these studies are concerned solely with *3.5 MeV* alpha particles, except for Ref.[43], where the effects of the pitch-angle-scattering are excluded.

The alpha particles slow down from *3.5 MeV* to about *400 KeV* mainly

through Coulomb collisions with the electrons, keeping the direction of the initial velocities. When the energy decreases below *400 KeV*, the alpha particles come to collide with the field ions as well as with the electrons and suffer pitch-angle-scattering. However, if high-Z impurities exist in the plasma core, the alpha particles suffer large-angle scattering even in the energy range above *1 MeV*. Hence, the effects of pitch-angle-scattering should not be neglected in the study of alpha particle loss during slowing-down, particularly in a contaminated plasma. In this chapter, the effects of pitch-angle scattering on the loss of alpha particles during slowing-down and on the alpha heating profiles are studied by using Monte-Carlo calculations.

5.2. Analytical Model and Assumptions

A DT-fueled axisymmetric tokamak reactor is taken for the numerical model. It is also assumed that the cross-sections for magnetic surfaces are concentric circles and no radial electric field exists. The loss of alpha particles brings about the radial electric field, which causes an additional drift due to $E \times B$ and has the effect of decreasing the alpha particle loss. However, the $E \times B$ drift will only be effective when the electrical potential has reached a value comparable to the alpha particle energy. Such a potential would drastically affect the transport of the field plasma. This problem is very interesting, but beyond the scope of the present work.

Although the containment properties of the alpha particles strongly depends on the radial profile of the toroidal current density[33,35,42], we shall, for simplicity, assume a flat current distribution. On these assumptions, the magnetic field is given by (Fig.4.1.)

$$B = \frac{\mu_0 j r}{2} \left(\frac{R_0}{R}\right) \hat{\theta} + B_{\phi_0} \left(\frac{R_0}{R}\right) \hat{\phi} \qquad (5.1)$$

where μ_0 is the permeability of free space, j the current density,

R_0 the major radius, and B_{ϕ_0} the toroidal magnetic field at the central plasma axis. The hat (^) denotes the unit vector.

The plasma and reactor parameters shown in Table 4.1 are used in this study. The plasma density and temperature are taken to have the following hypothetical profiles:

$$T_i(r) = T_e(r) = 8 \ (KeV) \tag{5.2}$$

$$n_e(r) = 1.0\times10^{20}[1-\gamma_e(r/a)^{K_e}]^{L_e} \ (1/m^3) \tag{5.3}$$

$$n_I(r) = n_{I_0}[1-\gamma_I(r/a)^{K_I}]^{L_I} \ (1/m^3) \tag{5.4}$$

where T_i and T_e are the ion and electron temperatures, n_e and n_I the electron and impurity densities and K_ℓ, L_ℓ and γ_ℓ (ℓ=e,I), parameters used in the numerical calculations. The density of the DT ions n_i can be obtained from the charge neutrality conditions,

$$n_i(r) = n_e(r) - Z_I n_I(r) \tag{5.5}$$

where Z_I is the charge number of the impurity ions.

The production rate of alpha particles at the minor radius r is given by[6]

$$S_\alpha(r) = 1.63\times10^{-23} \ n_i^2(r) \ (1/m^3 sec) \tag{5.6}$$

The alpha particles are assumed to be born isotropically in velocity space. (Appendix B)

5.3. Properties of Alpha Particles in a Tokamak Plasma

5.3.1. Coulomb collisions

It may be assumed that alpha particles slow down only through Coulomb interactions with the field plasma, i.e. there are no micro-instabilities affecting the slowing-down of the alpha particles. Although an Alfven wave may interact with the alpha particles during

slowing-down in a tokamak fusion plasma and affect the slowing-down process[44,45], its effect is assumed to be negligible in this study. Hence, when the alpha particles slow down in a plasma with a Maxwellian distribution, the rate of change of the mean deviation of the longitudinal velocity is given by[47]

$$<\Delta V_{//}> = - \sum_{j=e,i,I} q_\alpha (1+\frac{m_\alpha}{m_j}) \frac{n_j \mu(v_j^2)}{m_\alpha v_\alpha^2} \quad (m/s^2) \tag{5.7}$$

The rates of change of the mean square deviations of the longitudinal and perpendicular velocities are given by

$$<(\Delta V_{//})^2> = \sum_{j=e,i,I} \frac{K}{v_j} \frac{\mu(v_j^2)}{2v_j^2} \quad (m^2/s^3) \tag{5.8}$$

and

$$<(\Delta V)_\perp^2> = \sum_{j=e,i,I} \frac{K}{v_j} (\mu(v_j^2) + \mu'(v_j^2) - \frac{\mu(v_j^2)}{2v_j^2}) \quad (m^2/s^3) \tag{5.9}$$

$$v_j^2 = v_\alpha^2/v_j^2 = v_\alpha^2/(2kT_j/m_j)$$

$$q_\alpha = 1.015\times10^{21}\ e_\alpha^2 e_j^2 \ell n\Lambda/m_\alpha \quad (Kg\ m^6/s^4)$$

$$K = 2.030\times10^{21}\ n_j e_\alpha^2 e_j^2/v_\alpha m_\alpha^2 \quad (m^2/s^3)$$

where $\mu(x)$ denotes the error function, $\ell n\Lambda$ is the Coulomb logarithm which is assumed to be *20* and k is 1.603×10^{-16} *(Joul/KeV)*.

Figure 5.1 shows the change of the mean velocity deviation per second versus the energy of the alpha particles for a pure DT plasma($Z_{eff}=1$) and for a plasma contaminated by *1%* F_e ions($Z_{eff}=7.5$), where the electron density n_e is 1.0×10^{20} *(1/m³)* and the temperatures of electrons, ions and impurities are assumed to be *8 KeV*. In the case of a pure DT plasma, the alpha particles with energies above *400 KeV* slow down mainly through collisions with the electrons. When the energy decreases

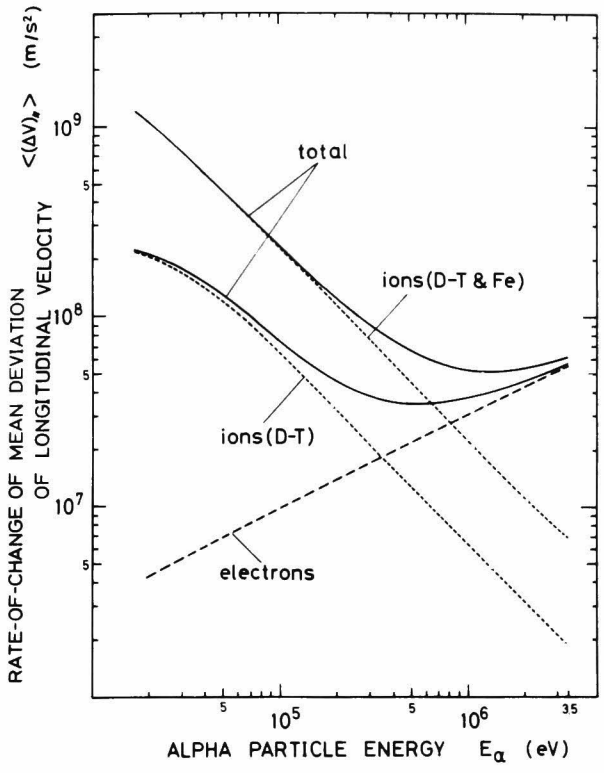

Fig.5.1. Rate-of-change of the mean velocity deviation for alpha particles during slowing down in a pure DT plasma and in a plasma contaminated by 1% Fe ions. The dotted curves and broken curves present the rate-of-change due to the ions and the electrons, respectively.

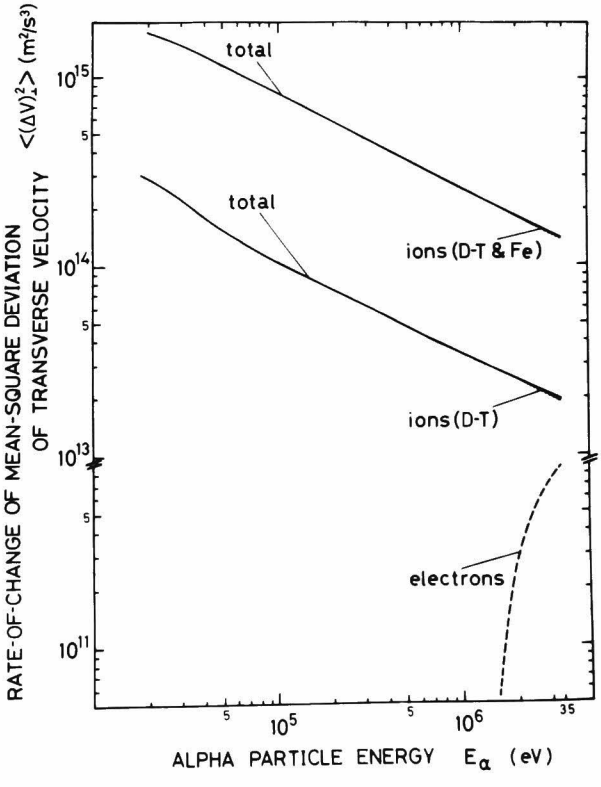

Fig.5.2. Rate-of-change of the mean square deviation of perpendicular velocity of alpha particles.

below *300 KeV*, collisions with the field ions are the dominant process during slowing-down. In a contaminated plasma, the rate of change of velocity in the low energy range of the alpha particles is several times as large as in the pure DT plasma.

Figure 5.2 presents the relation between the alpha-particle energy and the change of the mean square deviation of the perpendicular velocity per second, which is related to the rate of pitch-angle scattering. The electrons make little contribution to the pitch-angle scattering, while the ions scatter the alpha particles through large angles. The alpha particles in the pure DT plasma slow down without suffering the large angle scattering until their energy reaches *400 KeV*. When the energy drops below *400 KeV*, they are deflected in a direction perpendicular to the initial velocity. However, note that the alpha particles in the contaminated plasma are subject to remarkable pitch-angle scattering, even when the energy is about *1 MeV*.

5.3.2. Drift orbit and velocity

Three constants of motion of the alpha particles,i.e.

Magnetic moment; $\mu_\alpha = \frac{1}{2} m_\alpha v_\perp^2/B$ *(5.10)*

Canonical angular moment; $P_\phi = e_\alpha R A_\phi + m_\alpha v_{//} R$ *(5.11)*

Total particle energy; $E_\alpha = \frac{1}{2} m_\alpha (v_{//}^2 + v_\perp^2)$ *(5.12)*

are conserved within a time interval much shorter than the relaxation times due to Coulomb collisions. The relaxation times are given as follows[47]:

Slowing down time; $\tau_s = - \frac{v_\alpha}{<\Delta v_{//}>}$

Deflection time; $\tau_d = \frac{v_\alpha^2}{<(\Delta v)_\perp^2>}$

Energy exchange time; $\tau_\varepsilon = \dfrac{v_\alpha^2}{4\langle(\Delta v_{//})^2\rangle}$

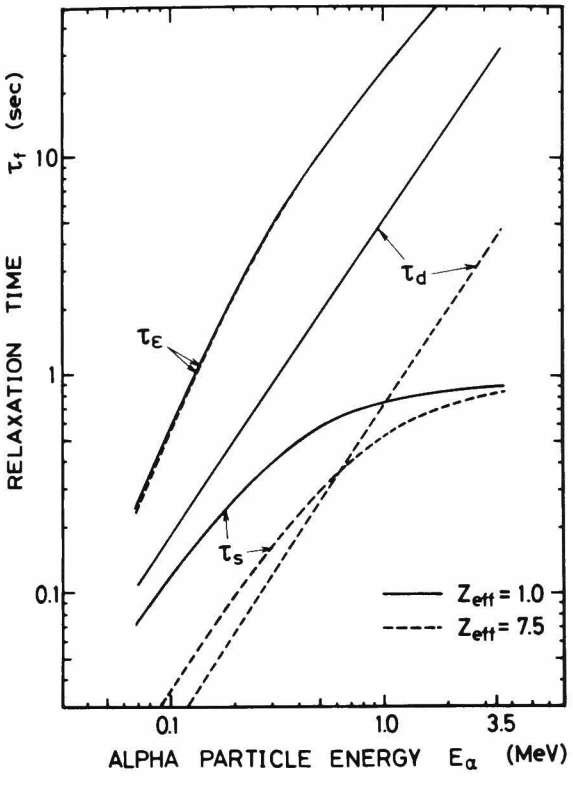

Fig.5.3. Relaxation times of the alpha particles with various energies in a pure DT plasma(solid curves) and in a highly contaminated plasma(broken curves), where T_e=8 KeV and n_e= 1.0×10^{20} $1/m^3$.

Figure 5.3 shows the relaxation times. The following inequalities hold for a pure DT plasma;

$$\tau_\varepsilon > \tau_d \gg \tau_s \quad \cdots\cdots\cdots \quad E_\alpha \gtrsim 1\ MeV,$$

$$\tau_\varepsilon > \tau_d > \tau_s \quad \cdots\cdots\cdots \quad E_\alpha < 1\ MeV,$$

and for a highly contaminated plasma (Z_{eff}=7.5);

$$\tau_\varepsilon \gg \tau_d > \tau_s \quad \cdots\cdots\cdots \quad E_\alpha \gtrsim 1\ MeV,$$

$$\tau_\varepsilon \gg \tau_d \simeq \tau_s \quad \cdots\cdots\cdots \quad E_\alpha < 1\ MeV.$$

Therefore, the slowing-down time τ_s can be taken as the characteristic

time for non-conservation of the above invariants.

The motion equation for the guiding center is derived from Eqs. (5.10)-(5.12) as follows[34],

$$e_\alpha\left(\frac{\mu_0 j R_0}{4}\right) r^2 + \varepsilon m_\alpha v_{//} R = P_\phi \tag{5.13}$$

$$\varepsilon = \begin{cases} +1 \cdots & \vec{v}\cdot\vec{j} \le 0 \\ -1 \cdots & \vec{v}\cdot\vec{j} > 0 \end{cases}$$

where P_ϕ is the integration constant. The drift velocity V_d in the x-y plane (Fig.4.1) is given by

$$V_d = \sqrt{v_x^2 + v_y^2} \tag{5.14}$$

where $$v_x = v_{//}\left(\frac{\mu_0 j}{2}\right)\frac{y}{B_{\phi_0}} \tag{5.15}$$

$$v_y = -v_{//}\left(\frac{\mu_0 j}{2}\right)\frac{x}{B_{\phi_0}} + \frac{m_\alpha}{e_\alpha BR}\left(v_{//}^2 + v_\perp^2/2\right) \tag{5.16}$$

Figure 5.4a shows numerical examples of the **drift orbit** for various pitch angles χ, i.e. for the angles between the magnetic field and the velocity of the alpha particles. In Fig.5.4b, we see the drift velocities corresponding to the drift orbits shown in Fig.5.4a. The vertical and horizontal axes denote the velocity normalized to the maximum velocity and the relative position along the orbit, respectively. The velocity of the banana-trapped particles (e.g. $\cos\chi=-0.4$) is found to change substantially during one bounce time. The drift velocity should be carefully dealt with in estimating the collision points.

5.3.3. Slowing down motions

Since alpha particles moving in the plasma change both speed and direction of their motion because of collisions with the field electrons and ions, Eqs.(5.10)-(5.12) cannot be assumed to be invariable under

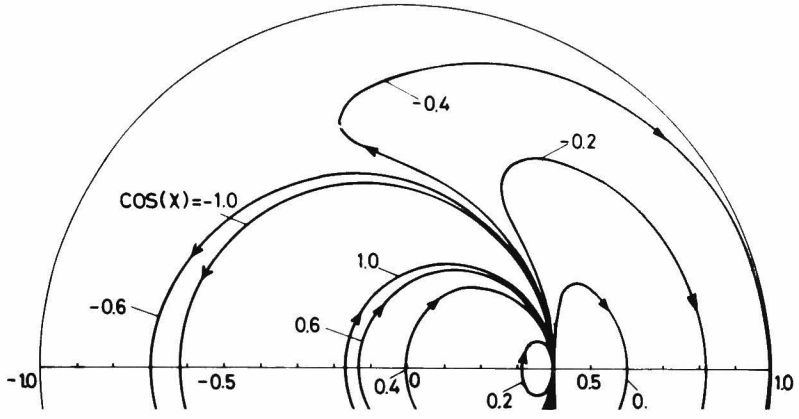

Fig.5.4a. The drift orbit of 3.5 MeV alpha particles for various pitch angles χ. The particles are born at x=0.4 on x axis.

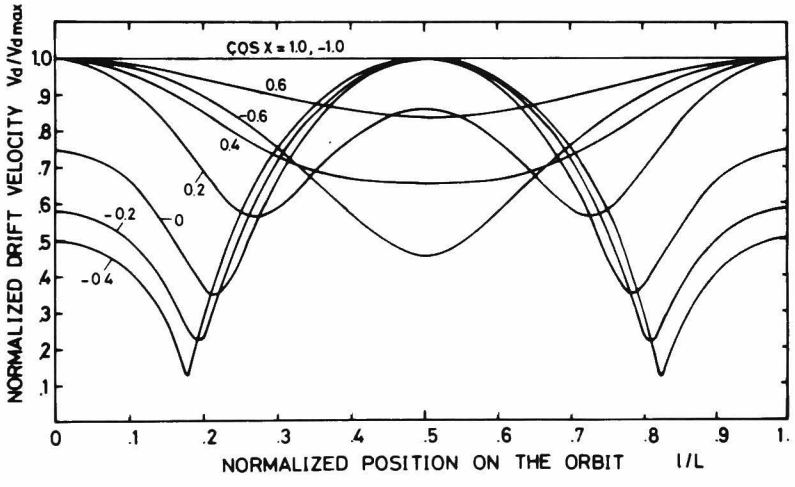

Fig.5.4b. The drift velocities on the orbits. The vertical and horizontal axes present the velocity normalized by the maximum velocity ($V_d/V_{d\,max}$) and the relative position on the orbit (ℓ/L), where L is the length of bounce orbit and ℓ being the orbit length from birth point to objective point.

all circumstances. Jassby, et al.[46] studied the ripple trapping of fast ions produced by neutral-beam injection in tokamaks by meams of the Monte-Carlo technique making use of the angle scattering operater. We shall now use the following collision model to obtain the particle motion during slowing-down: The Coulomb collisions are simulated by discrete collisions taking place every time interval Δt ($\tau_b \ll \Delta t \ll \tau_s$, τ_b is the orbit bounce time) at one point on the bounce orbits[48]. When the field particles have Maxwellian distributions, the changes in longitudinal and perpendicular velocities due to Coulomb collisions during the time interval Δt *sec* correspond to Gaussian distributions with mean values (m) and variances (σ^2) as follows:

$$m_{/\!/} = \langle \Delta V_{/\!/} \rangle \cdot \Delta t, \quad m_{\perp} = 0 \tag{5.17}$$

and

$$\sigma^2_{/\!/} = \langle (\Delta V_{/\!/})^2 \rangle \cdot \Delta t, \quad \sigma^2_{\perp} = \langle (\Delta V)^2_{\perp} \rangle \cdot \Delta t \tag{5.18}$$

Therefore, the changes in velocity can be obtained by using normal random numbers.(Appendix B) The collision point on the orbit can be determined by random numbers with a collision probability density P_c as follows:

$$P_c \propto 1/(V_d \, \tau_s) \tag{5.19}$$

The orbit after a collision is successively calculated from the amount of the velocity change and the collision point. The trajectories during slowing-down can be obtained from this collision model.

Figure 5.5a and b illustrates the motions of the alpha particles during slowing-down in a tokamak plasma (Z_{eff}=7.5). Figure 5.5a and b, respectively, correspond to trajectories from *3.5 MeV* to *350 KeV* and from *3.5 MeV* to the energy at which the particles are lost. Although the changes in magnitude of the velocity do not affect the orbits substantially,the changes in direction of the velocity alter the orbits remarkably. The trajectories are not much different from the birth

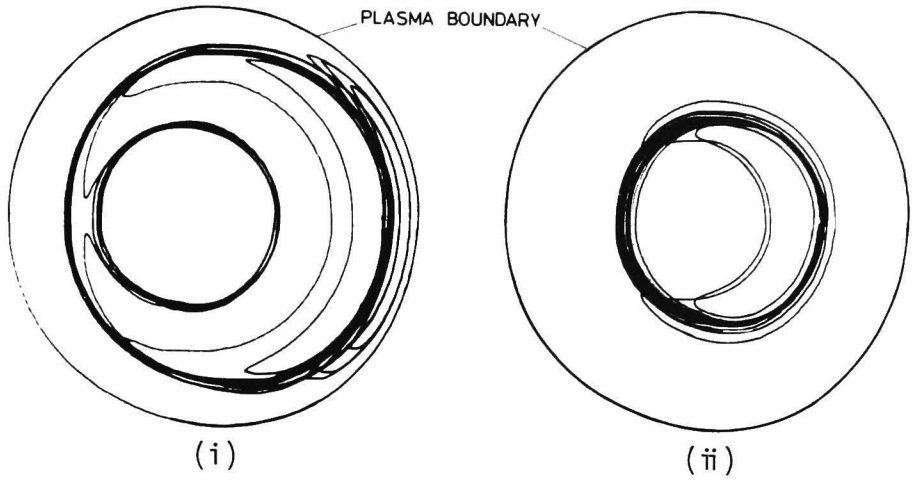

a) Thermalization

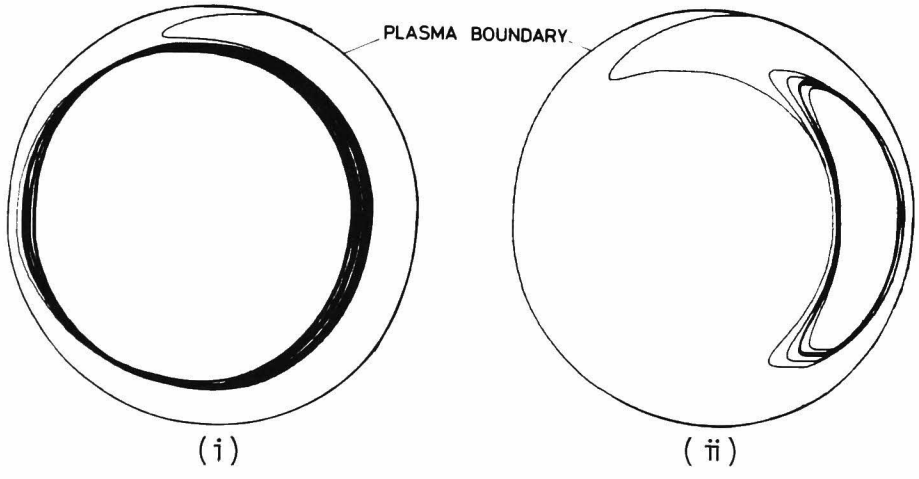

b) Loss

Fig.5.5. The trajectories of alpha particles during slowing down in a plasma (Z_{eff}=7.5). a) and b) show the cases of thermalization and loss, respectively. The energies at which the particles are lost from the plasma surface are 840 KeV in (i) and 2.13 MeV in (ii).

orbits until the energy of the alpha particles drops below *1 MeV*. When the alpha particles slow down to several hundred *KeV*, they suffer the pitch-angle scattering due to the field ions and change the trajectories appreciably.

Figure 5.6 shows the azimuthally-averaged loss fractions of the alpha particles which are assumed to be isotropically born with various energies. When the ion density is taken to be $n_i = 1.0 \times 10^{20} \sqrt{1-(r/a)^3}$ $1/m^3$, the percentages of total loss of *3.5 MeV* and *350 KeV* particles are roughly calculated to be *18%* and *2%*, respectively. Hence, the alpha particles with an energy below *350 KeV* may almost completely be confined in the reactor. We can compute the loss fractions and energy deposition profiles of the alpha particles by tracking the individual orbits from birth until they are lost or slow down to *350 KeV*.

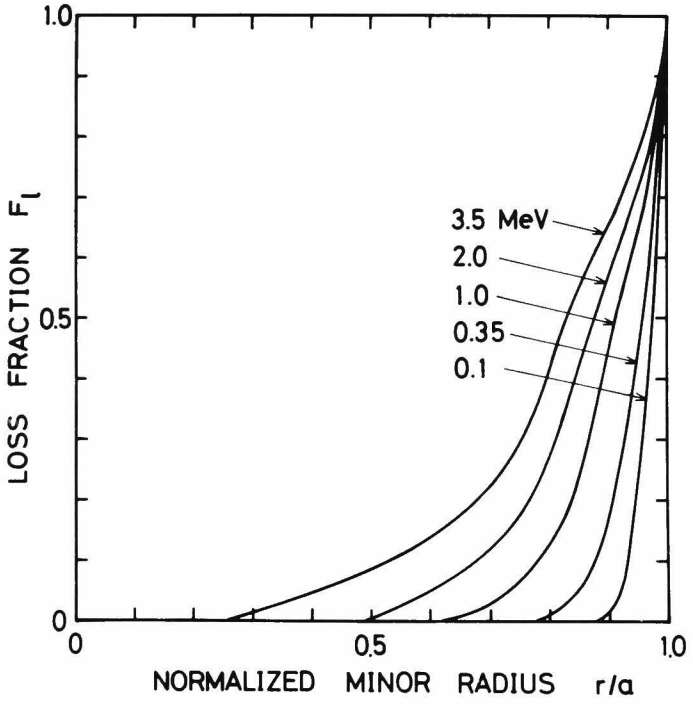

Fig.5.6. Loss fractions of alpha particles at normalized minor radius r/a in assuming that they are born isotropically with various energies.

5.4. Numerical Results

5.4.1. Loss

Figure 5.7 shows the energy spectra of the loss flux of alpha particles at the plasma surface for pure DT plasma ($Z_{eff}=1$) and for plasmas contaminated by iron ions ($Z_{eff}=4.3$ and 7.5). The loss of 3.5 MeV alpha particles is about 18% and the loss of the alpha particles during slowing

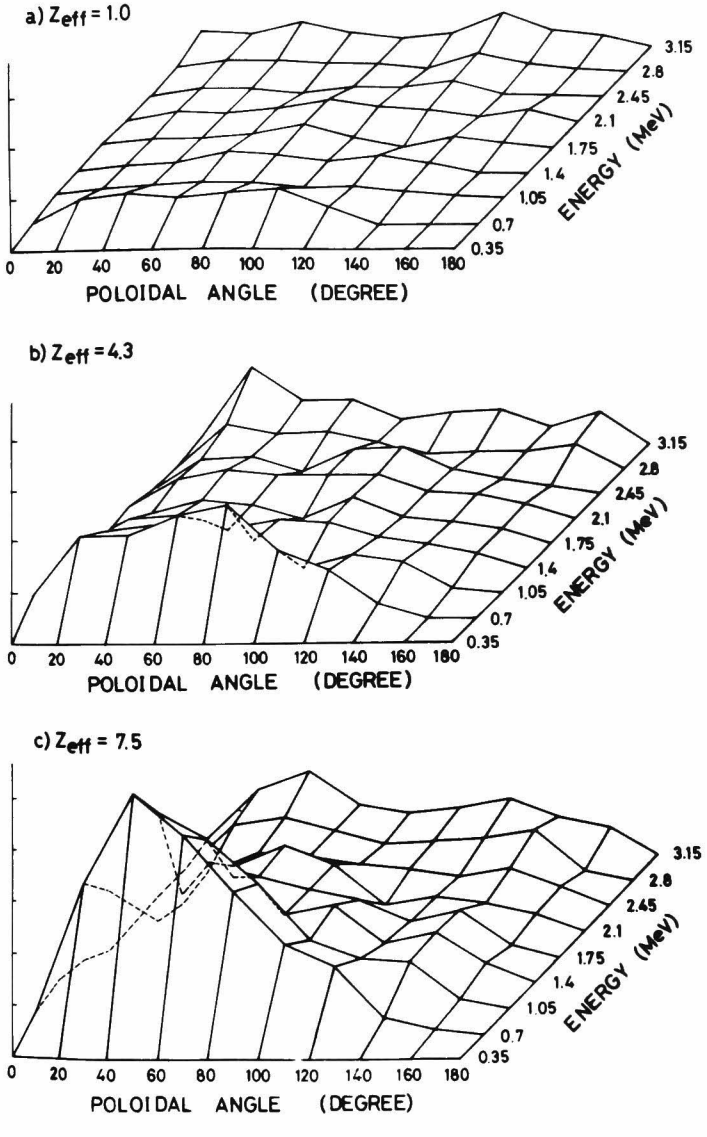

Fig.5.7. Energy spectra of the alpha particles lost from the plasma column, where T=8 KeV, $n_e=1.0\times10^{20}\times\sqrt{1-(r/a)^3}\,1/m^3$ and $n_I=n_{I0}\sqrt{1-(r/a)^3}\,1/m^3$. (a),(b) and (c) correspond to the cases of a pure DT plasma and contaminated plasmas, respectively. The vertical axes denote the loss flux in arbitrary units.

down amounts to *1%* for Z_{eff}=*1*, *4%* for Z_{eff}=*4.3* and *8%* for Z_{eff}=*7.5*. While the slowing down alpha particles are almost completely confined in the pure DT plasma, the loss cannot be neglected in the contaminated plasmas. The loss flux for a plasma with Z_{eff}=*7.5* has a peak energy close to *700 KeV* at a poloidal angle of *40°*. It is found from the calculations that the alpha particles with an energy less than *350 KeV* are completely confined.

Figure 5.8 shows the relationship between the loss and the effective charge number for the following radial density profiles for impurities and electrons:

Case *1*: $\gamma_I = \gamma_e = 0.8$, $K_I = K_e = 2$ and $L_I = L_e = 1$

Case *2*: $\gamma_I = \gamma_e = 0.8$, $K_I = K_e = 2$, $L_I = 2$ *and* $L_e = 1$

In Case *1*, the loss of *3.5 MeV* alpha particles is *15%* irrespective of

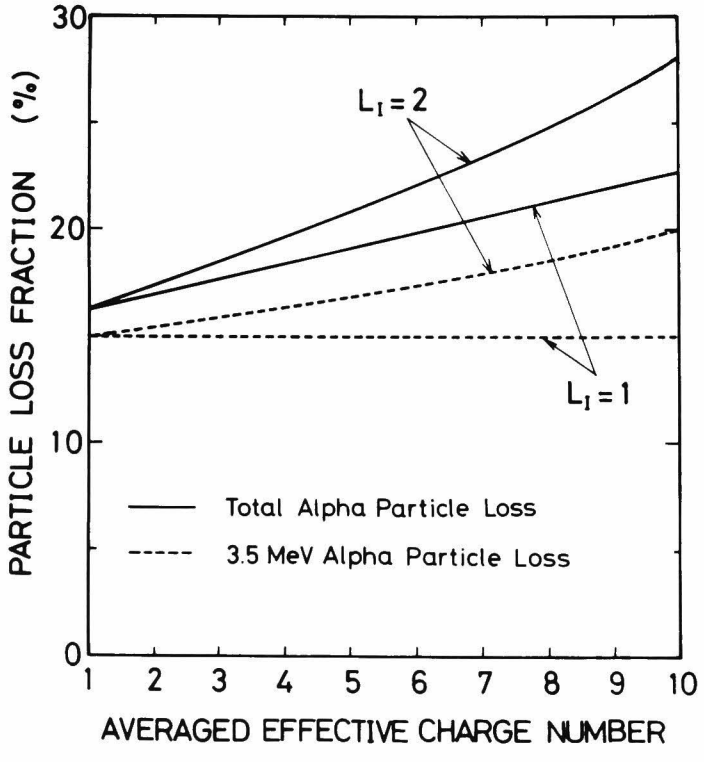

Fig.5.8. The relationship between the loss and the averaged effective charge number of a plasma, where T=8 KeV, $n_e = 1.0\times10^{20}\{1-0.8\times(r/a)^2\}$ *1/m*^{3} *and* $n_I = n_{I0}\{1-0.8(r/a)^2\}^{L_I}$ *1/m*^{3}.

the effective charge number. The total loss is about 16% for $Z_{eff}=1$ and increases proportionally to Z_{eff}. In Case 2, i.e. when the impurities are concentrated at the plasma center, the loss of the 3.5 MeV alpha particles rises as the effective charge number increases. This is due to the fact that the birth rate of the alpha particles increases in the outer region because of the concentration of impurities.
The loss fraction during slowing-down increases at the same rate as in Case 1, because the loss during slowing-down depends only on the rate of pitch-angle scattering, i.e. on the effective charge number.

5.4.2. Alpha heating

Figure 5.9 shows the birth profiles of the alpha particles and the relative power density deposited by the alpha particles until their energy decreases to 350 KeV. The alpha heating profile becomes smaller and flatter compared to the birth profiles because of the particle loss and the drift motion of the alpha particles. This tendency becomes a little more pronounced as the effective charge number of the plasma increases. The reason is that the pitch-angle-scattering caused by the impurity ions enhances the particle loss and makes the alpha particles move in broader regions.

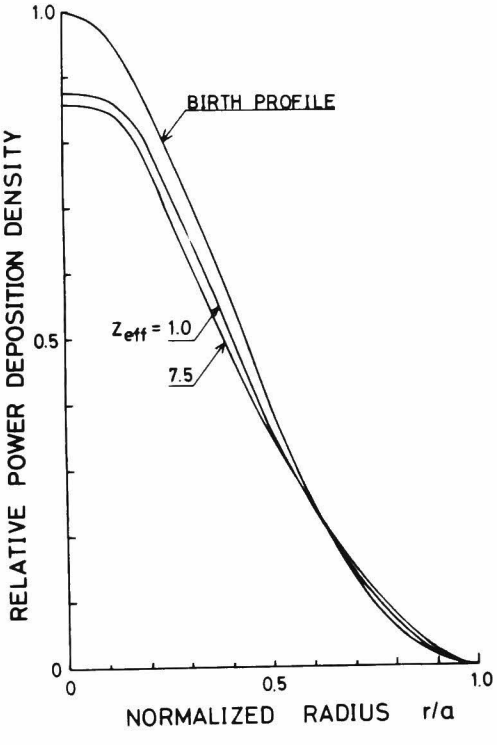

Fig.5.9. The relative power density deposited by alpha particles, where T=8 KeV, $n_i=1.0\times10^{20}\{1-(r/a)^2\}$ $1/m^3$ and $n_I=n_{I0}\{1-(r/a)^2\}$ $1/m^3$.

5.5. Concluding Remarks

It is concluded that alpha particles during the slowing-down process are almost completely confined in the pure DT plasma, but the loss during slowing-down cannot be neglected in a plasma contaminated by heavy impurities compared with the *3.5 MeV* particle loss. Above all, the loss of alpha particles with energies below *1 MeV* becomes large. The results suggest an important aspect of plasma diagnosis. Since the loss of alpha particles during slowing-down depends only on pitch-angle scattering, i.e. on the effective charge number, it may be possible to determine the concentration of impurities by measuring the energy spectrum of the alpha particles which are lost from the plasma surface. The power density deposited by the alpha particles is reduced by the loss of the alpha particles and its profile becomes broader than the birth profile due to drift motion. This tendency is a little more pronounced as the effective charge number of plasma increases.

Although the alpha particle trajectories are tracked from *3.5 MeV* to only *350 KeV* in this study, we can follow the alpha particles to energies of several tens of *KeV*. Therefore, the source profiles of the thermalized alpha particles can be found using the Monte-Carlo code developed for this study. We do not consider the effects of the radial electric field and the profiles of the current density and plasma temperature, but it is possible to include these effects in our Monte-Carlo code.

SUMMARY AND CONCLUSION

Conclusions obtained by this study were described in detail at the end of each chapter in this thesis. The major results and conclusions are briefly summarized.

Thermal stability and start-up characteristics of a D-T fusion reactor were studied in chapter 1 by making use of the static relation between the ion temperature and the injection beam energy. The reactor must be operated inevitably in the thermally unstable region for attaining the high Q value (= energy multiplication ratio) and some proper control mechanisms are necessary to stabilize the operation in the unstable region. The exploitation of the adequate stabilizing methods would be an important problem for a future power reactor. The beam energy of several tens *KeV* is sufficient for ignition of a D-T plasma, but some sequence controls of neutral beam energy, fueling rate, magnetic field,etc.are necessary for aiming at the operation in the unstable region.

Chapter 2 was devoted to investigating the effects of the slowing down process of energetic particles on the dynamics and control, which have been lightly treated as a pure time delay in chapter 1. Comparison between the instantaneous slowing-down approximation and the multigroup slowing-down approximation on the plasma heating by the energetic ions was made on the eigenvalues of the linearized dynamic equations as well as on the numerical integration of the non-linear dynamic equations.

The proper treatment of the slowing down process by the multi-group formulation indicates that the slowing down process does not appreciably change the critical temperature of the thermal stability but cannot be neglected in discussing the dynamics and control problems.

In chapter 3, the study on the reactor parameters of self-sustaining Cat.D tokamak presented the possibility of realizing the compact reactor comparable to the D-T reactor keeping the average beta value to be reasonable ($\beta < 10\%$). The dynamic transition processes from D-T reactor to Cat.D reactor were also studied by numerical integration of the kinetic equations of a plasma core with the initial conditions of D-T burning mode. The Cat.D operating mode is attained in roughly three hundreds seconds only by adequate controls of the fuel injection rate and mixture. The long transition time does not seem to provide us any serious problems in practice, because the reactor operating in the arbitrary D-T mixture mode continuously supplies the output power through the transition process. The feedback control to keep the stationary operation is one of the most important tasks for the Cat.D reactor, because the Cat.D plasma is unstable in wider temperature region than the D-T plasma.

Chapter 4 treated the orbit loss of *3.5 MeV* alpha particles born in axially symmetric tokamak reactors. When the plasma minor radius is less than *1.5 m* and the plasma current is below *3 MA*, the alpha particles more than ten per cent of the formation are lost from the reference reactor. The loss of the alpha particles causes the serious problems such as the damage of the first wall and divertor materials, the production of impurities due to bombardment of the alpha particles, the electrostatic potential build-up and the rotation of field plasma. The studies of these problems related to the alpha particle loss must be carried out for the sake of construction of the future D-T burning devices.

In the last chapter, the loss of alpha particles during slowing down process was studied by using the Monte Carlo technique. The alpha

particles are almost completely confined in the pure D-T plasma, but the loss during slowing down cannot be neglected in a plasma contaminated by heavy impurities compared with the *3.5 MeV* particle loss. Above all, the loss of alpha particles with energies below *1 MeV* becomes large. The power deposition density due to the alpha particles is reduced by the loss of the alpha particles and its profile becomes broader than the birth profile. This tendency is a little pronounced as the effective charge number of plasma increases.

Appendix A

FUSION REACTION TIMES AND SLOWING DOWN TIMES

Let us consider the collision between particle *1* and particle *2*, which have the number densities n_1 and n_2 and the distributions $f_1(v_1)$ and $f_2(v_2)$, respectively. The averaged reaction rate per second and unit volume are given by the sixfold integral over all space[50].

$$R_{12} = \int_{\vec{v}_1 \vec{v}_2} d\vec{v}_1 d\vec{v}_2 [n_1 f_1(\vec{v}_1)][n_2 f_2(\vec{v}_2)]\ v_r \sigma_{12}(v_r) \qquad (A.1)$$

where $v_r = |\vec{v}_1 - \vec{v}_2|$ and $\sigma_{12}(v_r)$ is the fusion cross section between particle *1* and particle *2*. The averaged quantity $\langle \sigma v \rangle_{12}$ is useful and is given by

$$\langle \sigma v \rangle_{12} = \int_{\vec{v}_1 \vec{v}_2} d\vec{v}_1 d\vec{v}_2 f_1(\vec{v}_1) f_2(\vec{v}_2)\ v_r \sigma_{12}(v_r) \qquad (A.2)$$

Using terms of energy variable $kU = m_1 v_r^2/2$, where $k = 1.602 \times 10^{-19}$ *(joul/eV)*, $\sigma_{12}(U)$ is approximated within *i*th interval of energy by fitting the curves of Ref.[51] and the values listed in Ref.[6] as follows,

$$\sigma_{12}(U) = \sum_{j=1}^{N} C_{ij}\, U^{N-j} \qquad (U_i \le U \le U_{i+1},\ i = 1, \cdots M) \qquad (A.3)$$

where M is the number of mesh points of energy variable.

If f_1 and f_2 are both Maxwellian at temperature T, it is possible to perform the integrals Eq.(A.2) by changing variables to the center mass systems. After simple calculations, we obtained the following equation.

$$\langle\sigma v\rangle_{12}^{M} = \frac{4}{\sqrt{2\pi m_1}} \left(\frac{m_r}{m_1 kT}\right)^{3/2} \int_0^{\infty} dU\, kU\, \sigma_{12}(U)\, \exp\left(-\frac{m_r kU}{m_1 kT}\right)$$

$$= \left(\frac{2}{\pi k}\right)^{1/2} \frac{2}{m_1^2} \left(\frac{m_r}{T}\right)^{3/2} \sum_{i=1}^{M} \sum_{j=1}^{N} C_{ij}\, J_{N+1-j}(U_i) \qquad (A.4)$$

where

$$m_r = m_1 m_2/(m_1+m_2) \quad \text{and} \quad J_n(U_i) = \int_{U_i}^{U_{i+1}} U^n \exp\left(-\frac{m_r U}{m_1 T}\right) dU\ .$$

When particle *1* is the particle injected or produced in fusion events with the single velocity $\vec{v}_B$,

$$f_1(\vec{v}_1) = \delta(\vec{v}_1 - \vec{v}_B)\ . \qquad (A.5)$$

By substituting Eq.(A.5) into Eq.(A.2), the averaged reaction rate between the superthermal particle and the maxwellian particles can be written by

$$\langle\sigma v\rangle_{12}^{B} = \left(\frac{m_2}{2\pi kT}\right)^{1/2} \frac{1}{v_1} \int_0^{\infty} dv_r\, v_r^2\, \sigma(v_r)\, \exp\left[-\frac{m_2}{2kT}(v_1^2 + v_r^2)\right]$$

$$\times\left\{\exp\left(\frac{m_2}{kT} v_1 v_r\right) - \exp\left(-\frac{m_2}{kT} v_1 v_r\right)\right\} \qquad (A.6)$$

Transforming into the energy integral and carring out the integral, the following equation is obtained.

$$\langle\sigma v\rangle_{12}^{B} = \frac{1}{m_1}\sqrt{\frac{2m_2 k}{\pi E_B}} \sum_{i=1}^{M} \sum_{j=1}^{N} C_{ij} \sum_{k=0}^{2N+2-2j} T^{N+1-j-\frac{k}{2}} E_B^{k/2} \binom{2N+2-2j}{k}$$

$$\times\{I_{2N+2-2j-k}(u_i^-) - I_{2N+2-2j-k}(u_i^+)\} \qquad (A.7)$$

where

$$E_B = \frac{1}{2} m_1 v_B^2 / k$$

$$I_n(u_{i+1}) = \int_{u_i}^{u_{i+1}} u^n \exp(-\frac{m_2}{m_1} u^2)\, du$$

$$u_i^{\pm} = (\sqrt{U_i} \mp \sqrt{E_B})/\sqrt{T}$$

The reaction time of Maxwellian particles of i-species, τ_{ri}^M is defined by

$$\tau_{ri}^M = \frac{2}{(1+\delta_{ij})\, n_j \langle\sigma v\rangle_{ij}^M} \qquad (A.8)$$

$$\delta_{ij} = \begin{cases} 1 & \cdots\cdots\ i=j \\ 0 & \cdots\cdots\ i\neq j \end{cases}$$

where n_t is the total field ion density.
The reaction time of a superthermal particle of i-species in Maxwellian field particles of j-species τ_{ri}^B is also defined by

$$\tau_{ri}^B = \frac{1}{n_j \langle\sigma v\rangle_{ij}^B} \qquad (A.9)$$

where n_j is the density of field ions.

Figure A.1 shows the reaction times between Maxwellian particles versus field ion temperature. Figure A.2 presents the reaction times between superthermal ions and thermal ions. Figure A.3 shows the thermalization times of superthermal ions versus particle energy, where the particles in the parenthesize denote the field ions. Since the reaction times between superthermal and thermal ions are about ten times larger than the slowing down times, it is reasonable to neglect the reaction of superthermal ions during slowing-down process.

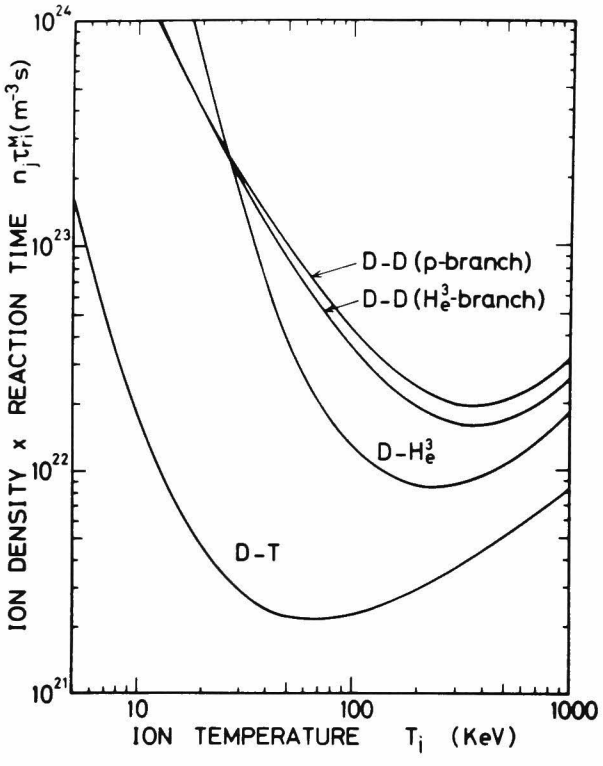

Fig.A.1. Products of field ion density and reaction time of Maxwellian particles vs. ion temperature.

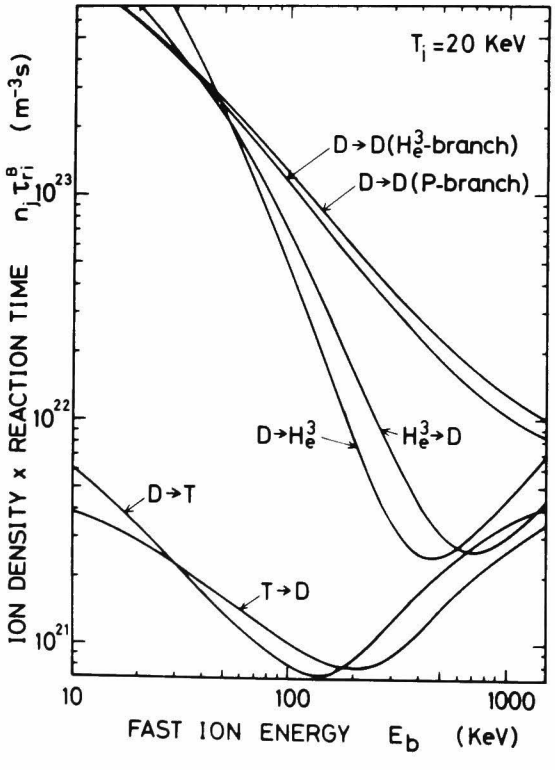

Fig.A.2. Products of field ion density and reaction time of superthermal particles vs. energy of superthermal particles, where the expression of D→T indicates that D and T are superthermal particles and Maxwellian particles, respectively.

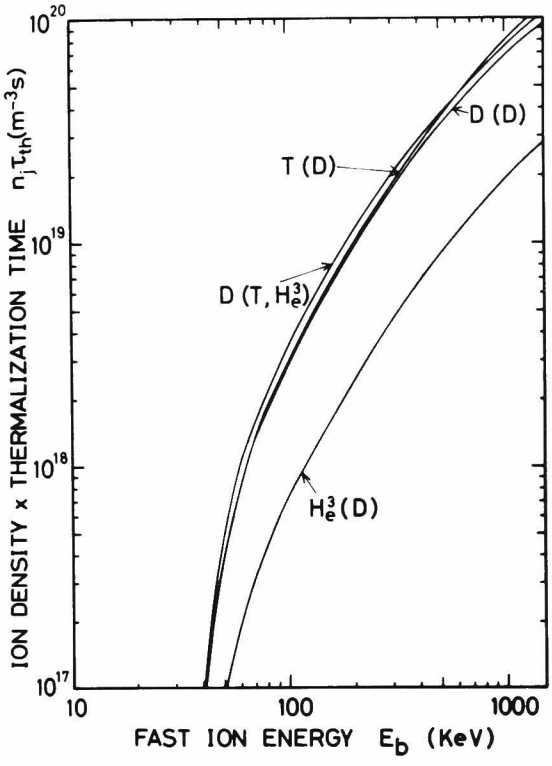

Fig.A.3. Thermalization times vs. energy of superthermal ions, where the expression of T(D) indicates that T and D are superthermal ions and field ions, respectively.

Appendix B

ALPHA PARTICLE FORMATION AND COULOMB COLLISION IN MONTE CARLO TECHNIQUE

B.1. Alpha Particle Formation

Alpha particles are assumed to be born isotropically in velocity space with the single energy of $3.5\,MeV$. Let us consider the spherical co-ordinate shown in Fig.B.1[52], where Z axis is taken to be parallel to the direction of magnetic field. The drift motion of alpha particles does not depend on the angle between X axis and $v_\perp$, but depends on solely the pitch angle χ between Z axis and $\vec{V}$. The angle χ is determined by uniform random number r_N as follows. A chosing point (x,y,z) is uniformly distributed on the unit sphere $x^2+y^2+z^2=1$. The element of area for this sphere in spherical co-ordinates χ, ϕ is $\sin\chi d\chi d\phi = -dz\,d\phi$, where $z=\cos\chi$. The probability density function $P(z)$ is given by $P(z)\,dz = -2\pi\sin\chi\,d\chi\,/4\pi = \frac{1}{2}dz$.

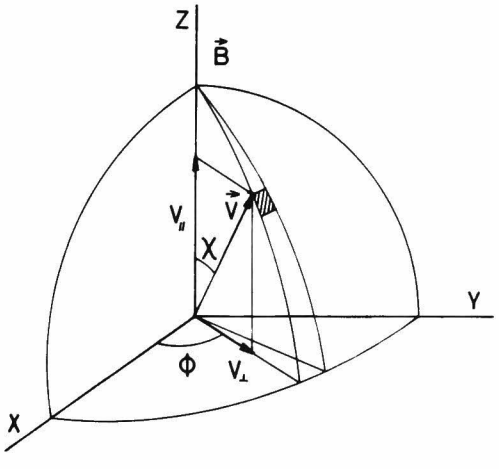

Fig.B.1. Spherical co-ordinate systems for isotropic source.

We may determine z by

$$r_N = \int_{-1}^{z} \frac{1}{2} dz = \frac{1}{2}(z+1) \qquad (B.1)$$

Therefore, $\chi = \cos^{-1}(2r_N - 1)$ (B.2)

is obtained. Next, we shall determine the birth position on vertical cross section of plasma core. If the production rate of alpha particles at the radial direction is assumed to be $f_b(r/a)$, then the birth position (r,θ) is derived from

$$r_N = \int_0^r x f_b(x)\, dx \Big/ \int_0^a x f_b(x)\, dx \qquad (B.3)$$

and

$$\theta = \pi r_N \qquad (B.4)$$

where $x=r/a$

B.2. Determination of Velocity after a Collision

The amounts of velocity change due to a Coulomb collision $\Delta V_{/\!/}$ and $\Delta V_{\perp}$ are given by the normal random numbers with the meanvalues $m_{/\!/}$ and $m_{\perp}$, and the variances $\sigma_{/\!/}^2$ and $\sigma_{\perp}^2$ presented by Eqs.(5.17) and (5.18). The velocity after a collision $\vec{V}(t+\Delta t)$ is expressed by the velocity before the collision $\vec{V}(t)$ and the changes of velocity due to the collision, $\Delta\vec{V}_{/\!/}$ and $\Delta\vec{V}_{\perp}$;

$$\begin{aligned}\vec{V}(t+\Delta t) &= \vec{V}(t) + \Delta\vec{V}_{/\!/} + \Delta\vec{V}_{\perp} \\ &= \{(V(t)+\Delta V_{/\!/})\cos\chi_0 - \Delta V_{\perp}\cos\psi\,\sin\chi_0\}\vec{i} \\ &\quad +\{(V(t)+\Delta V_{/\!/})\sin\chi_0 + \Delta V_{\perp}\cos\psi\,\cos\chi_0\}\vec{j} \\ &\quad + \Delta V_{\perp}\sin\psi\,\vec{k}\end{aligned} \qquad (B.5)$$

where $/\!/$ and $\perp$ denote the directions parallel and perpendicular to the initial velocity, respectively.

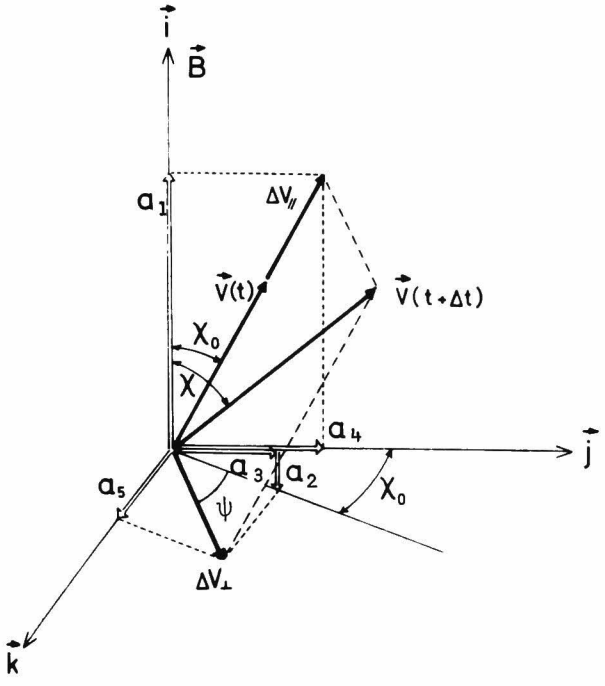

Fig.B.2. Velocity change due to a collision.

and $\vec{i}=\vec{B}/|\vec{B}|$, $\vec{k}\perp\vec{B}$, $\vec{k}\perp\vec{V}(t)$ and $\vec{i}\perp\vec{j}\perp\vec{k}$. (Fig.B.2) χ_0 is the initial pitch angle and ψ is the angle between the projection of $\vec{V}(t)$ on $\vec{j}$-$\vec{k}$ plane and $\Delta\vec{V}_\perp$, and constant a_i $(i=1,\cdots 5)$ are given as follows;

$$a_1 = (V(t)+\Delta V_{//})\cos\chi_0$$
$$a_2 = \Delta V_\perp \cos\psi \sin\chi_0$$
$$a_3 = \Delta V_\perp \cos\psi \cos\chi_0$$
$$a_4 = (V(t)+\Delta V_{//})\sin\chi_0$$
$$a_5 = \Delta V_\perp \sin\psi$$

The pitch angle after a collision χ is calculated as follows;

$$\chi = \tan^{-1}\left(\frac{\sqrt{(a_3+a_4)^2+a_5^2}}{a_1-a_2}\right). \qquad (B.6)$$

REFERENCES

[1] MILLS, R. G., "The Problems of Control of Thermonuclear Reactors", Proc. Symp. Los Alamos Scientific Laboratory LA-4250 (1969) B1.

[2] OHTA, M., YAMATO, H., MORI, S., in Plasma Physics and Controlled Nuclear Fusion Research (Proc. 4th Int. Conf. Madison, 1971) 3, IAEA, Vienna (1971) 423.

[3] SIVUKHIN, D. V., "Coulomb Collisions in a Fully Ionized Plasma", Reviews of Plasma Physics 4, Consultants Bureau, New York (1966) 93.

[4] ROSE, D. J., Nuclear Fusion 9 (1968) 183.

[5] SIGMAR, D. J., JOYCE, G., Nuclear Fusion 11 (1971) 447.

[6] TUCK, J. L., Nuclear Fusion 1 (1961) 201.

[7] SPITZER, L. Jr., "Physics of Fully Ionized Gases", Interscience Publishers, New York (1962) 135.

[8] STACEY, W. M. Jr., Nuclear Fusion 13 (1973) 843.

[9] FUJISAWA, T., Nuclear Fusion 14 (1974) 173.

[10] KOLESNICHENKO, Ya. I., REZNIK, S. N., Nuclear Fusion 13 (1973) 168.

[11] OHNISHI, M., YOSHIKAWA, H., WAKABAYASHI, J., Nuclear Fusion 13 (1973) 761.

[12] TSUJI, H., KATSURAI, M., SEKIGUCHI, T., Nuclear Fusion 16 (1976) 287.

[13] SAITO, H., KATURAI, M., TSUJI, H., SEKIGUCHI, T., in Plasma Physics and Controlled Nuclear Fusion Research (Proc. 6th Int. Conf. Berchtesgaden 1976) 3, IAEA, Vienna (1977) 337.

[14] RIVIERE, A. C., Nuclear Fusion 11 (1971) 363.

[15] CORMAN, E. G., LOEWE, W. E., COOPER, G. E., WINSLOW, A. M., Nuclear Fusion 15 (1975) 377.

[16] CORDEY, J. G., HOUGHTON, M. J., Nuclear FUSION 13 (1973) 215.

[17] YAMATO, H., OHTA, M., in the Technology of Controlled Nuclear Fusion (Proc. 1st Topical Meeting, San Diego, 1974) 2 (1974) 309.

[18] OHNISHI, M., HOSHINO, T., WAKABAYASHI, J., in the Technology of Controlled Nuclear Fusion (Proc. 2nd Topical Meeting, Richland, 1976) 3 (1977) 343.

[19] MILLS, R. G., in Engineering Problems of Controlled Fusion (Proc. 4th Symp. IEEE, Trans. Nucl. Science) 1 (1971) 205.

[20] MILEY, G. H., SOUTHWORTH, F. H., CHOI, C. K., GERDIN, G. A., in the Technology of Controlled Nuclear Fusion (Proc. 2nd Topical Meeting, Richland, 1976) 2 (1977) 119.

[21] GERDIN, G. A., STARK, R. A., MILEY, G. H., Proc. Int. Conf. on Plasma Science (1976) 53.

[22] MILLS, R. G., et al, Rep. MATT-1050.

[23] GOLOVIN, I. N., DNESTROVSKY, Yu. N., KOTOMAROV, D. P., Proc. Conf. Nuclear Fusion Reactors (1969) 194.

[24] STACEY, W. M. Jr., Nuclear Fusion 15 (1975) 583.

[25] KESNER, J., CONN, R. W., Nuclear Fusion 16 (1977) 829.

[26] JASSBY, D. L., TOWNER, H. H., "Optimization of Plasma Profiles for Ignited Low-Beta Toroidal Plasma Utilizing Advanced Fuels" PPPL-1360 (1977).

[27] LEHNERT, B., Proc. 3rd Int. Symp. Toroidal Plasma Confinement (1973) c1-1.

[28] GOTTLIEB, M. B., in the Technology of Controlled Nuclear Fusion (Proc. 2nd Topical Meeting, Richland, 1976) 267.

[29] IIYOSHI, A., UO, K., in Plasma Physics and Controlled Nuclear Fusion Research (Proc. 5th Int. Conf., Tokyo, 1974) 3, IAEA, Vienna (1974) 619.

[30] IIYOSHI, A., MOTOJIMA, O., OHNISHI, M., in Engineering Problems

in Fusion Research (Proc. 7th Symp., Knoxville, 1977) 2 (1978).

[31] STIX, T. H., Plasma Physics 14 (1972) 367.

[32] STRINGER, T. E., Plasma Physics 16 (1974) 651.

[33] ROME, J. A., McALEES, D. G., CALLEN, J. D., FOWLER, R. H., Nuclear Fusion 16 (1976) 55.

[34] McALEES, D. G., "Alpha Particle Energetics and Neutral Beam Heating in Tokamak Plasmas", ORNL-TM-4661 (1974).

[35] OHNISHI, M., TOKUNAGA, H., WAKABAYASHI, J., Nuclear Fusion 16 (1976) 690.

[36] MOROZOV, A. I., SOLOV'EV, L. S., "Motion of Charged Particles in Electromagnetic Fields", Reviews of Plasma Physics 2, Consultants Bureau, New York, (1966) 201.

[37] YANG, T. F., EMMERT, G. A., in the Technology of Controlled Nuclear Fusion (Proc. 1st Topical Meeting, San Diego, 1974) 2 (1974) 400.

[38] KADOMTSEV, B. B., POGUTSE, O. P., Nuclear Fusion 11 (1971) 67.

[39] CONN, R. W., EMMERT, G. A., Nuclear Fusion 14 (1974) 805.

[40] DAVIS, J.W., KULCINSKY, G. L., Nuclear Fusion 16 (1976) 355.

[41] KOLESNICHENKO, Ya. I., FURSA, A. D., YAVORSKII, V. A., Fizika Plazmy 2 (1976) 991.

[42] HIVELY, L. M., MILEY, G. H., Nuclear Fusion 17 (1977) 1031.

[43] PETRIE, T. W., MILEY, G. H., Nuclear Science and Engineering 64 (1977) 151.

[44] BELIKOV, V. S., KOLESNICHENKO, Ya. I., YAVORSKIL, V. A., Nuclear Fusion 16 (1976) 783.

[45] KALADZE, T. D., MIKHAJLOVSKIJ, A. B., Nuclear Fusion 17 (1977) 411.

[46] JASSBY, D. L., GOLDSTON, R. J., Nuclear Fusion 16 (1976) 613.

[47] TRUBNIKOV, B. A., "Particle Interactions in a Fully Ionized Plasma", Reviews of Plasma Physics 1, Consultants Bureau, New York, (1965) 105.

[48] AZUMI, M., Private Communication (1976).

[49] OHNISHI, M., AO, N., WAKABAYASHI, J., Nuclear Fusion 18 (1978)

859.

[50] ROSE, D. J., CLARK, M. JR., Plasmas and Controlled Fusion, MIT Press (1965) 80.

[51] BARNETT, C. F., RAY, J. A., THOMPSON, J. C., "Atomic and Molecular Collisions Cross Sections of Interested in Controlled Thermonuclear Research", ORNL-3113 (1964) 284.

[52] CASHWELL, E. D., EVERETT, C. J., A Practical Manual on the Monte Carlo Method for Random Walk Problems, Pergamon Press, London, (1959) 19.